ISTANBUL TECHNICAL UNIVERSITY ★ GRADUATE SCHOOL

NOVEL BIOPOLYMER APPLICATIONS AS ADSORBENT, DRUG ENCAPSULATION AND CONTROLLED DRUG RELEASE AGENTS

Ph.D. THESIS

Nilay KAHYA

Department of Chemistry

Chemistry Programme

OCTOBER 2023

<u>ISTANBUL TECHNICAL UNIVERSITY ★ GRADUATE SCHOOL</u>

NOVEL BIOPOLYMER APPLICATIONS AS ADSORBENT, DRUG ENCAPSULATION AND CONTROLLED DRUG RELEASE AGENTS

Ph.D. THESIS

Nilay KAHYA
(509162204)

Department of Chemistry

Chemistry Programme

Thesis Advisor: Prof. Dr. F. Bedia ERİM BERKER

OCTOBER 2023

ISTANBUL TEKNİK ÜNİVERSİTESİ ★ LİSANSÜSTÜ EĞİTİM ENSTİTÜSÜ

ADSORBAN, İLAÇ KAPSÜLLEME VE KONTROLLÜ İLAÇ SALIMI AJANLARI OLARAK YENİ BİYOPOLİMER UYGULAMALARI

DOKTORA TEZİ

Nilay KAHYA
(509162204)

Kimya Anabilim Dalı

Kimya Programı

Tez Danışmanı: Prof. Dr. F. Bedia ERİM BERKER

EKİM 2023

Nilay KAHYA, a Ph.D. student of ITU Graduate School student ID 509162204, successfully defended the thesis/dissertation entitled "NOVEL BIOPOLYMER APPLICATIONS AS ADSORBENT, DRUG ENCAPSULATION AND CONTROLLED DRUG RELEASE AGENTS", which she prepared after fulfilling the requirements specified in the associated legislations, before the jury whose signatures are below.

Thesis Advisor : **Prof. Dr. F. Bedia ERİM BERKER** ....
Istanbul Technical University

Jury Members : **Prof. Dr. Ayşegül GÖLCÜ** ....
Istanbul Technical University

Prof. Dr. Duri Şehvar ÜNAL ....
Istanbul University

Prof. Dr. Önder PEKCAN ....
Kadir Has University

Assoc. Prof. Dr. Aslı BAYSAL ....
Istanbul Technical University

Date of Submission : 02 September 2023
Date of Defense : 05 October 2023

To my mother,

FOREWORD

First of all, I would like to start by thanking my supervisor, Prof. Dr. F. Bedia ERİM, who contributed to the preparation of my thesis. If I include that I took her course as an undergraduate student in 2011 and my internship in her laboratory in 2013; she has been a guide for me over a 10-year studentship period throughout my undergraduate studies, graduate studies and ultimately my doctoral studies. She is a role model for me in many subjects, such as disciplined work, planning and doing things on time, being foresighted. I am grateful to her for providing me opportunity to work in her laboratory of Capillary Electrophoresis and Biopolymer Applications and most of the scientific experience I have gained. I would like to extend my respects to my PhD supervisor, who is also a real scientist, with a mother's feelings, protect and support her students and think of their well-being.

I would like to thank Assoc. Prof. Dr. Nevin ÖZTEKİN, who I have co-studied except my thesis's subject through my doctorate. I would like to thank all the members of my supervisor's research group, especially Lect. Dr. Zeynep KALAYCIOĞLU and Assoc. Prof. Dr. Hakan KAYGUSUZ as my colleagues, whom I worked sometimes together during my PhD years in the same laboratory environment. I would like to thank my thesis committee members of Prof. Dr. Ayşegül GÖLCÜ and Prof. Dr. Duri Şehvar ÜNAL for their valuable advices and comments though my doctoral studies.

I would like to thank my colleagues, with whom I worked as a research assistant in the ITU Chemistry Department in the years of my doctorate education. I am thankful to Asst. Prof. Dr. Esra SU for her friendship.

I also thank the Research Foundation of Istanbul Technical University for the financial support (Project ID: 42372) for my PhD studies.

In the last year of my PhD studentship, I have worked as a PhD scholar in the project of Assoc. Dr. Alper GÜRARSLAN. I would like to thank him for included me in his 3501 Career Development Program project (Project ID: 221M272). I thank the Scientific and Technical Research Council of Turkey (TÜBİTAK) for 2250 Performance-Based Scholarships Programme for PhD and Post-Doc Scholars.

I cannot thank my dear mother enough for being with me at every moment, supporting my decisions, guiding and supporting me. She is my everything and most important person of my life. I am grateful to my father for the importance and support he gave to my education. I would like to thank my sister for her support and friendship in my life. I would also like to express my gratitude and love to my little nephew, who joined our family.

I am grateful to all the good people I have come across; I would like to wish to share my future successes and beautiful moments with you.

September 2023

Nilay KAHYA
(Chemist, Chemical Engineer)

TABLE OF CONTENTS

Page

ABBREVIATIONS

Alg	: Alginate
Ba	: Barium
BSA	: Bovine Serum Albumin
Ca	: Calcium
Ce	: Cerium
CMC	: Carboxymethyl Cellulose
Cu	: Copper
DMSO	: Dimethyl Sulfoxide
EDX	: Energy Dispersive X-ray
EE%	: Encapsulation Efficiency %
EE%	: Entrapment Efficiency %
FTIR	: Fourier Transform Infrared
MTX	: Methotrexate
NPs	: Nanoparticles
PBS	: Phosphate Buffer Saline
R%	: Removal Efficiency %
SDBS	: Sodium Dodecyl Benzene Sulfonate
SDS	: Sodium Dodecyl Sulfate
SEM	: Scanning Electron Microscopy
SGF	: Simulated Gastric Fluid
SIF	: Simulated Intestinal Fluid
SR%	: Swelling Ratio %
SWR%	: Swelling Ratio %
TISAB	: Total Ionic Strength Adjustment Buffer
WHO	: World Health Organization
Zn	: Zinc

SYMBOLS

A	: Equilibrium binding constant of Temkin isotherm
B	: Temkin constant related to the heat of adsorption
b	: Temkin isotherm constant
C	: Intra-particle diffusion kinetic model constant
C_e	: Equilibrium concentration
C_i	: Initial concentration
C_t	: Equilibrium concentration of adsorbate at time
K_F	: Freundlich isotherm constant
K_L	: Langmuir isotherm constant
k_p	: Intra-particle diffusion kinetic model rate constant
k_1	: Pseudo-first-order kinetic model rate constant
k_2	: Pseudo-second-order kinetic model rate constant
m	: Mass
M_i	: Initial dry mass
M_i	: Initial mass of the beads
M_f	: Mass of swollen state of the beads
M_t	: Swelled mass
m_o	: Initial mass of the beads
m_t	: Mass of swollen beads
m_0	: Initial amount of drug present in alginate solution
m_1	: Total amount of drug present in alginate solution
q_e	: Amount of adsorbate per unit mass of adsorbent at equilibrium
q_t	: Amount of adsorbate per unit mass of adsorbent at time
q_{max}	: Maximum adsorption capacity
R	: Ideal gas constant
R_L	: Langmuir isotherm parameter
T	: Temperature
t	: Time
V	: Volume
1/n	: Freundlich isotherm parameter

α	**:** Elovich kinetic model rate constant
β	**:** Elovich kinetic model desorption constant

LIST OF TABLES

Page

LIST OF FIGURES

Page

NOVEL BIOPOLYMER APPLICATIONS AS ADSORBENT, DRUG ENCAPSULATION AND CONTROLLED DRUG RELEASE AGENTS

SUMMARY

Biopolymers are polymers derived from biological sources. Biopolymers can be subdivided into plant-derived polysaccharides and animal-derived proteins. Firstly, cellulose and then chitin as a polysaccharide are among the most well-known biopolymers thanks to their high abundance, wide distribution on earth and low production costs. The group of proteins mainly includes silk, gelatin, collagen and albumin. Similarly, chitin derivative chitosan, alginate (Alg), gum (gum), carboxymethyl cellulose (CMC) and starch are also included in the category of polysaccharides, and these biopolymers have found numerous applications by using them in various forms. The fact that biopolymers are non-toxic, biodegradable and create composite materials with different additives easily increases their applicability. Considering their sustainability, biocompatibility and mostly hydrophilic properties, biopolymers generally have high advantages over synthetic polymers. Due to their unique properties such as their renewable resources, abundance, biodegradability and ease of functionalization, biopolymers are being investigated for both academic and industrial applications.

Water treatment with biopolymers and biopolymer composites is one of the most sought-after research topics today. Reducing the resulting pollutants from wastewater is of vital importance for living organisms. Biopolymer-based adsorbents have the potential to replace traditional adsorbents such as silica, alumina, and activated carbon. They can compete with other adsorbents in terms of adsorption capacity, cost-effectiveness, and biocompatibility. In the first and second steps in this thesis, adsorption studies were carried out to remove harmful substances from the aqueous environment by means of biopolymer-based adsorbents. Different biopolymer-containing materials prepared as adsorbent materials in the physical form of films and beads were used in the removal studies from aqueous media. Biopolymers also have potential applications in the pharmaceutical industry for the development of controlled drug release systems. Biopolymers, with their abundance and natural content, are of great interest as carriers that will realize controlled drug release with the compatibility they will show in the stages of degradation in biological systems. In the ongoing third and fourth steps of this thesis study, drug encapsulation into new biopolymer materials and controlled release of drugs into the desired environment were investigated.

In the first stage of the thesis, an anionic surfactant sodium dodecyl benzene sulfonate (SDBS) was chosen as the harmful substance to remove from the aqueous medium. The uncontrolled mixing of surfactants into the environment is an important problem today. Cross-linked chitosan biopolymer films were utilized to the removal of SDBS from the aqueous solution. Sodium sulfate was chosen as the cross-linker. Batch adsorption studies show that the positively charged chitosan has an interaction with the negatively charged surfactant SDBS. In experimental studies, adsorption

parameters such as contact time, pH, cross-linker concentration and adsorbent dose were investigated. The maximum amount of adsorbed SDBS was reached at pH 2 and 180 minutes. Experimental data was modeled using kinetic and adsorption isotherm models and it was found that the adsorption system followed pseudo-second-order kinetics and the Langmuir adsorption isotherm model. The adsorption capacity of the films for SDBS adsorption was calculated as 714 mg/g. This study proposes a potential use of cross-linked chitosan films for the removal of anionic surfactants from the aqueous medium. The results of the study have been published in an SCI journal (Journal of Polymers and the Environment, 2018, *26*, 2166-2172).

In the second stage of the thesis, it was aimed to demonstrate the use of the novel composite material prepared by adding CeO_2 nanoparticles to carboxymethyl cellulose (CMC) beads cross-linked with Ce^{3+} ions as being an efficient adsorbent in fluoride ions removal from water. The characterization of the beads was carried out by swelling experiments, scanning electron microscopy and Fourier transform infrared spectroscopy. The adsorption of fluoride ions from aqueous solutions was carried out with both cerium ions cross-linked CMC beads (CMC-Ce) and CeO_2-nanoparticle loaded CMC-Ce beads (CeO_2-CMC-Ce) in a batch system. Optimized adsorption conditions were obtained under experimental conditions where parameters such as pH, contact time, adsorbent dose and agitation speed were investigated and a constant temperature value was 25 °C. Experimental data on adsorption showed good agreement with the Langmuir isotherm and pseudo-second-order kinetics. The maximum adsorption capacity of the adsorbents was obtained as 105 and 312 mg F^-/g adsorbent for CMC-Ce and CeO_2-CMC-Ce beads, respectively. Reusability studies have shown that adsorbent beads exhibit excellent sustainable properties up to 9 cycles. This study revealed that the CeO_2 nanoparticle doped CMC-Ce composite is a very effective adsorbent in removing fluoride from water. The results of the study have been published in a SCI journal (International Journal of Biological Macromolecules, 2023, *242(1)*, 124595).

In the third phase of the thesis, it was aimed to reduce the drug release in the acidic stomach environment and to transport the drug to the colon environment with the highest possible encapsulation amount. Protein-type drugs are disrupted at extremely acidic stomach pH. If such drugs reach the intestine without being degraded in the stomach environment, they can be absorbed by the intestinal mucosa. Therefore, research focuses on new approaches for colon-targeted delivery systems. The pH-sensitive properties of some polysaccharides make them colon-targeting agents. One of them is the biopolymer alginate. Alginate (Alg) shrinks in the stomach environment and mostly retains the drug encapsulated in the gel. In the thesis study, the biopolymer alginate was modified with sodium dodecyl sulfate (SDS), an agent whose interaction with protein is known. Bovine serum albumin (BSA) protein selected as the model drug was loaded onto SDS-modified calcium alginate beads (SDS/Ca-Alg). The encapsulation efficiency of BSA in SDS/Ca-Alg beads was found to be 96.3% with a high yield, which can be called complete confinement. The second remarkable result from the experimental studies is that the protein release from the SDS-modified calcium alginate beads into the artificial gastric fluid medium is significantly reduced compared to the protein release from the calcium alginate beads. At the same time, the release time of the entire drug from the SDS/Ca-Alg beads into the artificial intestinal medium was significantly prolonged compared to the Ca-Alg beads. SDS-modified alginate beads are recommended as suitable carriers for the passage of oral protein-type drugs into the colonic environment by preventing their degradation in acidic gastric fluid. The results of the study have been published in an SCI journal (Carbohydrate Polymers, 2019, *224*, 115165).

In the fourth phase of the thesis, barium alginate-carboxymethyl cellulose composite hydrogel beads were prepared as a controlled release agent that retards the release of the cancer drug methotrexate (MTX) into a phosphate-buffered saline (PBS) medium with a pH value of 7.4. The biggest advantage of alginate as a drug carrier in oral drug applications is its low level of swelling in the acidic gastric fluid environment. Thus, the drug entrapped in the alginate gel and taken orally is largely transported to the intestinal environment. However, in the basic pH environment, uncontrolled and rapid release of the drug is observed with sudden swelling and disintegration of the alginate gel. Recent innovative studies have focused on slowing the swelling rate of alginate in basic medium with suitable additives or forming composites of alginate and other polysaccharides. According to the literature review, this is the first study on MTX release from an alginate-carboxymethyl cellulose matrix into a PBS medium. Ba-Alg/CMC beads to be used in drug release experiments were prepared by adding the solution, which is a mixture of sodium alginate (NaAlg)/sodium carboxymethyl cellulose (NaCMC) biopolymers, into barium chloride solution. As a method in the preparation of the beads, dropping the polymer solution with a syringe into the solution containing barium ions was applied. Since MTX has low water solubility, the drug was first dissolved in DMSO and added to the polymer solution. The amount of DMSO added to the beads to dissolve the drug in the biopolymer solution (10% v/v) positively affected the morphology, swelling and release profiles of the beads. Scanning electron microscopy (SEM) and Fourier-transformed infrared (FTIR) spectroscopy analysis were used to characterize Ba-Alg/CMC composites. The results showed that the release of almost all the amount of MTX loaded on the beads was completed in 5 hours in PBS (pH 7.4 and 37 ^{o}C) with a release percentage of 98.1±2.64%. In addition, the synthesized Cu(II) (MXT-Cu) and Zn(II) (MXT-Zn) metal complexes of the drug were also loaded onto Ba-Alg/CMC beads and subjected to drug release studies. The entrapment efficiency of metal complexes of MTX in Ba-Alg-CMC and their release behaviour into PBS were compared with MTX. The data of the controlled release experiments was process to the first-order, Higuchi and Hixson-Crowell kinetic models, which are the most widely used drug release kinetic models. The results of the study have been published in an SCI journal (Journal of Drug Delivery Science and Technology, 2019, *54*, 101324).

The successive steps of this thesis study were completed in four stages on the applicability of new biopolymer-based materials for adsorption and controlled drug release. The results obtained from the experiments at each stage were presented to the literature as four original research articles published in journals within the scope of SCI in the Q1 (3) and Q2 (1) category. The fact that the materials containing biopolymer, which are successful adsorbent and controlled drug release agents, prepared in line with the outputs of the thesis study, will be beneficial to humanity in the coming years will be a complete indicator of the realization of the purpose. It is foreseen that the thesis will contribute to scientific knowledge through the articles published as a result of the research carried out within the scope of the thesis.

ADSORBAN, İLAÇ KAPSÜLLEME VE KONTROLLÜ İLAÇ SALIMI AJANLARI OLARAK YENİ BİYOPOLİMER UYGULAMALARI

ÖZET

Biyopolimerler, biyolojik kaynaklardan elde edilen polimerlerdir. Biyopolimerler, bitki kaynaklı polisakkaritler ve hayvan kaynaklı proteinler olmak üzere alt sınıflara ayrılabilirler. Polisakkarit olarak özellikle selüloz ve ardından kitin, yüksek bollukları, yeryüzünde geniş dağılımları ve düşük üretim maliyetleri sayesinde en bilinen biyopolimerlerdendir. Proteinler grubu esas olarak ipek, jelatin, kollajen ve albümini içerir. Benzer şekilde kitin türevi kitosan, aljinat (Alg), zamk (gum), karboksimetil selüloz (CMC) ve nişasta da polisakkaritler kategorisine girerler ve bu biyopolimerler de çeşitli formlarda kullanılarak çok sayıda uygulama alanı bulmuşlardır. Biyopolimerlerin toksik olmaması, biyolojik olarak parçalanabilir olması ve farklı katkı maddeleri ile kompozit malzemeler oluşturması uygulanabilirliklerini kolayca artırmaktadır. Biyopolimerler sürdürülebilirlikleri, biyouyumlulukları ve çoğunlukla hidrofilik özellikleri göz önüne alındığında sentetik polimerlerin yanında genel olarak yüksek avantajlara sahiptir. Doğal kaynaklarının yenilenebilirliği, bollukları, biyolojik olarak parçalanabilirlikleri ve işlevselleştirme kolaylığı gibi benzersiz özellikleri sayesinde biyopolimerler, hem akademik hem de endüstriyel uygulamalar için araştırılmaktadır.

Biyopolimerler ve biyopolimer kompozitlerle su iyileştirme, günümüzde en fazla rağbet gören araştırma konularından biridir. Ortaya çıkan kirleticilerin atık sudan azaltılması canlılar açısından hayati öneme sahiptir. Biyopolimer bazlı adsorbanlar, silika, alümina, aktif karbon gibi geleneksel adsorbanların yerini alma potansiyeline sahiptir. Adsorpsiyon kapasitesi, maliyet etkinliği, biyouyumluluk gibi açılardan diğer adsorbanlara rekabet edebilirler.

Bu tez içerisindeki birinci ve ikinci basamaklarda, biyopolimer bazlı adsorbanlar aracılığıyla sulu ortamdan zararlı maddelerin giderilmesi için adsorpsiyon çalışmaları yapılmıştır. Film ve boncuk fiziksel formundaki birer adsorban malzeme olarak hazırlanan farklı biyopolimer içerikli malzemeler sulu ortamdan giderim çalışmalarında kullanılmıştır. Biyopolimerler kontrollü ilaç salım sistemlerinin geliştirilmesi amacıyla ilaç sektöründe potansiyel uygulamalarda da yer almaktadır. Biyopolimerler, bollukları ve doğal içerikli olmalarıyla biyolojik sistemlerde parçalandıkları aşamalarda gösterecekleri uyum ile kontrollü ilaç salımını gerçekleştirecek taşıyıcılar göreviyle büyük ilgi görmektedirler. Bu tez çalışmasının devam eden üçüncü ve dördüncü basamaklarında yeni biyopolimer malzemelere ilaç enkapsülasyonu ve ilaçların istenilen ortama kontrollü olarak salımı için araştırılmıştır.

Tezin birinci aşamasında, sulu ortamdan zararlı maddelerin uzaklaştırma çalışmaları için anyonik yüzey aktif sodyum dodesil benzen sülfonat (SDBS) seçilmiştir. Yüzey aktif maddelerin çevreye kontrolsüz olarak karışması günümüzde önemli bir sorundur. SDBS’nin sulu çözeltiden uzaklaştırılması için, çapraz bağlı kitosan biyopolimer filmler kullanıldı. Çapraz bağlayıcı olarak sodyum sülfat seçildi. Kesikli adsorpsiyon

çalışmaları, pozitif yüklü kitosanın negatif yüklü yüzey aktif SDBS'ye karşı bir etkileşime sahip olduğunu göstermektedir. Deneysel çalışmalarda temas süresi, pH, çapraz bağlayıcı konsantrasyonu ve adsorban dozu gibi adsorpsiyon parametreleri incelenmiştir. Maksimum adsorbe edilen SDBS miktarına pH 2'de ve 180 dakikada ulaşıldı. Deneysel veriler, kinetik ve adsorpsiyon izoterm modelleri kullanılarak modellendi ve adsorpsiyon sisteminin Langmuir izoterm modeli ile sözde ikinci dereceden kinetiği izlediği bulundu. Filmlerin SDBS adsorpsiyonu için elde edilen adsorpsiyon kapasitesi 714 mg/g olarak bulunmuştur. Bu çalışma, sulu ortamından anyonik yüzey ektif maddelerin uzaklaştırılması için çapraz bağlı kitosan filmlerinin potansiyel bir kullanımını önermektedir. Çalışmanın sonuçları bir SCI dergisinde yayınlanmıştır (Journal of Polymers and the Environment, 2018, *26*, 2166-2172).

Tezin ikinci aşamasında yapılan çalışmada, CeO_2 nanoparçacıklarının Ce^{3+} iyonları ile çapraz bağlı karboksimetil selüloz (CMC) boncuklarına ilavesiyle hazırlanan yeni bir kompozit malzemenin florürün sudan uzaklaştırılmasında etkili bir adsorban olarak kullanımının gösterilmesi amaçlanmıştır. Boncukların karakterizasyonu, şişme deneyleri, taramalı elektron mikroskobu ve Fourier dönüşümlü kızılötesi spektroskopisi ile gerçekleştirildi. Sulu çözeltilerden florür iyonlarının adsorpsiyonu, kesikli bir sistemde hem seryum iyonu çapraz bağlı CMC boncukları (CMC-Ce) hem de CeO_2-nanoparçacık ilaveli CMC-Ce boncukları (CeO_2-CMC-Ce) ile gerçekleştirildi. Optimize edilmiş adsorpsiyon koşulları pH, temas süresi, adsorban dozu ve çalkalama hızı gibi parametrelerin incelendiği deney koşullarında ve sabit sıcaklık değeri 25 °C'de elde edildi. Adsorpsiyona ait deneysel veriler Langmuir izotermi ve sözde ikinci dereceden kinetik ile iyi bir şekilde uyum göstermiştir. Maksimum adsorpsiyon kapasitesi CMC-Ce ve CeO_2-CMC-Ce boncukları için sırasıyla 105 ve 312 mg/g F^- olarak bulundu. Yeniden kullanılabilirlik çalışmaları, adsorban boncukların 9 döngüye kadar mükemmel sürdürülebilir özellikler sergilediğini göstermiştir. Bu çalışma, CeO_2 nanoparçacık katkılı CMC-Ce kompozitinin florürün sudan uzaklaştırılmasında çok etkili bir adsorban olduğunu ortaya koymuştur. Çalışmanın sonuçları bir SCI dergisinde yayınlanmıştır (International Journal of Biological Macromolecules, 2023, *242(1)*, 124595).

Tezin üçüncü aşamasında yapılan çalışmada, asidik mide ortamında ilaç salınımını azaltmak ve ilacı olabilecek en yüksek kapsülleme miktarı ile kolon ortamına taşımak için kontrollü ilaç salımı hedeflenmiştir. Protein tipi ilaçlar aşırı asidik mide pH'sında bozulur. Bu tür ilaçlar mide ortamında bozunmadan bağırsağa ulaşırsa, bağırsak mukozası tarafından emilebilirler. Bu nedenle araştırmalar, kolon hedefli dağıtım sistemleri için yeni yaklaşımlar üzerinde yoğunlaşmaktadır. Bazı polisakkaritlerin pH'a duyarlı özellikleri onları kolon hedefli ajanlar yapar. Bunlardan biri biyopolimer aljinattır. Aljinat (Alg) mide ortamında büzülür ve jel içerisine kapsüllenmiş ilacı çoğunlukla tutar. Yapılan tez çalışmasında, biyopolimer aljinatın protein ile etkileşiminin bilindiği bir ajan olan sodyum dodesil sülfat (SDS) ile modifiye edilmiştir. Model ilaç olarak seçilen sığır serum albümin (BSA) proteini SDS ile modifiye edilmiş kalsiyum aljinat boncuklarına (SDS/Ca-Alg) yüklenmiştir. BSA'nın SDS/Ca-Alg boncuklarındaki kapsülleme etkinliği tam hapsetme denilebilecek olan yüksek verimle %96,3 olarak saptanmıştır. Yapılan deneysel çalışmalardan alınan ikinci dikkat çekici sonuç, SDS ile modifiye edilmiş kalsiyum aljinat boncuklarından yapay mide sıvısı ortamına protein salınımının, kalsiyum aljinat boncuklarının yaptığı protein salınımına kıyasla önemli ölçüde azalmasıdır. Aynı zamanda, ilacın tamamının SDS/Ca-Alg boncuklarından, yapay bağırsak ortamına salınma süresi Ca-Alg boncuklara göre önemli ölçüde uzamıştır. SDS ile modifiye edilmiş aljinat boncukları, ağızdan alınan protein tipi ilaçların asidik mide sıvısında bozulmalarını önleyerek kolon ortamına geçişi için uygun taşıyıcılar olarak önerilmektedir. Çalışmanın sonuçları bir SCI dergisinde yayınlanmıştır (Carbohydrate Polymers, 2019, *224*, 115165).

Tezin dördüncü aşamasında yapılan çalışmada, baryum aljinat-karboksimetil selüloz kompozit hidrojel boncukları, kanser ilacı metotreksatın (MTX) pH değeri 7,4 olan fosfat tamponlu tuz çözeltisi (PBS) ortamına salınımını yavaşlatıcı bir kontrollü salım ajanı olarak hazırlandı. Aljinatın ağızdan alınan ilaç uygulamalarında bir ilaç taşıyıcısı olarak en büyük avantajı asidik mide sıvısı ortamda düşük seviyedeki şişme özelliğidir. Böylece aljinat jeli içine hapsolmuş ve ağızdan alınan ilaç büyük ölçüde bağırsak ortamına taşınır. Bununla birlikte, bazik pH ortamında, aljinat jelinin ani şişmesi ve parçalanması ile ilacın kontrolsüz ve hızlı salımı gözlenir. Son zamanlarda yapılan yenilikçi çalışmalar, uygun katkı maddeleri ile aljinatın bazik ortamda şişme hızının yavaşlatılması veya aljinat ile diğer polisakkaritlerin kompozitlerinin oluşturulması üzerinedir. Literatür araştırmasına göre bu çalışma aljinat-karboksimetil selüloz matrisinden PBS ortamına MTX salımı üzerine yapılan ilk çalışmadır. İlaç salım deneylerinde kullanılacak Ba-Alg/CMC boncukları sodyum aljinat (NaAlg)/sodyum karboksimetil selüloz (NaCMC) biyopolimerlerinin karışımı olan çözeltinin, baryum klorür çözeltisi içerisine eklenmesiyle hazırlandı. Boncukların hazırlanmasında yöntem olarak baryum iyonları içeren çözeltiye polimer çözeltisinin şırınga ile damlatılması uygulanmıştır. MTX'in suda çözünürlüğü düşük olduğu için ilaç öncelikle DMSO içinde çözüldü ve polimer solüsyonuna eklendi. İlacı çözmek için boncuklara eklenen DMSO'nun biyopolimer çözeltisindeki (%10 h/h) miktarı boncukların morfolojisini, şişmesini ve salım profillerini olumlu yönde etkiledi. Ba-Alg/CMC kompozitlerini karakterize etmek için taramalı elektron mikroskobu ve Fourier dönüştürülmüş kızılötesi spektroskopisi kullanıldı. Sonuçlar, boncuklara yüklenen neredeyse tüm MTX miktarının %98.1±2.64 salım yüzdesi ile PBS içerisinde (pH 7,4 ve 37 ^{o}C) 5 saatte tamamlandığını gösterdi. Ayrıca ilacın sentezlenen Cu(II) (MXT-Cu) ve Zn(II) (MXT-Zn) metal kompleksleri de Ba-Alg/CMC boncuklarına yüklenmiş ve ilaç salım çalışmalarına tabi tutulmuştur. MTX'in metal komplekslerinin Ba-Alg-CMC içerisine hapsolma verimliliği ve PBS içerisine salım davranışları MTX ile karşılaştırıldı. Kontrollü salım deneylerinin verileri en çok kullanılan ilaç salım kinetik modelleri olan birinci derece, Higuchi ve Hixson-Crowell kinetik modellerine uygulanmıştır. Çalışmanın sonuçları bir SCI dergisinde yayınlanmıştır (Journal of Drug Delivery Science and Technology, 2019, *54*, 101324).

Bu tez çalışmasının birbirini takip eden basamakları adsorpsiyon ve kontrollü ilaç salımı konusunda yeni biyopolimer bazlı malzemelerin uygulanabilirliğinin araştırılması üzerine dört aşamada tamamlanmıştır. Her bir aşamada deneylerden elde edilen sonuçlar Q1 (3) ve Q2 (1) kategorisindeki SCI kapsamındaki dergilerde yayınlanmış dört adet özgün araştırma makalesi olarak literatüre sunulmuştur. Tez çalışmasının çıktıları doğrultusunda hazırlanmış olan başarılı birer adsorban ve kontrollü ilaç salım ajanı olan biyopolimer içerikteki malzemelerin, ilerleyen yıllarda insanlığa yararlı olması tezin amacının gerçekleştiğinin tam anlamıyla göstergesi olacaktır. Tez kapsamında gerçekleştirilmiş araştırmaların sonucunda yayınlanan makaleler aracılığıyla, tezin bilimsel bilgi birikimine katkısının olacağı öngörülmektedir.

1. INTRODUCTION

Today, biopolymers are highly valued as alternative sources that can replace petroleum-based products and chemicals that have been used in countless uses. Many types of biopolymers are obtained naturally from plants, animals and microorganisms. The suffix "bio" in the term biopolymer emphasizes the availability of these polymers from living things. At the same time, biopolymers obtained from natural sources are biodegradable. The monomer units of biopolymers can be composed of nucleic acids, amino acids or sugars, thus resulting in biopolymer groups that can be divided into three main classes: Polypeptides, polynucleotides, and polysaccharides, respectively. The most abundant biopolymer is cellulose, and then followed by chitin, are at the top of the polysaccharides of natural origin. Anionic and water-soluble cellulose derivative biopolymers, such as carboxymethyl cellulose and hydroxethyl cellulose, can also be produced from the abundant polysaccharide of cellulose. In addition, chitosan, cationic charged polysaccharide obtained from chitin, is a well-known and common biopolymer, which is soluble in acidic solutions. Alginate, which is obtained from seaweeds, is a polysaccharide-structured marine biopolymer that is also very abundant. Polysaccharide biopolymers such as alginate, chitosan, and carboxymethyl cellulose provide the most important features that carry them to a wide range of uses, as well as their abundance, biocompatibility, biodegradability and non-toxicity. In addition to these, biopolymers belonging to different subclasses of plant and animal origin can be included in the subject.

In many aspects of human life, besides the cheapness of the use of any material, it is important that it is degradable, cheap and harmless to living creatures and the environment. The increasing world population and many products produced to maintain daily life in order to meet the needs of this population accumulate in the environment as irreversible waste. In addition, the irreversible pollution and consumption of many earth resources have also started to create awareness among people and have become one of the problems sought solutions. At this point, the replacement of synthetic polymers produced from fossil-based sources with biopolymers can be provided as an urgent solution to this part of the problem. In today’s world, there is a trend towards sustainability and many biopolymer and bioplastic-based products have been growing in the market at increasing rates. Biopolymers are currently used in applications in different industrial areas, such as food, medicine, water treatment, and medical products. With an increasing trend, researchers from all over the world bring numerous academic studies to the literature to prove the preparation and usability of different biopolymer-based materials with the principle of progressing towards the better. The knowledge and experience gained carries the appropriate information from these research products, from laboratory scale to industrial scale application. Water is essential for humanity, and it is the source of life. As long as there is water, life exists. Inevitably, potable water resources in the world are also limited. Moreover, an increasing population and all kinds of water consumption that comes with it cause pollution and destruction of many water resources. When the effects caused by climate change are added to these problems, it is obviously clear that the remaining time for the adequacy of usable natural source water is rapidly shortening. There are different techniques for cleaning and purifying water after contamination with harmful and toxic substances from different sources. Adsorption is known to be the easiest and most widely applicable of these methods. Simply, the substance that is desired to be drawn from the water is attached to the adsorbent and separated. In two separate studies carried out within the scope of this thesis, studies have been carried out to demonstrate the applicability of biopolymers as adsorbent materials for the separation of undesirable harmful components from water by novel materials prepared.

For humanity to survive, the struggle against diseases and their sources has been going on since the early ages. In addition to preventing diseases, drugs are taken into the body for therapeutic purposes. As a primitive method of treatment since ancient times, when the active ingredient of drugs is present in natural sources such as edible plants, the drug can enter the body and thus the disease can be cured. However, this method, which is expressed under the name of treatment and from a very limited point of view, is of course not applicable today in the treatment of many very different diseases that require the delivery of drugs to a controlled and targeted environment. There are many methods for delivering drugs to the body. Delivery of the drug to the desired environment via the agent that will carry it locally or systematically can be done through controlled release systems. Polysaccharides are also polymers suitable to act as a vehicle to deliver the drug as a carrier to the release medium. Thanks to their advantages such as biodegradability and biocompatibility, biopolymers can also be diversified with a wide variety of fillers in drug delivery systems, either alone as a matrix or in composites. They can play a role in different material forms in release systems that can deliver drugs from such natural sources to the body. Within the scope of this thesis, two original studies were carried out for drug encapsulation and controlled release of new biopolymer composites for the use of new biopolymer composites in the medical field for pharmaceutical applications.

1.1 Purpose of Thesis

This thesis aims to prepare new biopolymer-based composites and to use these emerging materials in adsorption and drug release applications. For this reason, the thesis is divided into four parts to show the applications of biopolymers in the main topics mentioned. In the first two parts of this thesis, adsorbent materials produced from biopolymers have been used to remove pollutants that cause harm to the environment and living organisms in the aqueous medium. In the third and fourth stages of the thesis, the release studies of two different drugs were carried out following the encapsulation of the drugs into the biopolymer matrix in order to ensure the controlled release of the selected drugs into body fluids in vitro.

In the first part of the thesis, adsorption studies were carried out with chitosan biopolymer films prepared for the removal of negatively charged surfactant sodium dodecyl benzene sulfonate as a pollutant that can mix with domestic or industrial waters. Uncontrolled pollution of surfactants to aquatic environment is a crucial problem of today's earth. In this study, sodium dodecyl benzene sulfonate was chosen as a model surfactant for removal studies by the chitosan films. A study on the adsorption of the related surfactant by chitosan films has not yet been published in the literature. Chitosan films, prepared as a harmless adsorbent and cross-linked with sodium sulfate ions, were subjected to removal studies in a series of systematic adsorption experiments to determine pH, time, adsorbent amount and adsorbate concentration effects in order to determine the optimum conditions of adsorption. In addition, considering the energy efficiency, all adsorption experiments were carried out at 25 °C and according to the results obtained in the optimization stages, the highest

SDBS removal was performed at pH=2 and at the end of 180 minutes. Chitosan is a biopolymer with a positive charge in acidic medium and its interaction with negatively charged surfactant was strong at pH of acidic medium. The maximum adsorption capacity of the adsorbent chitosan films was calculated as 714 mg SDBS per gram adsorbent. As a result of fitting the experimental data to the adsorption isotherms and kinetic models, it was seen that the system adapts to the Langmuir isotherm and follows the pseudo-second-order kinetic model. The results of the SDBS removal study of chitosan films, which is an easy-to-prepare and low-cost adsorbent, were published as an original research article in an SCI journal in 2018.

In the second part of the thesis, fluoride adsorption studies were carried out using beads prepared with CeO_2 nanoparticle-loaded carboxymethyl cellulose biopolymer which is cross-linked with cerium ions in order to remove the polluting fluoride from water. Fluoride is an inorganic anion that, causes health problems in humans with its excessive accumulation in drinking water as well as its deficiency in water. The biopolymers with their non-toxicity and biodegradability have been drawn attention with their usage areas as adsorbent and the fact that they form composite materials with different additives increases their application areas. Based on this, a nanoparticle-loaded cross-linked biopolymer adsorbent was prepared considering the interaction of cerium and fluoride ions. The presence of nanoparticles in the biopolymer beads increased the adsorption capacity of fluoride ions by the beads from 105 mg/g to 312 mg/g. Adsorption experiments at pH 6.2 which is the initial pH value of the fluoride solution and at 25 ^{o}C, showed that equilibrium was reached in 120 minutes. Among the studies in the literature, no study has yet been reported that, carboxymethyl cellulose spheres doped with CeO_2 nanoparticles and cross-linked with cerium (III) ion effectively remove fluoride anions from aqueous media. All results including fluoride removal studies of the new adsorbent from aqueous media and SEM, FTIR, SEM-EDX analyzes were published as an original research article in a journal within the scope of SCI in 2023.

In the third part of the thesis, after the encapsulation of the BSA protein, selected as a model drug, into SDS-modified calcium alginate beads, the release behavior of the orally taken drug into the simulated gastric and intestinal environment was investigated. In some diseases that require colon-targeted drug delivery, when protein-containing drugs are taken orally, the desired behaviour is that the protein-structured drug passes into the intestine with the lowest possible level of denaturation in the gastric fluid at acidic pH. To serve this purpose, BSA protein was encapsulated in the beads modified with SDS, and it was observed that, SDS additive provided an almost complete entrapment efficiency of 96.3% to the drug, and also significantly reduced its cumulative release from the spheres in SGF, which is the first body fluid it enters when the drug is taken orally. As a result, the drug was delivered by the beads into the SIF of the colon with a time-dependent controlled release. Thereby, it is recommended that, SDS modified alginate drug carriers to the pharmaceutical industry as a novel material for orally taken protein-type drugs that are target to deliver the drug into the colon. The results of this study were presented to the literature as an original research article in an SCI indexed journal in 2019.

In the fourth part of the thesis, it was studied to monitor the controlled release of methotrexate (MTX) drug encapsulated in barium ion cross-linked alginate-carboxymethyl cellulose into phosphate buffer saline (PBS) medium. The study aims to reveal the release of the drug into the body environment, which is simulated with a PBS solution at pH 7.4. MTX is a drug with a very low water solubility and was first dissolved in DMSO and added to disperse it in the alginate-carboxymethyl cellulose composite biopolymer solution. The addition of DMSO to the formulation of the beads used as a drug release agent reduced the swelling of the beads and was also effective in controlling the MTX release. In this study, the MTX drug loaded on the biopolymer-based material showed a controlled release profile from the spheres and was completely released into the PBS as much as it was trapped within the 5-hour release follow-up period. The results of this controlled drug release study were published as an original research article in a scientific journal within the scope of SCI in 2019.

2. AQUEOUS REMOVAL OF SODIUM DODECYL BENZENE SULFONATE BY CROSSLINKED CHITOSAN FILMS [1]

Nowadays, environmental pollution is one of the important problems of earth. Surfactants are among the major pollutants of wastewaters due to their widespread use in detergent formulations [1]. Industrial and domestic wastewaters containing surfactant residues are discharged into the environment. Organisms in aquatic systems are directly affected by the polluted waters. Surfactants are present in four different types depending on their charge being cationic, anionic, nonionic, or amphoteric. Sodium dodecyl benzene sulfonate (SDBS) is a negatively charged surfactant in the family of linear alkyl benzene sulfonates and one of the commonly used surfactants in the industrial applications. In the literature, various techniques were reported for the removal of SDBS from aqueous media. The most widely used method is adsorption, being one of the most economic and environmentally friendly techniques [2–5]. In this context, biopolymers have been used for the development of novel adsorbents for pollutants [6–10].

Chitosan is a positively charged polymer made of chitin. It has reactive amino and hydroxyl groups on its chains. Via amino groups, chitosan can be protonated in acidic pH values. It has antibacterial properties and can be doped with natural products in order to improve its physical and antimicrobial properties [11, 12]. Chitosan is currently in various applications such as in food industry, medicine, and cosmetics. In these fields, chitosan finds use due to its biodegradable and biocompatible nature. It forms gel structures in different shapes, including beads, microspheres, and films. Crosslinking of chitosan is made ionically or covalently [13]. Removal of SDBS by non-crosslinked chitosan was reported before [14].

In this work, sodium sulfate crosslinked chitosan films were used for adsorption of SDBS from its aqueous solution. The effects of contact time, pH, crosslinker amount,

---

[1] This chapter was published as "Kahya, N., Kaygusuz, H., Erim, F.B. (2018). Aqueous removal of sodium dodecyl benzene sulfonate (SDBS) by crosslinked chitosan films. J. Polym. Environ. 26, 2166-2172".

and adsorbent dose were studied. Adsorption experimental data was modeled by isotherm and kinetic models. The maximum adsorption capacity of this novel adsorbent was calculated.

2.1 Experimental

2.1.1 Materials

Chitosan (low molecular weight, with a degree of deacetylation 75–85%, viscosity 20–300 cP) and sodium dodecyl benzene sulfonate (SDBS) were purchased from Sigma-Aldrich (St. Louis, MO, USA). Sodium sulfate was obtained from Merck (Darmstadt, Germany). The mentioned chemicals were of analytical grade and used without any further purification. All solutions were prepared using deionized water from Elga Purelab Option-Q system (London, UK).

2.1.2 Preparation of adsorbent: sodium sulfate crosslinked chitosan films

Chitosan was dissolved in 1% (v/v) acetic acid solution to give a 1% (w/v) solution. The polymer solution was stirred 6 h for homogenization. The chitosan solution was degassed in an ultrasonic bath for 30 min to remove air bubbles before casting films into Petri dishes. Films were prepared by pouring 1% (w/v) chitosan solution into round shaped plates and the solvent was evaporated at room temperature. After that, the films were ionically crosslinked by sodium sulfate solution. Firstly, the films were dipped into 10% (or 20%) (w/v) sodium sulfate aqueous solutions for 1 h at 25 °C. Then, the films were taken out and washed with deionized water. Finally, the films were dried at room temperature. Films in dried state were used in adsorption experiments.

2.1.3 Adsorption studies

Adsorption experiments were carried out in a batch method. In order to investigate the adsorption behavior of system, several experiments were done as preliminary studies. Experimental parameters such as initial SDBS concentration, contact time, crosslinker concentration, pH and adsorbent dose were studied in order to determine optimized conditions for adsorption. In optimization experiments; SDBS concentrations varied from 100 to 3000 ppm in a batch volume of 10 mL, adsorbent film dose from 5 to 25 mg, and pH between 2 and 8. SDBS solution vessels were shaken in a temperature controlled Nüve ST-402 water bath (Ankara, Turkey) at 25 °C and at a speed of 200 rpm. Adsorbent sodium sulfate chitosan films were cut in square shapes about 1×1 cm^2 sizes and then weighed. The thickness of the films (0.15±0.03 mm) was measured with a Mitutoyo digital caliper (Kanagawa, Japan). A linear calibration curve was obtained by measuring absorbance of standard SDBS solutions at 223 nm using a Shimadzu UV-1800 (Kyoto, Japan). All experiments were repeated three times. Removal percentage of SDBS was calculated from equation 2.1.

$$Removal\ \% = \frac{(C_i - C_e)}{C_i} x\ 100 \qquad (2.1)$$

here, C_i and C_e (ppm) represent initial and final concentrations of SDBS in solutions, respectively. Another parameter q_e (mg/g) which explains adsorption capacity of adsorbent or SDBS removal capability of the films at equilibrium time was expressed as:

$$q_e = \frac{(C_i - C_e)}{m} x\ V \qquad (2.2)$$

where V is volume of adsorbate solution (L) and m is mass (g) of adsorbent.
Adsorption experiments were performed by placing film samples in SDBS solutions of varying concentration at pH 2 and shaking them at 25 °C during 180 min. In kinetic studies, 20 mg of the film was shaken in 10 mL of SDBS the solution (40 or 300 ppm) and varying concentrations of SDBS in solution over time (C_t) were determined at different time intervals.

2.1.4 Isotherm modeling of adsorption

Batch adsorption experimental results are modeled by three isotherms: Langmuir [15], Freundlich [16] and Temkin [17] models. The related equations of these models can be expressed as:

$$\frac{C_e}{q_e} = \frac{1}{q_m} C_e + \left(\frac{1}{q_m K_L}\right) \qquad (2.3)$$

$$ln\, q_e = ln\, K_f + \frac{1}{n} ln\, C_e \qquad (2.4)$$

$$q_e = \left(\frac{RT}{b}\right) ln\, A + \left(\frac{RT}{b}\right) ln\, C_e \qquad (2.5)$$

where C_e is the concentration of SDBS at equilibrium (mg/L), q_e is the amount of SDBS on adsorbent (mg/g) which was expressed in equation 2.2, q_m is the maximum adsorption capacity, and K_L is the Langmuir constant (L/mg). In the Freundlich isotherm model, the 1/n value indicates the nature of adsorption. The Temkin isotherm is related to the heat of adsorption that is $B = (RT/b)$ in (J/mol), R is the ideal gas constant, T is temperature (K), b is the isotherm constant, and A (L/g) is the equilibrium binding constant that states maximum binding energy.

2.1.5 Kinetic modeling of adsorption

Kinetic models describe kinetic behavior of adsorbate onto adsorbent and are relevant to the rate of adsorption. Pseudo-first-order and pseudo-second-order kinetic model equations were applied to experimental data and their equations are given below, respectively:

$$log(q_e - q_t) = log\, q_e - \frac{k_1}{2.303} t \qquad (2.6)$$

$$\frac{t}{q_t} = \frac{1}{k_2 {q_e}^2} + \frac{t}{q_e} \qquad (2.7)$$

where t is time (min). Pseudo-first-order and pseudo-second-order rate constants are k_1 (min^{-1}) and k_2 ($g\ mg^{-1}\ min^{-1}$) respectively.

2.2 Results and Discussion

2.2.1 Characterization of films

Figure 2.1 (A-B-C) shows Fourier transform infrared spectra of non-crosslinked chitosan films and crosslinked chitosan films before and after SDBS adsorption, respectively. In noncrosslinked film spectra, the peak at 3260 cm^{-1} is related to O–H and N–H stretching. The peaks located 2882, 2886, and 2891 cm^{-1} can be associated C–H stretching vibrations. Characteristic chitosan peaks are related to the peaks at 1540 cm^{-1} (N–H bending) and 1634 cm^{-1} (C=O stretching).

Crosslinking of the chitosan film with sodium sulfate decreased the C–N stretching peak at 1407 cm^{-1} and the peak at 1379 cm^{-1} (amide III) sharply became evident. The distance between chitosan chains became closer by interactions of sulfate and amine groups of the chains. C–O–C vibrations appeared at 1022, 1024, and 1026 cm^{-1}. SDBS adsorption onto chitosan film just changed the overlapped O–H and N–H stretching peaks and shifted to 3275 cm^{-1}. Similar to these results, the report by Parhizgar et al. showed small shifts of peaks after SDBS adsorption onto noncrosslinked chitosan [14].

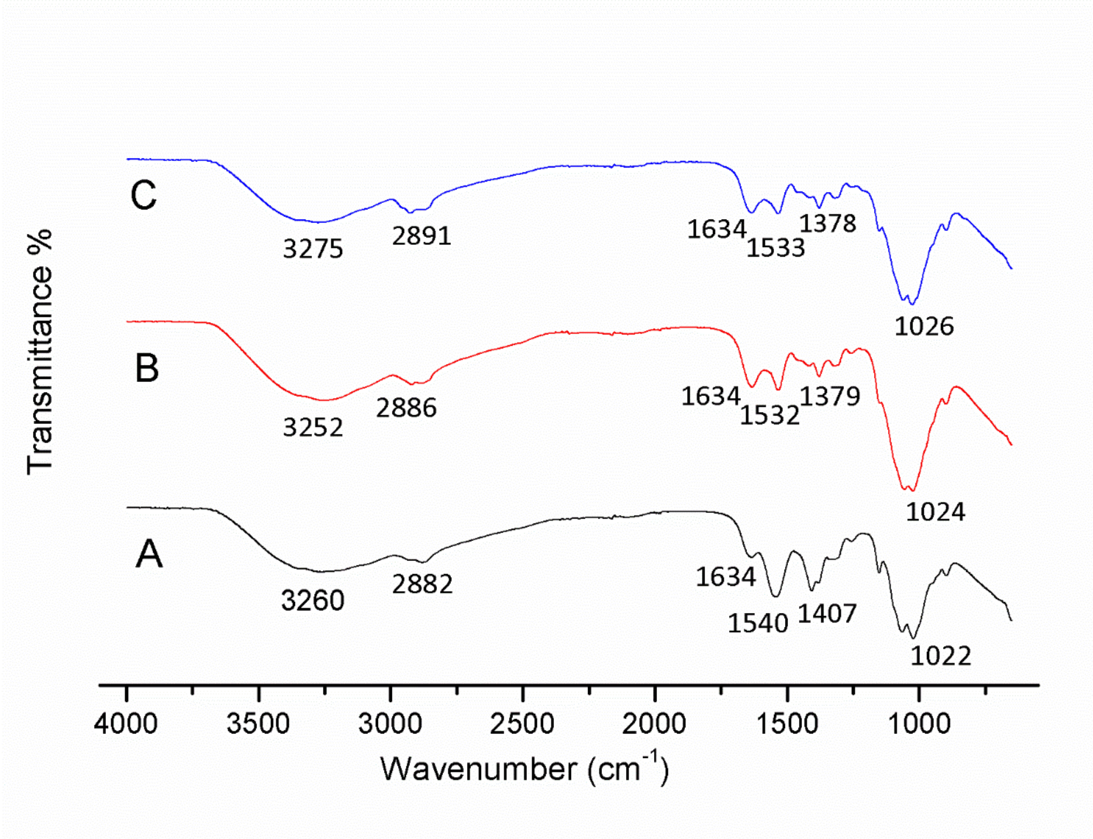

Figure 2.1 : FTIR spectra of non-crosslinked (A), sodium sulfate crosslinked (B) and SDBS adsorbed crosslinked chitosan films (C), respectively.

2.2.2 Optimum conditions for adsorption of SDBS

Figure 2.2 (A-D) shows the effect of time, pH, crosslinker amount, and adsorbent dose on the removal efficiency of SDBS by chitosan films. Removal percentages were calculated from equation 2.1. For the effect of contact time, 40 and 300 ppm of SDBS solutions were shaken at 25 °C and it was seen that equilibrium time was reached at 180 min. After that time, the removal percentage of SDBS did not change significantly (Figure 2.2 A). 40 ppm of SDBS solutions was prepared at pH values between 2 and 8. The maximum efficiency was obtained at pH 2 (Figure 2.2 B). The effect of the sodium sulfate amount as crosslinker was tested for 10% (w/v) and 20% (w/v) sodium sulfate solutions for the removal of 40 ppm SDBS solution. It did not seem to be a significant difference between the two concentrations; thereby the 10% (w/v) sodium sulfate solutions were used to crosslink chitosan films (Figure 2.2 C). As it can be seen from Figure 2.2 D, increasing the adsorbent amount after 20 mg did not show any further effect on adsorption. All optimization experiments were done at a fixed temperature of 25 °C. The optimum conditions were selected as 180 min of contact time, pH 2, and 20 mg adsorbent dose.

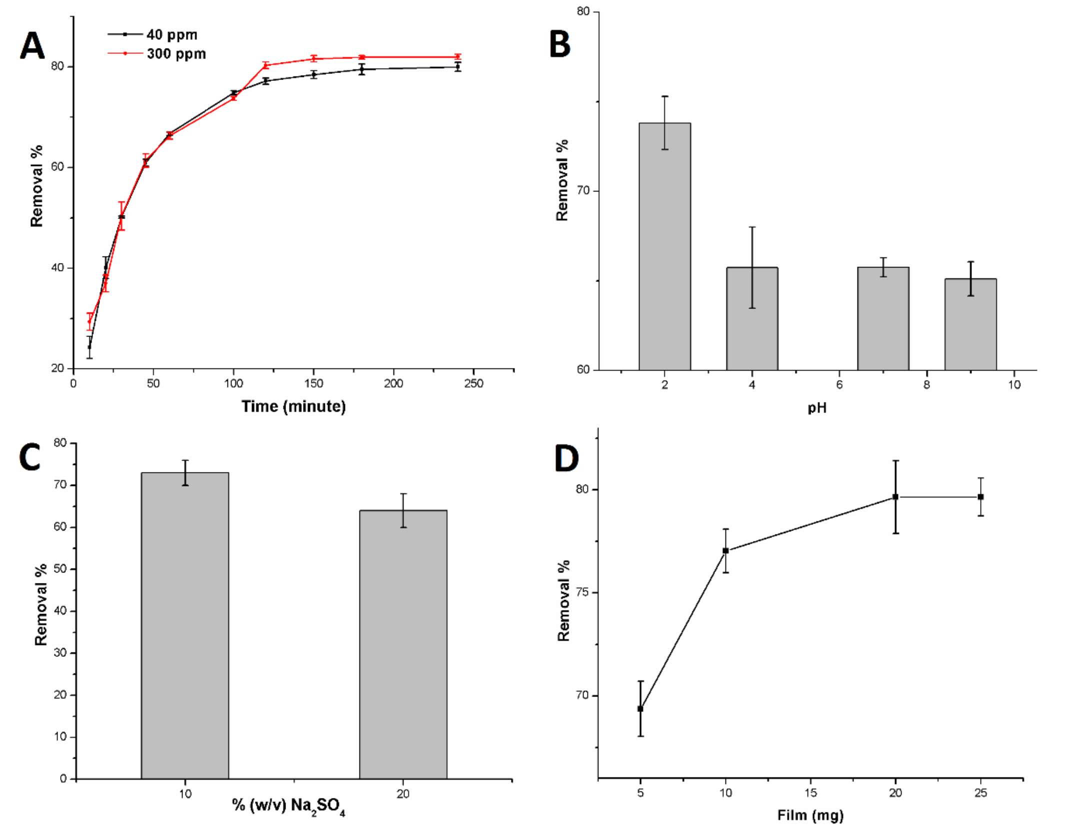

Figure 2.2 : The removal efficiency graphs of the effect of time (A), pH (B), crosslinker amount (C), and adsorbent dose (D) on SDBS adsorption, respectively.

2.2.3 Adsorption isotherm and kinetic models

Langmuir, Freundlich, and Temkin isotherm models were used to model SDBS adsorption. SDBS solutions with varying concentrations of 100 to 3000 ppm were shaken at the mentioned optimized conditions. Figure 2.3 A–C shows the fits of these three isotherm models. Figure 2.3 D shows the q_e–C_e graph. The most linear curve belongs to the Freundlich isotherm model with a high R^2 value. Depending on the value of the *1/n* parameter, a determination of the favorability of adsorption can be done [18]. Since the *1/n* parameter is 0.76, which indicates a linear Freundlich isotherm curve, it can be concluded that SDBS adsorption onto chitosan films is favorable. The R^2 of the Langmuir isotherm curve is above 0.961 and q_m was calculated as 714 mg/g. Table 2.1 shows the calculated isotherm constants and Table 2.2 shows the comparison of adsorption capacities of some other adsorbents in the literature [3–5, 14, 19–22].

Table 2.1 : Calculated isotherm constants of Langmuir, Freundlich and Temkin models.

Langmuir		Freundlich		Temkin	
q_m (mg/g)	714 ± 84	K_f (mg/g)	13.89 ±6.65	b (J/mol)	17.35 ± 1.33
K_L (L/mg)	0.013 ± 0.008	1/n	0.76 ± 0.04	A (L/mg)	0.16 ± 0.05
R^2	0.961	R^2	0.981	R^2	0.932

Table 2.2 : Adsorption capacities, experimental pH values and temperatures of some adsorbents in literature.

Adsorbent	q_m (mg/g)	pH	T (°C)
Silica magnetic nanoparticle [4]	61.73	2	25
$CuCl_2$ doped polyaniline [5]	32.3	2	23
$ZnCl_2$ doped polyaniline [5]	29.5	3	23
Non-crosslinked chitosan [14]	6.38	4	25
K_2CO_3 and KOH/active carbon [19]	152.51	3	25
Chromium leather waste [20]	386	4-8	20
PEI modified bentonite clay [21]	443.1	8.5	25
Na Alginate-g-P(AA-co-AM) [22]	471.99	7	25
Quaternary ammonium modified activated carbon [3]	77.82	2.22	25
Current study	714	2	25

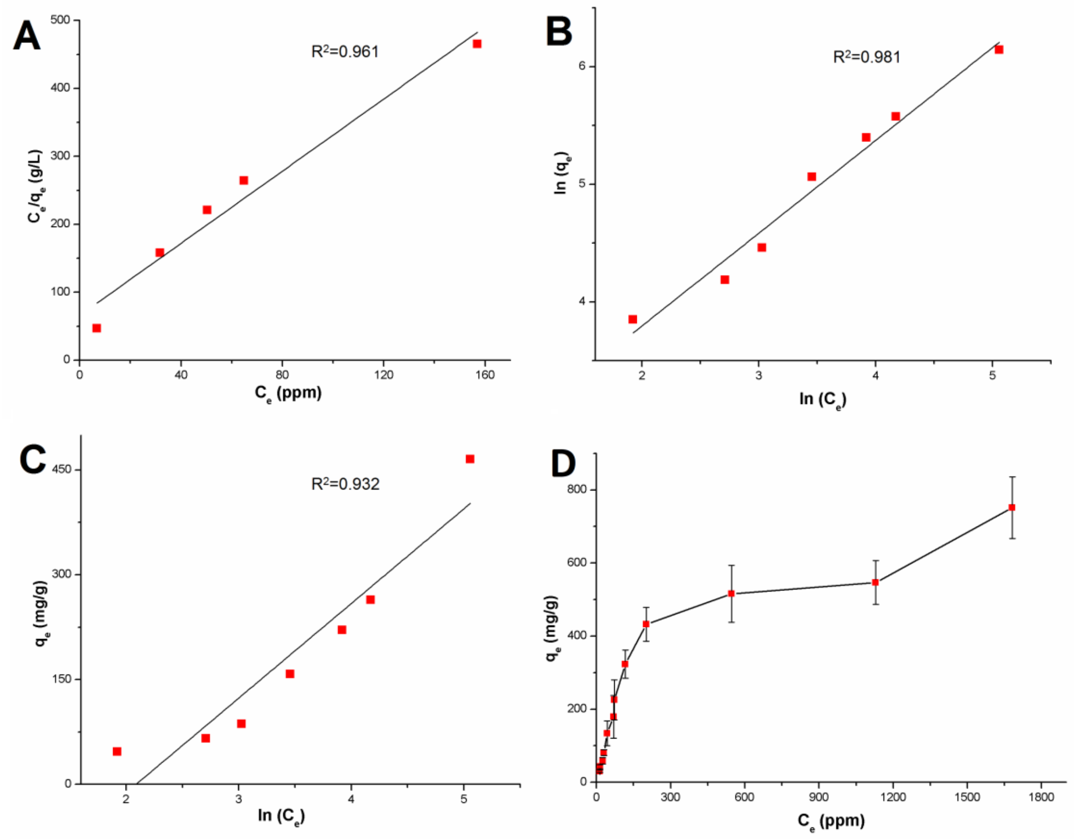

Figure 2.3 : Fits of Langmuir (A), Freundlich (B), Temkin (C) models, and q_e-C_e graph (D).

Pseudo-first-order and pseudo-second-order kinetic models were applied to the adsorption experimental data. Figure 2.4 shows the linear fits of pseudo-first-order (A) and pseudo-second-order (B) kinetic models. The pseudo-second-order kinetic model was found as the best model that fits the experimental data. Using the slopes and intercepts of the fits, the rate constants k_1 (min^{-1}) and k_2 (g/mg/min) were determined. Table 2.3 shows the calculated constants of the kinetic models. The theoretically calculated q_e from the pseudo-first-order model, showing the adsorbed amount of SDBS at the equilibrium time, has almost same value with the experimental $q_e^{(exp)}$. However, the R^2 of the model is not high enough.

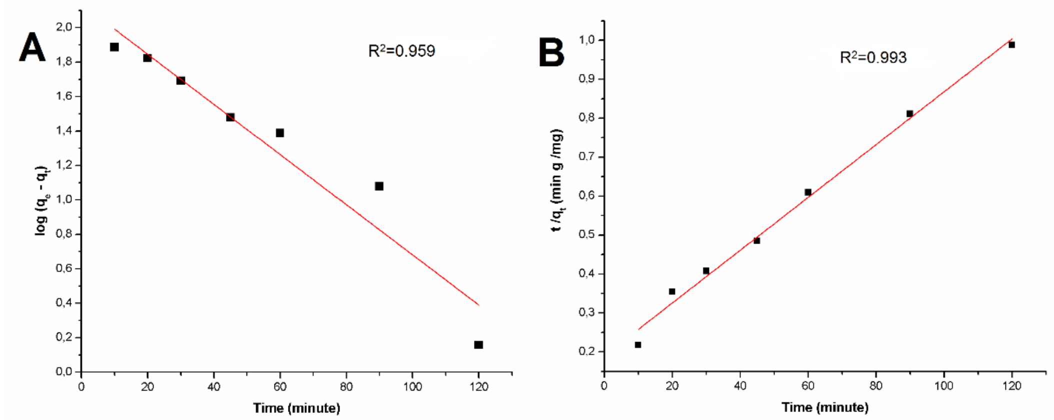

Figure 2.4 : Fits of pseudo-first-order (A) and pseudo-second-order (B) kinetic models.

Table 2.3 : Calculated kinetic model constants of pseudo-first-order and pseudo-second-order models.

Pseudo-first-order		Pseudo-second-order	
q_e (mg/g)	123.4 ± 11.9	q_e (mg/g)	147.1 ± 1.2
$q_e^{(exp)}$ (mg/g)	122.9 ± 0.5	$q_e^{(exp)}$ (mg/g)	122.9 ± 0.5
$k_1 \times 10^{-3}$ (min^{-1})	30.25 ± 2.93	$k_2 \times 10^{-3}$ (g mg^{-1} min^{-1})	0.25 ± 0.01
R^2	0.959	R^2	0.993

The results show that the mechanism of adsorption of SDBS onto crosslinked chitosan films is based on the electrostatic interactions. Maximum removal percentage is achieved at pH 2, and this suggests the conversion of local amine-sulfate complexes into positively charged centers at the chitosan chain, so that SDBS tends to bind these positively charged centers. Besides the electrostatic interaction between oppositely charged SDBS and chitosan, the hydrophobic interaction between the aliphatic part of the SDBS and the chitosan chain is possible; however, the interaction between oppositely charged groups is the driving force behind the highest removal percentage at pH 2.

2.3 Conclusions

This study indicates a potential usage of a biopolymer based adsorbent for the removal of surfactants from an aquatic environment. Chitosan films were ionically crosslinked by sodium sulfate solutions to increase durability of films in water. SDBS adsorption was found to be favorable and the kinetic behavior follows the pseudo-second-order kinetics. Optimization studies revealed that pH 2 is the optimum pH value. This behavior can be explained by chitosan being positively charged when it is in acidic conditions. In conclusion, crosslinked chitosan films are candidates for practical adsorbents for removal of anionic surfactants with a long alkyl chain.

3. REMOVAL OF FLUORIDE IONS FROM WATER BY CERIUM-CARBOXYMETHYL CELLULOSE BEADS DOPED WITH CeO_2 NANOPARTICLES[2]

Fluoride contamination has become a considerable health threat worldwide [23]. While the presence of low content of fluoride ions in drinking water is necessary for health, exceeding certain limits causes important health issues such as dental and skeletal fluorosis, cardiovascular problems, neurological disorders, and bladder cancer [23, 24]. Fluoride, an ion with high water solubility, easily mixes with drinking water with the dissolution of rocks, and fluoride limits in drinking water around the world exceed the limits that, will threaten human health [23]. The international guidelines, World Health Organization (WHO), is recommending a daily fluoride limit of 1.5 mg F^-/L [25]. Therefore, the removal of fluoride ions from drinking water is a current research topic. Besides several methods such as precipitation and flocculation, membrane technology, and ion exchange technology, the removal of fluoride ions from drinking water by adsorption stands out due to its ease of application and economy, and the research generally focuses on the development of new types of adsorbents [26-29]. Carbon-based materials such as activated carbon, graphene, carbon nanotubes, as well as the biopolymers, and inorganic nanoparticles are adsorbents that, have been tried to remove fluoride from water, either alone or as composite materials [29,30]. Alumina and aluminum-containing composite materials have been widely applied in fluoride removal because of their affinity for fluoride ions [31, 6, 7]. On the other hand, the fluoride ion has an affinity for rare earth elements. Cerium has been known the most abundant rare earth element in nature. Therefore, adsorbents containing cerium are good candidates for fluoride removal from water. Cerium-modified bone char [32], Zirconium–Cerium complexed polyvinyl alcohol

---

[2] This chapter was published as "Kahya, N., Erim, F.B. (2023). Removal of fluoride ions from water by cerium-carboxymethyl cellulose beads doped with CeO_2 nanoparticles. Int. J. Biol. Macromol. 242, 124595".

[33], cerium immobilized cross-linked chitosan composite [34], and Al–Ce hybrid adsorbent [35] have been tried as adsorbents for fluoride removal. On the other hand, recently CeO_2 nanoparticles (NPs) have received immense interest due to their wide application areas [36]. The unique feature of these particles is related to redox transitions between Ce^{3+} and Ce^{4+} ions. CeO_2 nanoparticles have been widely used in wound dressing materials and other biotechnology fields due to their antioxidant and antimicrobial properties [37-39]. CeO_2 nanoparticles have been considered to be non-toxic [40]. Recently, CeO_2 nanoparticles synthesized with the green synthesis method have been expanding their application areas with their different properties [41, 42]. Morphology-dependent adsorption performance of CeO_2 for fluoride removal has been reported by Kang et al. [43]. However, an important obstacle to the use of nanoparticles as adsorbent is the difficulties in their recovery from the water after removal. The use of nanoparticles by entrapping them in a polymeric medium is a solution to this problem [44]. In recent years, studies on the use of biopolymers obtained from natural sources instead of synthetic polymers have increased in terms of environmental sensitivity [45]. The non-toxicity of biopolymers, their biodegradability and the fact that, they form composite materials with different additives increase their application areas. Applications, where CeO_2-NPs are compatible with biopolymers, have been demonstrated [38, 39]. Carboxymethyl cellulose (CMC) is one of the biopolymers that, draws attention with its usage areas both as an adsorbent and as a food coating and wound dressing material [46]. CMC is a water-soluble biopolymer that, usually forms water-insoluble hydrogels with trivalent metal ions. Therefore, cerium (III) ions are ideal ionic crosslinking agents for CMC. This study aims to demonstrate the use of composite material, which is formed by trapping CeO_2 nanoparticles in CMC spheres cross-linked with Ce^{3+} ions, as an effective adsorbent in fluoride removal from water. In the literature, there is one study created by adding CeO_2-NPs into CMC to prevent the corrosion of steel [47]. As far as we know, the removal of fluoride ions from both Ce ions and CeO_2-doped CMC composite material has not been reported yet.

3.1 Experimental

3.1.1 Materials and methods

Sodium carboxymethyl cellulose (4% solution's viscosity in water is 50-200 cps at 25 ^{o}C, product number from the producer: C5678), cerium(III) nitrate hexahydrate, and cerium (IV) oxide nanopowder (<25 nm size particles) were purchased from Sigma-Aldrich (St. Louis, MO, USA). Acetic acid (glacial), sodium bicarbonate, sodium chloride, sodium citrate tribasic dihydrate, sodium fluoride anhydrous, sodium carbonate, sodium hydroxide, sodium nitrate, sodium sulfate, and sodium phosphate dodecahydrate were from Merck (Darmstadt, Germany). All solutions were prepared with distilled water from Elga Purelab Option-Q 15 system (London, UK). pH adjustments were done by using an Orion Dual Star pH-ISE meter (Thermo Fisher Scientific Beverly, MA, USA) with a combined glass pH electrode. The zeta potential of the CeO_2-NPs was measured using a zeta potential analyzer (Malvern Panalytical, Malvern, United Kingdom). The surface charge of CMC-Ce and CeO_2-CMC-Ce beads was determined by the pH drift method. Beads were shaken for 24 hours in 0.1 M $NaNO_3$ solution, and pH values were adjusted with HCl and NaOH. The pH value in the point zero charges was determined by plotting the difference between the initial and final pH of the solution against the initial pH values. Scanning electron microscopy (SEM) images and energy dispersive X-ray spectroscopy (EDX) spectra of beads were taken by Tescan Vega3 SEM/EDX scanning electron microscope (TESCAN, Brno, Czech Republic) by coating samples with gold/palladium before the analysis. A structural analysis was performed by Fourier transform infrared spectroscopy (FTIR) with Shimadzu IRAffinity-1S model infrared spectrophotometer (Kyoto, Japan) in the wavenumber range of 4000–400 cm^{-1}. The statistical analysis was conducted by two-way ANOVA in Microsoft Excel.

3.1.2 Preparation of adsorbents

CMC was weighed and dissolved at room temperature for 6 h by stirring to give a uniform 5% (*w/v*) solution. To prepare cerium ions cross-linked CMC beads (CMC-Ce), a volume of 20 mL of 5% (*w/v*) CMC solution was dropped by using a syringe of a 21-gauge needle into 50 mL 0.2 M $Ce(NO_3)_3$ aqueous solution. The formation step of the wet beads was followed by curing the gel beads in $Ce(NO_3)_3$ solution by stirring gently the mixture with a magnetic stirrer. The dropping and curing of the beads were completed in 15 minutes. Then, the CMC-Ce beads were filtered from a stainless-steel filter and waited in 100 mL water for 1 minute to remove excess salt ions from the surface of the beads. The freshly prepared wet beads were placed on a plastic Petri dish and left to drive in an oven at 40 ^{o}C (Nüve EV 018, Ankara, Turkey). The beads doped by CeO_2-NPs were prepared similarly to the CMC-Ce beads. After the dispersion of CeO_2-NPs in 20 mL of distilled water for 24 h by continuously stirring with a magnetic stirrer at 1000 rpm, weighed amount of CMC was added to the dispersion. The mixture of 5% (*w/v*) CMC and 1% (*w/v*) CeO_2 was continued to stirring for homogenization for 8 h. Then, this polymer mixture was treated similarly to the preparation steps of CeO_2-CMC-Ce beads. The beads of CMC-Ce and CeO_2-CMC-Ce were used in adsorption experiments of fluoride ions in their dry states. The characterization of the prepared adsorbents was carried out by FTIR, SEM-EDX, and swelling experiments.

3.1.3 Adsorption experiments

A stock solution of 1000 mg/L sodium fluoride was prepared by dissolving NaF in distilled water in a polyethylene volumetric flask. Batch adsorption studies were performed systematically to determine the optimum conditions by conducting experiments on the effect of pH, contact time, adsorbent dose, shaking rate, initial concentration of adsorbate, and effect of coexisting anions in F^- solution. For optimization, initial experiments were performed with 40 mL of 20 mg/L fluoride ion solution. All experiments were done at 65±5% humidity and ambient temperature of the laboratory, which is stabilized by the air conditioners at 25±1 ^{o}C.

To determine the concentration of fluoride, Orion DUAL STAR pH/ISE benchtop meter combined with Orion Fluoride Electrode (Thermo Fisher Scientific Inc, Beverly, MA, USA) was used. The limit of detection of ion-selective electrode is 10^{-5} M fluoride. Total ionic strength adjustment buffer (TISAB I) was prepared by dissolving 58 g of sodium chloride, 0.3 g tri-sodium citrate, and 57 mL glacial acetic acid in 500 mL distilled water. Then, the pH of the mixture was adjusted to 5.0 by the addition of 5 M sodium hydroxide solution, and finally, the volume was made up to 1 L with distilled water. Equal volumes of 5 mL of sample solution and 5 mL of TISAB I were mixed in a 25 mL plastic beaker, while the mixture was stirred continuously using a magnetic stirrer during the voltage measurements, and duplicate measurements were made. A series standard solution of fluoride was prepared for the calibration curve, and the same procedure was applied for the voltage measurements of the solutions. The measured potential in mV is plotted against the logaritmic concentration of F^- in mg/L, and a linear calibration curve equation was used to calculate the F^- concentration in solutions (y = -32.930x – 82.979, R^2 = 0.9922).

The percentage removal efficiency (*R%*) for F^- ions was calculated using equation 3.1:

$$R\% = \frac{(C_i - C_e)}{C_i} \text{ x } 100 \tag{3.1}$$

where C_i and C_e are the initial and equilibrium F^- ions concentrations in the solutions in mg/L, respectively.

The adsorption isotherms for F^- removal were studied by using the initial F^- ion concentration of 20–500 mg/L. By the addition of 0.04 g adsorbent to 40 mL solutions of each concentration, the solutions were mixed for 120 minutes with a stirring speed of 200 rpm (IKA HS 260 Basic Shaker, IKA-Werke GmbH & Co. KG, Staufen, Germany). The temperature was kept constant at 25±1 °C and the pH at 6.2. Kinetic studies were carried out under the same experimental conditions with the initial concentrations of 20 mg/L F^-. While the samples were stirred continuously, at regular intervals of time, a known volume of adsorbate solution was taken by a micropipette and analyzed for residual F^-. The same volume removed from the media was added immediately to be able to keep the volume of the adsorbate solution in the container constant during the adsorption process.

The adsorption capacity of the adsorbent at equilibrium (q_e) and any time t (q_t) was obtained by using equation 3.2 and equation 3.3, respectively.

$$q_e \left(\frac{mg}{g}\right) = \frac{(C_i - C_e)}{m} xV \tag{3.2}$$

$$q_t \left(\frac{mg}{g}\right) = \frac{(C_i - C_t)}{m} xV \tag{3.3}$$

where q_e and q_t are the amount of F^- ions adsorbed per unit mass of the adsorbent at equilibrium and time t in mg/g, respectively. C_t is the concentration of the F^- ions at time t in mg/L. V is the volume of the adsorbate solution (L) and m is the mass of the adsorbent (g).

All experiments were repeated two times (*N=2*), and the calculated results were represented by mean and standard deviation.

3.1.4 Reusability of adsorbent

To investigate the reusability of adsorbent, 0.04 g of either CMC-Ce or CeO_2-CMC-Ce beads were shaken in 40 mL of 20 mg/L initial concentration F^- solution at 200 rpm for 2 h. The wet beads were treated with distilled water as a desorbing agent, and the treated beads were dried at room temperature for 24 h. Then, the same group of beads was reused in F^- removal in the described experimental conditions of adsorption.

3.1.5 Swelling studies

The swelling ability of adsorbent beads was tested in distilled water by measuring the changing mass (g) of beads over time. For this purpose, 0.04 g of dry beads in 40 mL of distilled water at 25 ^oC were agitated at 200 rpm for certain times (5 to 240 min). At mass measurement times, the soaked wet beads were taken out, and excess water on them was removed on filter paper. The swelling ratio of the beads was calculated from the following equation 3.4:

$$Swelling\ Ratio\ (\frac{g}{g}) = \frac{(M_t - M_i)}{M_i} \tag{3.4}$$

where M_i and M_t are the initial dry mass (g) and swelled mass of the beads by time (g), respectively.

3.2 Results and Discussion

3.2.1 Characterization of the beads

The digital photographs of wet CMC-Ce and CeO_2-CMC-Ce beads were given in Figure 3.1 A and Figure 3.2 B, respectively. It is seen from Figure 3.1 A that, the wet CMC-Ce beads have an opaque and white color with spherical shapes. CeO_2-NPs incorporation altered the color of the CMC beads from white to yellowish due to the light-yellow color of NPs (Figure 3.1 B). After drying at 40 ^oC for 24 h, even though both types of beads shrank with the loss of water, their shapes remained mostly spherical (Figure 3.1 C and Figure 3.1 D).

Zeta potential measurements of CeO_2-NPs were performed to determine their surface charge as a function of pH at room temperature as shown in Figure 3.2 A. The isoelectric point of CeO_2-NPs was determined to be 8.5. At pHs above the isoelectric point, the metal oxide surface gains a negative charge as a result of the dissociation of adsorbed -OH groups ($M–O^{-}$), while below the isoelectric point, NPs have a positive charge as a result of the protonation of the -OH groups ($M–OH^{2+}$) [22].

The plots of ΔpH vs. $pH_{initial}$ for determination of the point of zero charges (pH_{pzc}) of CMC-Ce and CeO_2-CMC-Ce beads were given in Figure 3.2 B. The pH_{pzc} values of beads were found as 6.45 and 6.71 from the plots. Below these pH values, the surface charge of the spheres is positive.

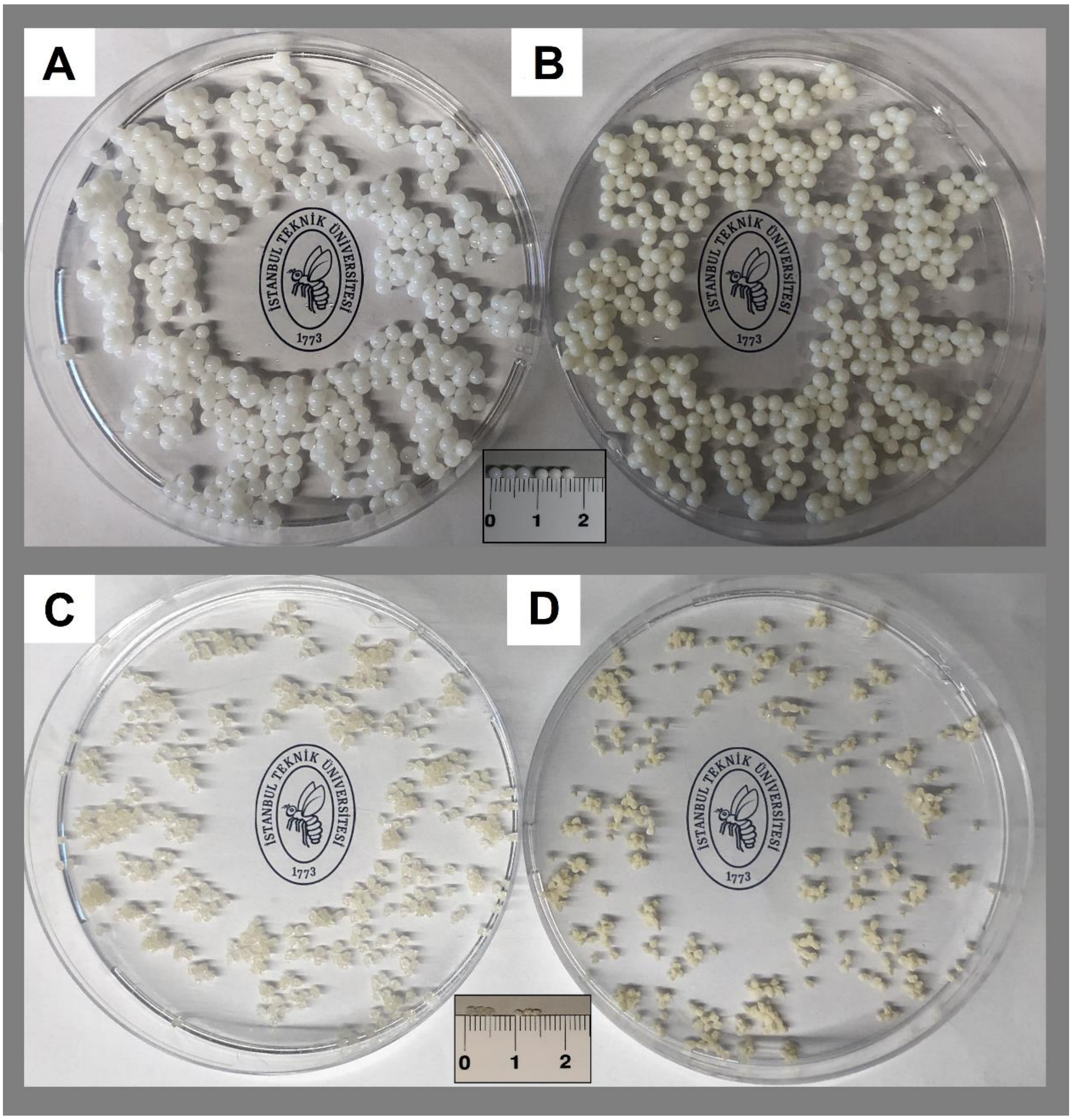

Figure 3.1 : Digital photographs of CMC-Ce (*left sides*) and CeO_2-CMC-Ce (*right sides*) in freshly prepared (A, B) and after drying states (C, D), respectively.

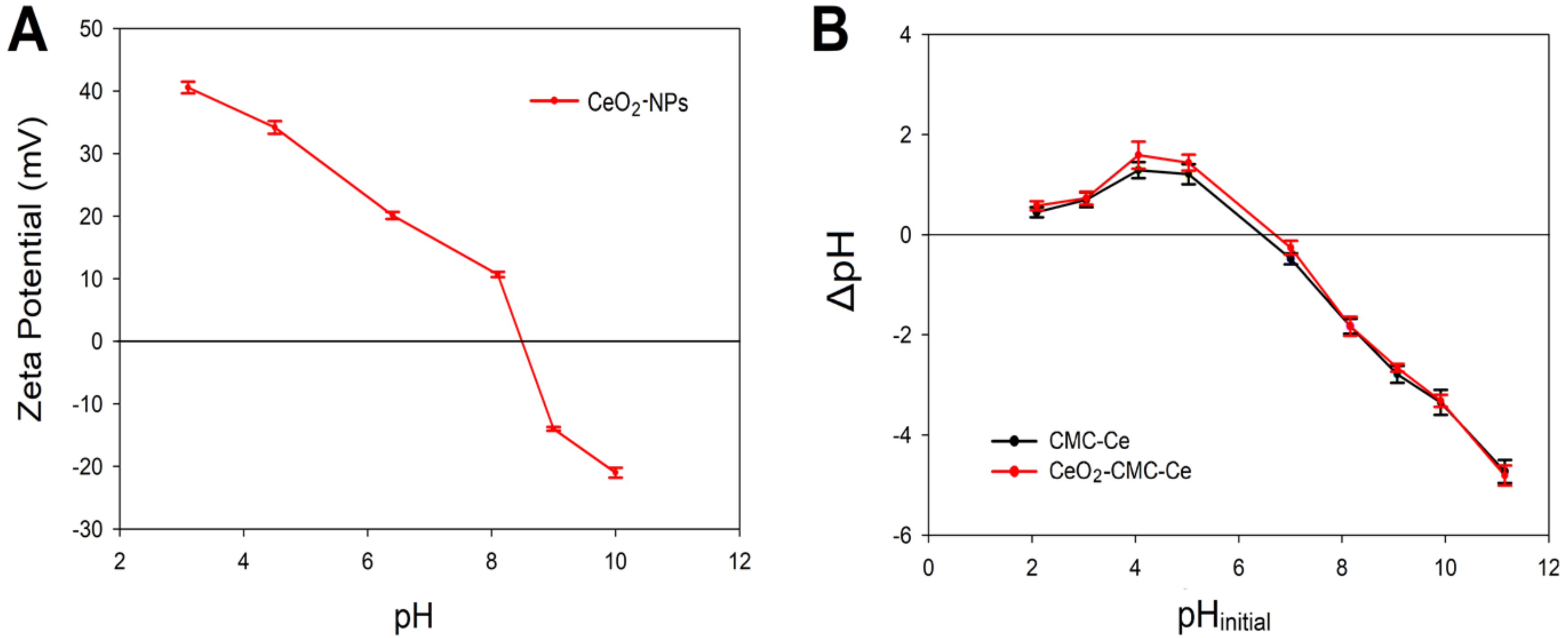

Figure 3.2 : (A) Zeta potential of CeO_2-NPs *vs*. pH. (B) Plot of ΔpH *vs*. $pH_{initial}$ for the determination of pH_{pzc} of CMC-Ce and CeO_2-CMC-Ce beads.

The surface morphologies of the prepared CMC-Ce and CeO_2-CMC-Ce adsorbents were analyzed using SEM. Figure 3.3 A and Figure 3.3 B show the SEM images of single CMC-Ce and CeO_2-CMC-Ce dry beads, respectively at low magnification. The sizes of these beads determined by ImageJ are 1489 x 1755 μm and 1315 x 1884 μm for CMC-Ce and CeO_2-CMC-Ce beads, respectively. The high-magnified SEM images of CMC-Ce and CeO_2-CMC-Ce beads are represented in Figure 3.3 C and Figure 3.3 D, respectively. The surface of the CMC-Ce bead has folds and slits together with smooth morphology (Figure 3.3 C). This similar flatted-folds image was reported before for titanium/CMC [48] and barium-alginate/CMC [49] composites. After the incorporation of CeO_2, the SEM surface image becomes heterogeneous (Figure 3.3 D). In a recent study, CeO_2-nanoparticle loaded CMC composite films prepared for corrosion resistance of mild steel has similar surface alteration after the incorporation of CeO_2 into CMC [47].

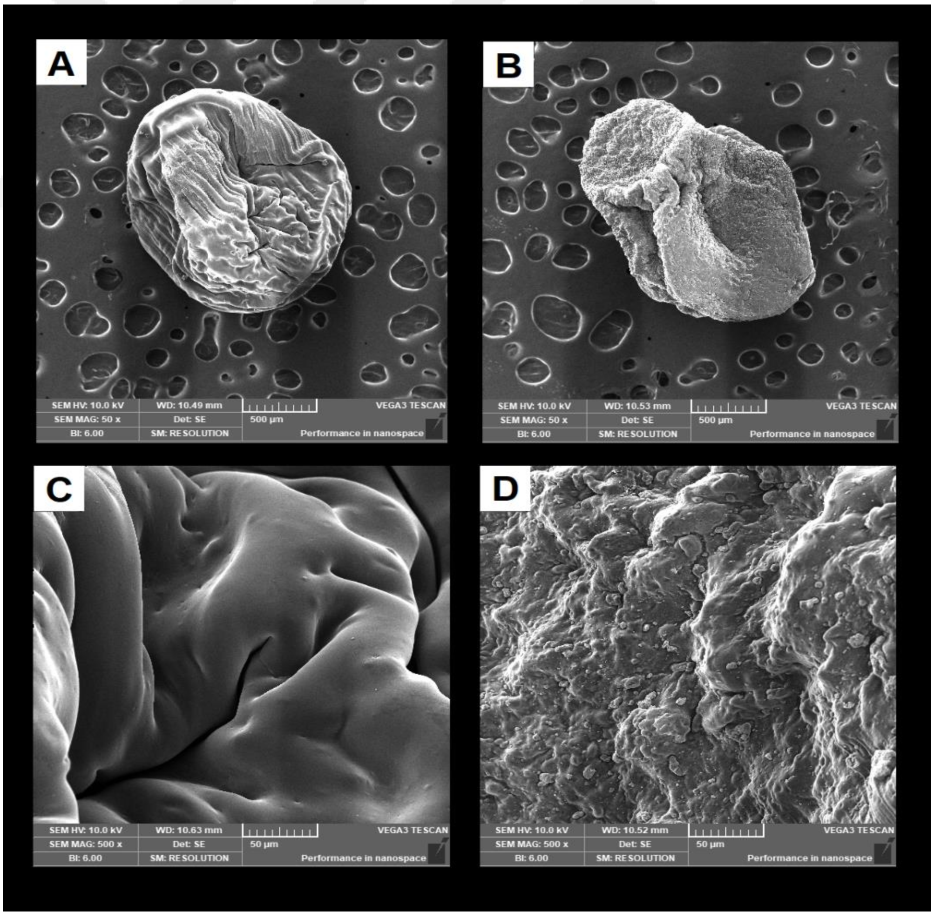

Figure 3.3 : SEM images of CMC-Ce (A, C) and CeO_2-CMC-Ce (B, D) beads from different magnifications.

SEM images and corresponding EDX mapping of CMC-Ce and CeO_2-CMC-Ce beads after F^- ions adsorption were shown in Figure 3.4 (A-D). The fluoride and cerium element peaks are distinctive in the spectra for CMC-Ce and CeO_2-CMC-Ce adsorbents. The mass and atomic % distribution of C, O, Ce, and F are shown on the EDX images. As seen in Figure 3.4 B and Figure 3.4 D, the mass and atomic percentages of fluoride adsorbed by CeO_2-CMC-Ce beads are higher than the fluoride adsorbed of CMC-Ce beads. That is, the incorporation of CeO_2-NPs in the biopolymer adsorbent cross-linked with Ce ions increases the removal effect of the adsorbent. By comparing the SEM morphology of the CMC-Ce and CeO_2-CMC-Ce beads before and after adsorption (Figure 3.3 and Figure 3.4, respectively), there was no significant change in the visual appearance of the adsorbents after the adsorption process.

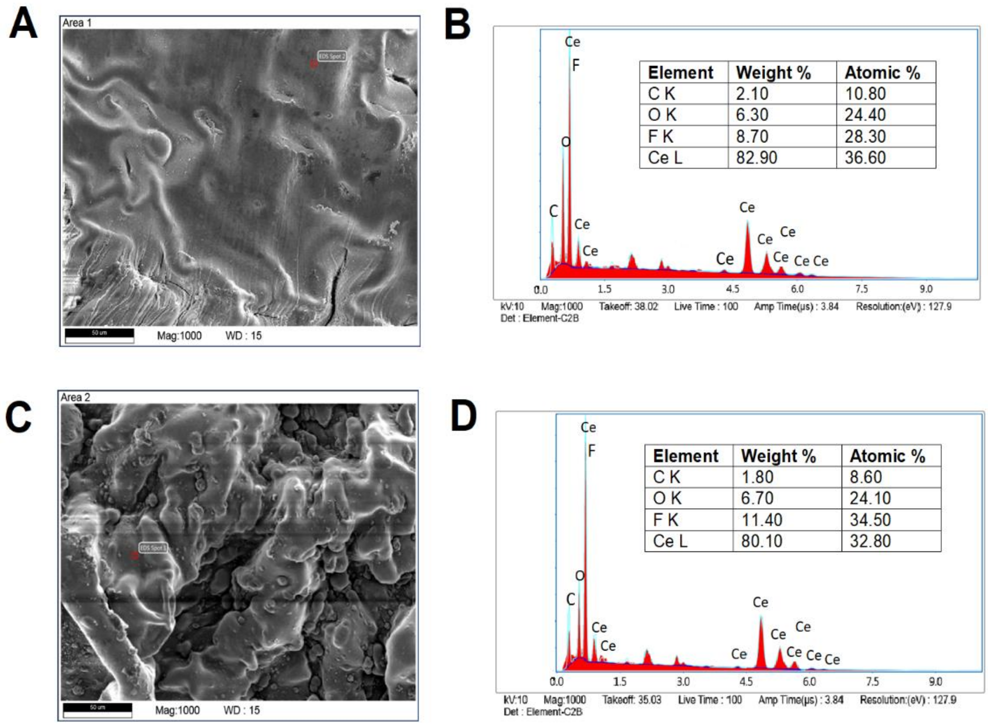

Figure 3.4 : SEM micrographs (A, C) and corresponding EDX spectra (B, D) for CMC-Ce (A, B) and CeO_2-CMC-Ce (C, D) beads after fluoride adsorption. 0.04 g of beads, 20 mg/L F^- (pH of 6.2, 40 mL), 200 rpm of shaking rate, 2 h equilibrium time, and 25 ^oC temperature.

FTIR spectra of CMC-Ce and CeO_2-CMC-Ce adsorbents were analyzed before and after F^- adsorption, and shown in Figure 3.5. The dry state of the beads was used in FTIR analysis. The broad peak at around 3290 and 3388 cm^{-1} for all types of beads is assigned to the O-H stretching of the carboxylic acid group of CMC. The peak at ~2920 cm^{-1} was evident in the spectra of all beads before and after F^- adsorption, and it illustrates the stretching vibrations of $–CH_2$ (aliphatic) bonds of CMC polysaccharide. Strong absorption bands seen at ~1580 cm^{-1} and ~1410 cm^{-1} refer to the asymmetric and symmetric stretching vibrations of carboxyl groups (COO^-) of CMC. The characteristic peak at around ~1325 cm^{-1} is the bending vibrations of surface hydroxyl groups (Ce-OH) of adsorbent [44]. The intensity of this peak decreased in the fluoride-adsorbed bead’s spectra. The decrease in peak intensity because of fluoride adsorption of CeO_2-CMC-Ce adsorbent is significant. This is due to the displacement of the surface -OH groups of the adsorbent with fluoride. Dong et al. observed a similar decrease in peak intensity around 1338 cm^{-1} in spectra of F^- adsorbed nanosized cerium oxides-impregnated porous polystyrene anion exchanger adsorbent [44]. The peaks at 817 cm^{-1} and 815 cm^{-1} belong to CMC-Ce and CeO_2-CMC-Ce beads’ spectra, respectively, have disappeared in both adsorbents after the fluoride adsorption. This may be due to the F^- ion and Ce metal ion interaction in the adsorption process.

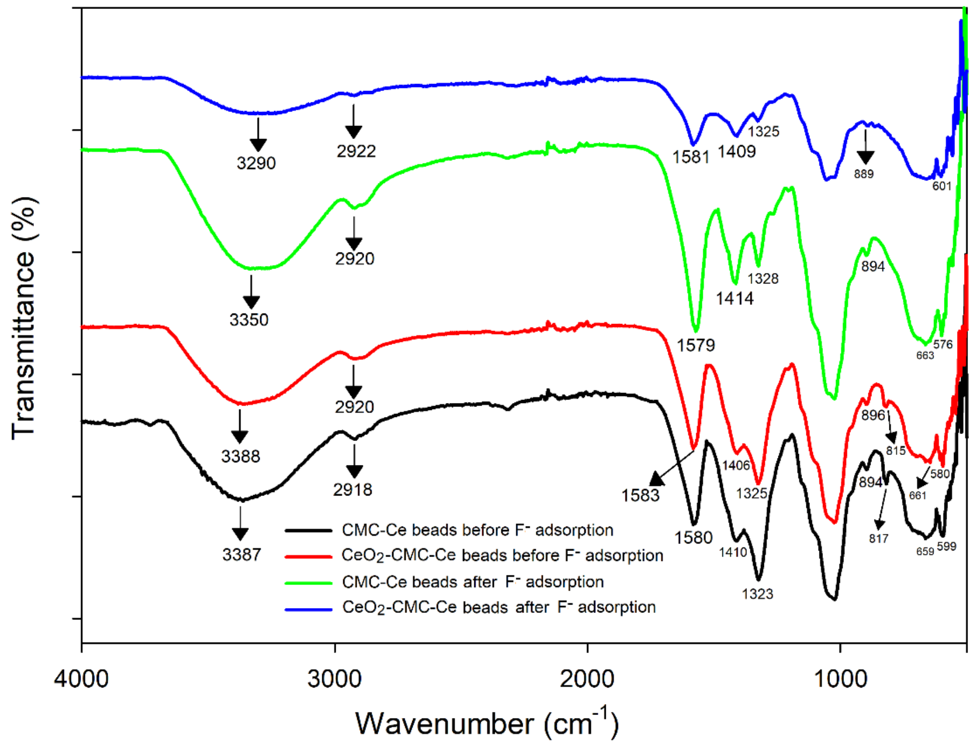

Figure 3.5 : FTIR spectra of CMC-Ce and CeO_2-CMC-Ce beads before and after F^- adsorption. 0.04 g of beads, 20 mg/L F^- (pH of 6.2, 40 mL), 200 rpm of shaking rate, 2 h equilibrium time, and 25 °C temperature.

Figure 3.6 shows the swelling degree curves of CMC-Ce and CeO_2-CMC-Ce beads. It is seen from Figure 3.6, both types of beads have reached the swelling equilibrium at approximately 60 min of the swelling test. After the time reached, the water absorption by the beads had not altered significantly. The swelling experiment of the beads in distilled water was followed up to 240 min, and it is observed that CeO_2 incorporation decreased the beads' swelling in distilled water. The addition of CeO_2 has been shown to reduce the degree of swelling in different biopolymer composites [38,39,50,51]. CeO_2 existence in hydrogel avoided the water absorption of CMC beads mostly expelling the H_2O molecules from the bead's structure creating a more hydrophobic nature.

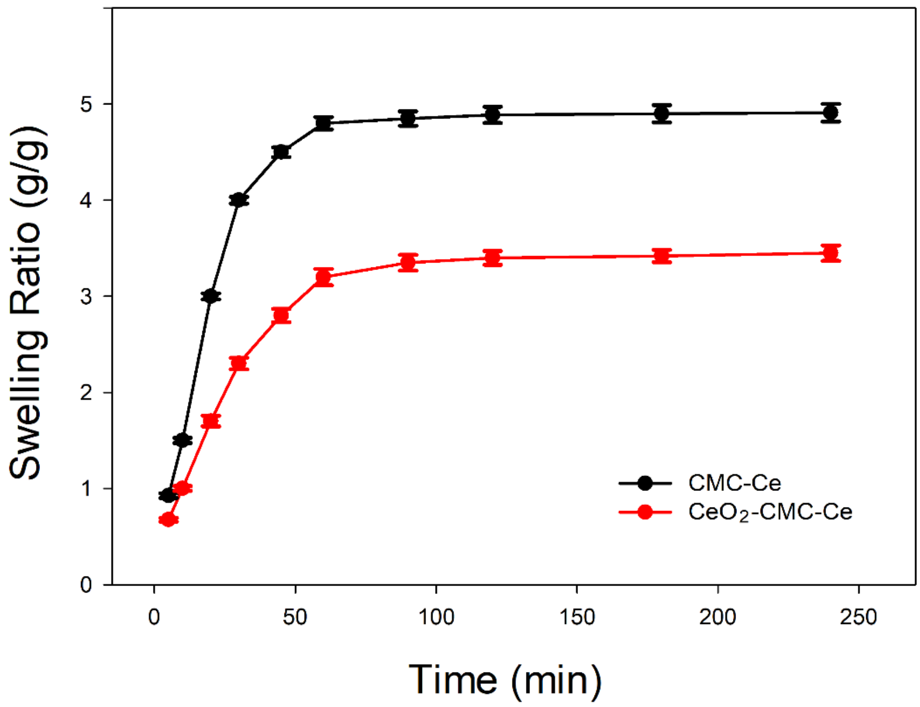

Figure 3.6 : Swelling degree *vs*. time curves of CMC-Ce and CeO_2-CMC-Ce beads in distilled water.

3.2.2 Fluoride adsorption studies

3.2.2.1 Effect of pH

The effect of pH is one of the most effective factors in adsorption processes. The effect of the pH of the adsorbate solution on the F^- removal was investigated by adjusting the pH of the solution to 2, 4, 8, and 10 as final pH values with HCl or NaOH solutions. The natural pH of the fluoride solution was measured as 6.2. This solution was used in the experiment without changing its pH. The concentration of 20 mg/L of F^- solutions having varying pH values was shaken with 0.04 g of adsorbent beads at 25 ^oC temperature for 2 h. Figure 3.7 A shows the fluoride removal performance of adsorbent beads as a function of pH. The removal of F^- ions increased by the increasing pH of solutions from 2 to 6 and then, followed by a decrease with increased pH values from 6 to 10. Since the maximum fluoride removal was around pH 6, the fluoride solution with a natural pH of 6.2 was used without pH adjustment in subsequent experiments.

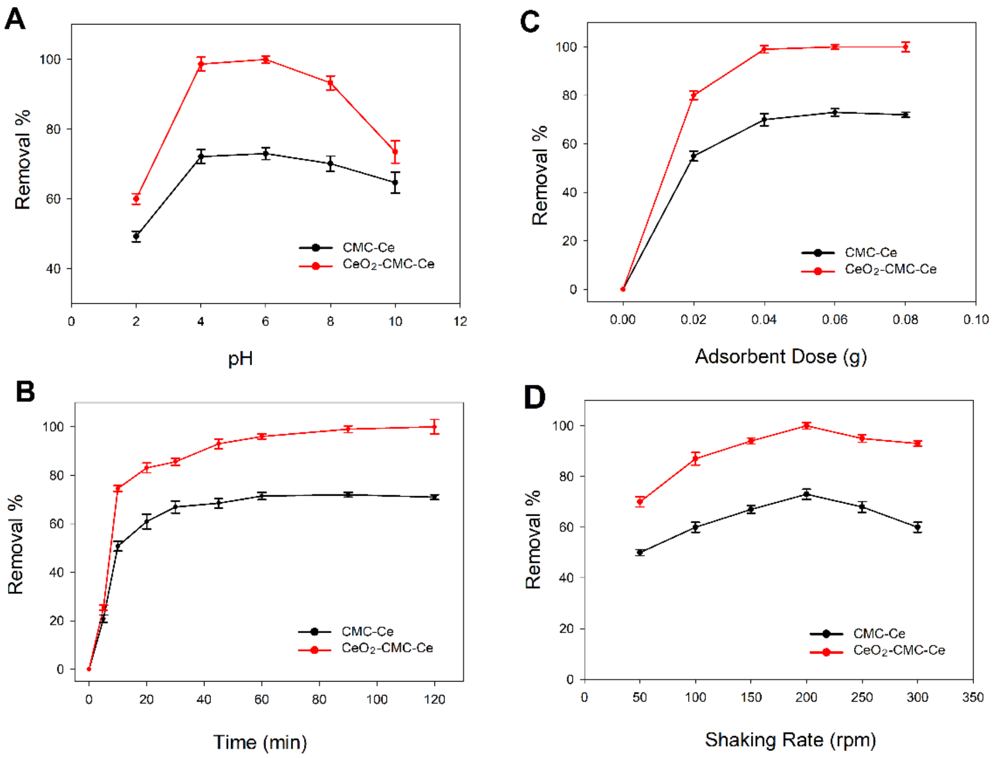

Figure 3.7 : (A): The effect of pH of F^- solution. 0.04 g of beads, 20 mg/L F^- (pH of 2, 4, 6, 8, and 10, 40 mL), 200 rpm of shaking rate, 2 h adsorption time, and 25 ^oC temperature. (B): The effect of time. 0.04 g of beads, 20 mg/L F^- (pH of 6.2, 40 mL), 200 rpm of shaking rate, 2 h adsorption time, and 25 ^oC temperature. (C): The effect of the amount of the adsorbent. Varying amount of beads (0.02 g, 0.04 g, 0.06 g, and 0.08 g), 20 mg/L F^- (pH of 6.2, 40 mL), 200 rpm of shaking rate, 2 h adsorption time, and 25 ^oC temperature. (D): The effect of the shaking rate. 0.04 g of beads, 20 mg/L F^- (pH of 6.2, 40 mL), the varied shaking rate of 50, 100, 150, 200, 250, and 300 rpm, 2 h adsorption time, and 25 ^oC temperature.

3.2.2.2 Effect of time

The effect of contact time on the fluoride adsorption onto the adsorbents, F^- solutions of 40 mL volume of 20 mg/L were agitated at 200 rpm for 2 h at 25 ^oC in 0.04 g adsorbent bead existence. The effect of the contact time on F^- removal by CMC-Ce and CeO_2-CMC-Ce beads was represented in Figure 3.7 B. As can be seen from the figure, about 70% and 100% removal efficiency was reached within 120 min at an adsorbent dose of 0.04 g for an initial fluoride concentration of 20 mg/L by CMC-Ce and CeO_2-CMC-Ce beads, respectively. In addition, the adsorption process was continued for 120 min, and it was understood that no more than that time would be required for complete equilibrium. In the adsorption experiments for the optimization to be continued, the equilibrium time has been kept at two h.

3.2.2.3 Effect of adsorbent dose

The effect of the amount of adsorbent dose on the adsorption of F^- ions was shown in Figure 3.7 C. The removal percentage of F^- increased from 80% to 99% by the increment of the amount CeO_2-CMC-Ce beads from 0.02 g to 0.04 g in the volume of 40 mL of 20 mg/L fluoride solution at pH of 6.2 shaken at 200 rpm for 2 h. After the amount of 0.04 g of bead in the studied conditions of adsorption, there is an equilibrium state which indicates the saturation occurred. The same trend was observed for CMC-Ce beads as seen in Figure 3.7 C.

3.2.2.4 Effect of shaking rate

The shaking rate with varied rates of 50, 100, 150, 200, 250, and 300 rpm at 25 ºC was investigated. The other conditions were 0.04 g bead, 20 mg/L of 40 mL of F^- solution of pH 6.2, and 2 h. The results showed reaching the maximum removal at 200 rpm, and the adsorption started to decline gradually with further the increase in agitation speed (Figure 3.7 D).

3.2.2.5 Statistical analysis

The two-way ANOVA test was applied to examine the influence of two different independent variables (The types of the bead and each effective factor on adsorption *i.e*. pH, time, adsorbent dosage, and shaking time) on the dependent variable (F^- removal percentage). ANOVA results showed that there is a significant interaction effect between the two independent variables and the dependent variable ($p < 0.05$). As a result, two adsorbents showed a significant difference in fluoride adsorption.

3.2.3 Adsorption isotherms

To evaluate the efficiency of the adsorption, experimental equilibrium data were fitted to the two well-known isotherm models *i.e*., Langmuir and Freundlich adsorption models. The isotherm model graphs were plotted using the experimental data in Figure 3.8 A and Figure 3.8 B, respectively.

The Langmuir isotherm model equation can be expressed as:

$$\frac{Ce}{qe} = \frac{1}{q_{max}K_L} + \frac{1}{q_{max}} \tag{3.5}$$

where q_e (mg/g) is the amount of fluoride adsorbed at the time of the equilibrium (mg/g), C_e (mg/L) is the equilibrium concentration of F^-, q_{max} (mg/g) is the maximum adsorption capacity of adsorbent, and K_L (L/mg) is the Langmuir constant, which is related to the affinity of the binding sites of adsorbent with the adsorbate. q_{max} and K_L values were calculated from the slope and intercept of the linear equation of the isotherm and were summarized in Table 3.1. From Table 3.1, it is seen that, the high R^2 (0.99) values refer that the experimental data being well-fitted with the isotherm model. The calculated Langmuir constant of K_L (L/mg) values are 0.037 and 0.076, for CMC-Ce and CeO_2-CMC-Ce, respectively. q_{max} (mg/g) were found 105 and 312 mg/g for CMC-Ce and CeO_2-CMC-Ce adsorbent beads, respectively. The CeO_2 addition to the bead formulation increased the adsorption capacity of the CMC-Ce bead about three times.

Langmuir constant of R_L, which is known as a dimensionless factor is given in equation (3.6) below as:

$$R_L = \frac{1}{1+K_L C_o} \tag{3.6}$$

Various values of the R_L parameter investigate the efficacy of adsorption: if $R_L > 1$, the adsorption process is unfavorable, $R_L = 1$, the adsorption is linear, $0 < R_L < 1$, the adsorption is favorable, and $R_L = 0$, the adsorption is irreversible. C_o is the maximum initial concentration of F^- solution, which is 500 mg/L F^-, and R_L parameters are found 0.35 and 0.21 for CMC-Ce and CeO_2-CMC-Ce, respectively showing the adsorption is a favorable process.

The linearized equation of Freundlich isotherm is given in equation (3.7):

$$\ln q_e = \ln K_F + \frac{1}{n} \ln C_e \tag{3.7}$$

where q_e (mg/g) is the adsorbed amount of F^- at equilibrium and C_e (mg/L) is the concentration of F^- at equilibrium time. *1/n* and K_F (mg/g)(L/mg)$^{1/n}$ are Freundlich isotherm parameters and are calculated from the slope and intercept of the straight line for the plot of ln q_e *vs*. ln C_e, respectively. The calculated Freundlich constants are represented in Table 3.1. The regression coefficient of the Freundlich isotherm of CeO_2-CMC-Ce is lower than those of the Langmuir isotherm model. This suggests that, the F^- adsorption on the beads is confirming monolayer adsorption on the homogeneous surface of the adsorbent. The both of calculated 1/n values given in Table 3.1 are between 0 and 1, it can be noted that, F^- adsorption is favorable for two types of beads.

The fluoride removal capacities of the cerium ion and CeO_2-NPs containing biopolymer adsorbents in the literature were summarized in Table 3.2. As seen in Table 3.2, the CeO_2-CMC-Ce composite material showed an exceptionally high adsorbent capacity of 312 mg F^-/g compared to the other adsorbents.

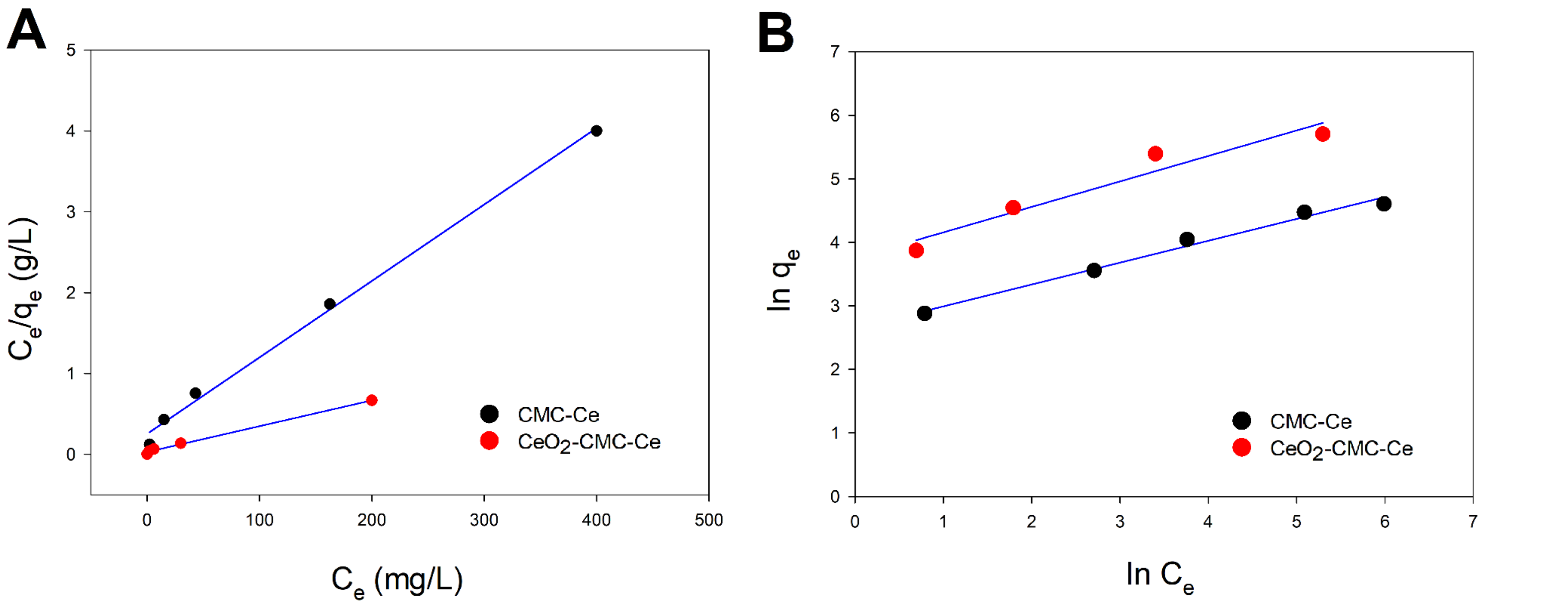

Figure 3.8 : Langmuir and Freundlich isotherm model graphs F^- adsorption. 0.04 g of beads, 20-500 mg/L F^- (pH of 6.2, 40 mL), 200 rpm of shaking rate, 2 h equilibrium time, and 25 ^oC temperature.

Table 3.1 : Isotherm model parameters of F^- adsorption obtained from Langmuir and Freundlich isotherm model equations.

Adsorbent	Langmuir			Freundlich		
	q_{max} (mg/g)	K_L (L/mg)	R^2	1/n	K_F (mg/g)(L/mg)$^{1/n}$	R^2
CMC-Ce	105±5	0.037±0.001	0.9961	0.34	14±1	0.9858
CeO_2-CMC-Ce	312±14	0.076±0.005	0.9998	0.49	30±3	0.9097

Table 3.2 : Comparison of maximum adsorption capacities of cerium containing adsorbents.

Adsorbents	q_{max} (mg/g)	pH	Experimental Conditions (Equilibrium time; temperature; adsorbent dosage; F^- concentration)	Reference
Cerium-immobilized cross-linked chitosan	153.0	3.0	12 h; 20 °C; 0.3 g/L; 30 mg/L	[34]
CeO_2-Rods-NPs CeO_2-Octahedrons-NPs CeO_2-Nanocubes-NPs	71.5 28.3 7.0	3.5	12 h; 25 °C; 0.5 g/L; 50 mg/L	[43]
Ce(III)-incorporated chitosan	33.43	3.0	40 min; 25 °C; 3.0 g/L; 20 mg/L	[52]
Luffa cylindrica functionalized cerium nanocomposite	212	7.0	60 min; 25 °C; 5.0 g/L; 10 mg/L	[53]
Cerium alginate cross-linking with biochar	34.86	5.5	30 min; 20 °C; 1.0 g/L; 10 mg/L	[54]
Ce ion crosslinked carboxymethyl cellulose (CMC-Ce) CeO_2-NPs incorporated cerium-carboxymethyl cellulose (CeO_2-CMC-Ce)	105 312	6.2	120 min; 25 °C; 1.0 g/L; 20 mg/L	This study

3.2.4 Adsorption kinetic modelling

Four kinetic models, which are the pseudo-first-order, pseudo-second-order, intra-particle diffusion and Elovich kinetic models, were applied to the adsorption kinetic data of F^- adsorption experiments and the model graphs were represented in Figure 3.9 (A-D) for CMC-Ce and CeO_2-CMC-Ce beads, respectively.

The pseudo-first-order model linearized equation is given in equation (3.8):

$$\ln(q_e - q_t) = -k_1 t + \ln(q_e) \tag{3.8}$$

where q_e (mg/g) and q_t (mg/g) are the amounts adsorbed F^- at equilibrium and time t, respectively. k_1 (min^{-1}) is the pseudo-first-order rate constant. The values of k_1 were calculated from the slopes of the linear plots of ln (q_e - q_t) *vs*. time (min), and represented in Table 3.3. The regression coefficients of the model can be acceptable to fit with the experimental data. However, the theoretically calculated adsorption capacity values ($q_{e\ (theo)}$) from the model was not in consistence with the experimental adsorption capacities ($q_{e\ (exp)}$).

The pseudo-second-order rate equation is represented in equation (3.9):

$$\frac{t}{q_t} = \frac{1}{k_2 q_e^2} + \frac{t}{q_e} \tag{3.9}$$

where k_2 (g/mg.min) is the rate constant of the kinetic model. From the slope and intercept of the plot of t/q_t *vs*. time (min), the rate constant and the equilibrium adsorption capacity are obtained (Table 3.3). The correlation coefficient of the kinetic model showed that, the pseudo-second-order kinetic model is well fitted with the high values (R^2 = 0.99). Moreover, the calculated adsorption capacity values from the model is obtained closely to the experimental values.

The intra-particle diffusion model can be explained as in equation (3.10):

$$q_t = k_p t^{1/2} + C \tag{3.10}$$

where k_p ($mg.g^{-1}.min^{-1/2}$) is the rate constant of the intra-particle diffusion kinetic model and C ($mg.g^{-1}$) is the constant on boundary layer thickness. According to equation 3.10, a plot of q_t versus $t^{1/2}$ will be plotted to calculate the rate constant of the model for the adsorption. However, it has been seen that, intra-particle diffusion has two linear regression region, indicating F^- adsorption on the adsorbent beads has been controlled by both external diffusion and intra-particle diffusion. Though, $k_{p\ (1)}$ ($mg/g.min^{1/2}$) and $k_{p\ (2)}$ ($mg/g.min^{1/2}$) rate constants have been calculated for first and second fitted lines of the model plot, and represented in Table 3.3.

The adsorption kinetic data was modelled by Elovich kinetic model using the linear equation represented below:

$$q_t = \frac{1}{\beta}\ln(\alpha\beta) + \frac{1}{\beta}\ln t \qquad (3.11)$$

where t is time in min, α (mg.g^{-1}.min^{-1}) and β (g.mg^{-1}) are the rate constant and desorption constant, respectively. These parameters are obtained by using the linear equation of a plot of q_t *vs*. ln (t), and given in Table 3.3. It is determined that, the R^2 values of the fits of the model is not enough compatible for kinetic experiments data of F^- adsorption. As a result of the modelling of the adsorption of F^- by CMC-Ce and CeO_2-CMC-Ce beads, the best fitting was achieved for the pseudo-second-order-kinetic model as explicated above.

Table 3.3 : Kinetic model parameters calculated from pseudo-first-order, pseudo-second-order, intra-particle diffusion, and Elovich kinetic model equations.

Kinetic Model	Parameter	Adsorbent	
		CMC-Ce	CeO_2-CMC-Ce
		$q_{e\ (exp)}$ = 17.81±0.97 mg/g	$q_{e\ (exp)}$ = 19.95±0.56 mg/g
Pseudo-First-Order Model	k_1 x 10^2 (min^{-1})	4.89±0.12	6.04±0.19
	$q_{e\ (theo)}$ (mg/g)	10.40±0.53	10.08±0.44
	R^2	0.9652	0.9837
Pseudo-Second-Order Model	k_2 x 10^3 (g/mg.min)	5.73±0.14	12.50±0.60
	$q_{e\ (theo)}$ (mg/g)	16.53±0.36	20.70±0.11
	R^2	0.9949	0.9997
Intra-particle Diffusion Model	$k_{p\ (1)}$ (mg/g.min$^{1/2}$)	3.61±0.07	2.29±0.09
	$R_{(1)}^2$	0.9951	0.8441
	$k_{p\ (2)}$ (mg/g.min$^{1/2}$)	0.30±0.02	0.18±0.03
	$R_{(2)}^2$	0.9513	0.7878
Elovich Model	α (mg/g.min)	3.35±0.13	49.62±1.25
	β (g/mg)	0.29±0.05	0.36±0.05
	R^2	0.8912	0.8350

(Mean±Standard deviation, N=2)

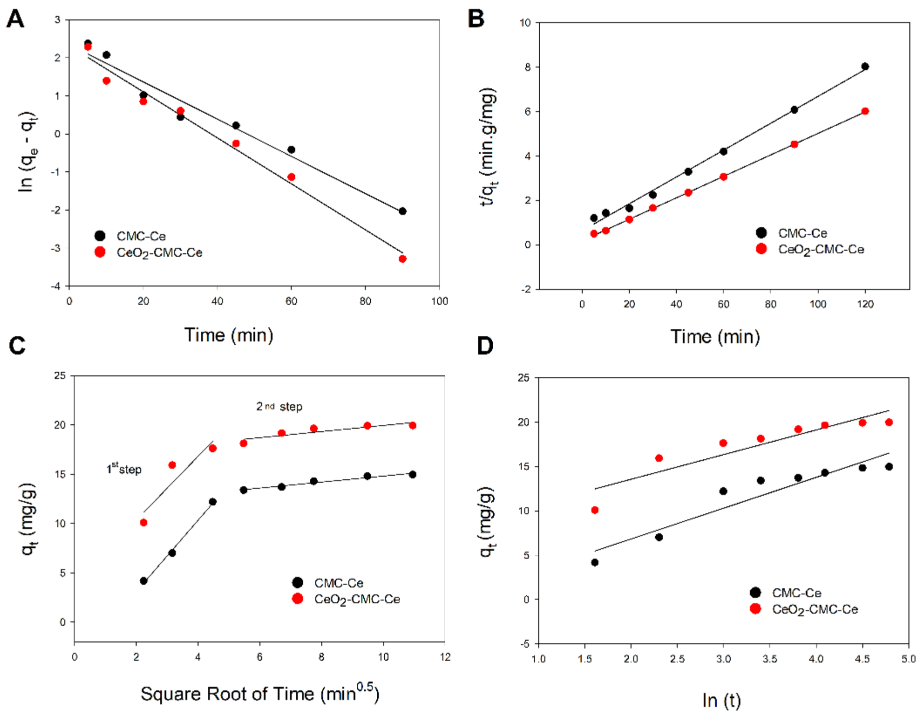

Figure 3.9 : Kinetic model graphs of pseudo-first order (A), pseudo-second-order (B), intra-particle diffusion (C), and Elovich kinetic models for CMC-Ce and CeO_2-CMC-Ce bead's F^- removal kinetics.

3.2.5 Effect of co-existing anions

To investigate the effect of co-existing ions for F^- removal of the adsorbent beads of this study, the adsorption of F^- was studied with 20 mg/L of F^- solutions in the existence of 20 mg/L of Cl^-, CO_3^{2-}, HCO_3^- NO_3^-, SO_4^{2-}, and PO_4^{3-} ions. Figure 3.10 A and Figure 3.10 B shows the effect of co-existing ions on adsorption of F^- by CMC-Ce and CeO_2-CMC-Ce beads, respectively. As can be seen from the Figure 3.10, although the amount of fluoride ions removed decreases somewhat, the fluoride ion is still highly selective against adsorbents. It is seen that, the ions affect F^- adsorption the most are HCO_3^- and CO_3^{2-} for CMC-Ce and phosphate for CeO_2-CMC-Ce. Probably because these ions are of basic character, the OH^- ions they form in the aqueous medium compete with F^- against the adsorbent [54].

3.2.6 Reusability of adsorbent

Considering the practical application and economical aspects, it is desirable for an efficient adsorbent to be regenerated and reused. Since F^- has high solubility in water, water was used as the regeneration solvent, which will both dissolve the fluoride from the adsorbent and not damage the structure of the adsorbent. The removal percentage of CeO_2-CMC-Ce reduced from ~100% to ~85% and, similarly adsorption percentage of CMC-Ce beads reduced to ~50% from ~71% after 9^{th} cycle of usage (Figure 3.11).

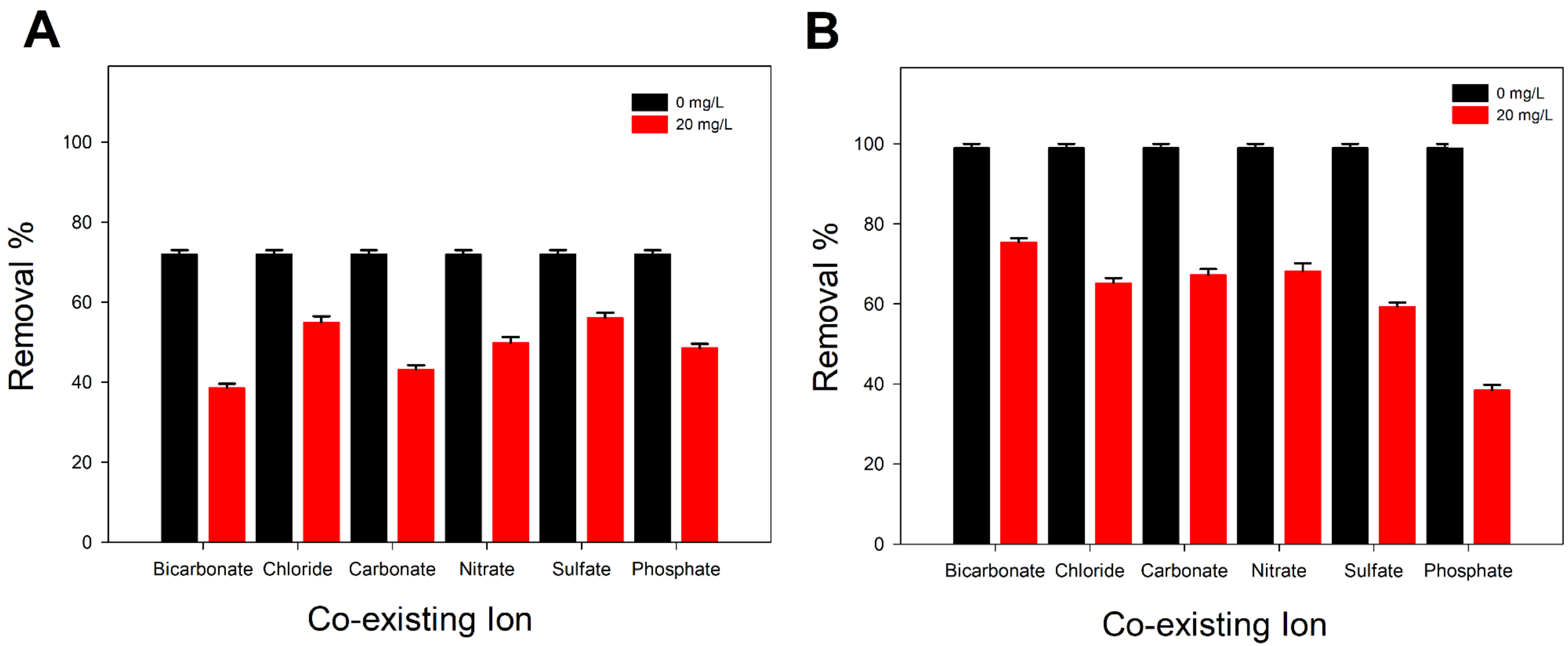

Figure 3.10 : The effect of co-existing ions of F^- adsorption. 0.04 g of beads, 20 mg/L of co-existing ion in 20 mg/L F^- (pH of 6.2, 40 mL), 200 rpm of shaking rate, 2 h equilibrium time, and 25 °C temperature.

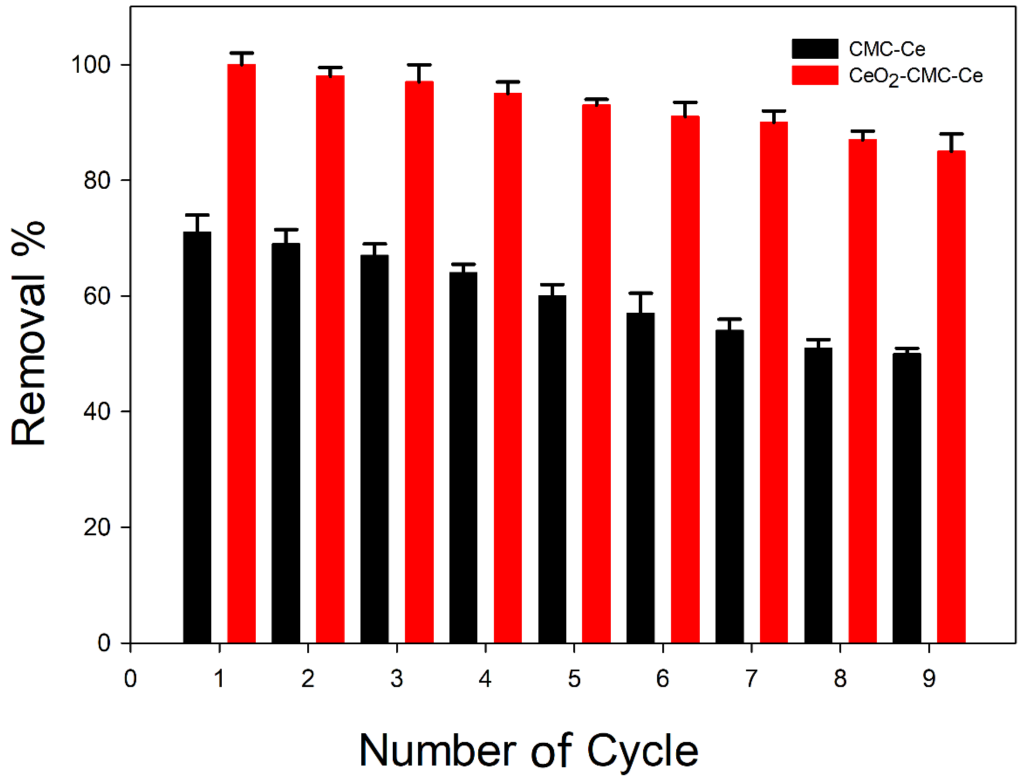

Figure 3.11 : Bar graphs of removal percentage of F^- per cycle in the reusability of adsorbent experiments. Adsorption: 0.04 g of beads, 20 mg/L F^- (pH of 6.2, 40 mL), 200 rpm of shaking rate, 2 h equilibrium time, and 25 °C temperature. Desorption: Distilled water.

The adsorption mechanism appears to be mostly electrostatic. The negatively charged carboxylic acid groups of CMC are blocked by Ce^{3+} ions. On the other hand, as can be seen from the distribution of Ce ion types against pH in the study of Bentouhami et al. [55], the percentage of free Ce^{3+} ions at pH 6 is around 75%. The presence of approximately 10% $Ce(OH)^{2+}$ ions at pH 6 indicates that, there is also anion exchange mechanism by replacing fluoride ions with OH^- ions, as it was previously suggested in the mechanism of cerium-containing adsorbents [32, 35]. As seen in Figure 3.2, since the isoelectric point of CeO_2 nanoparticles is 8.5, the nanoparticles will be highly positively charged at pH 6, which is well below the isoelectric point pH [42] due to protonated hydroxyl groups on the metal oxide surface. On the other hand, the optimum adsorption pH value being below the pH_{pzc} values of CMC-Ce and CeO_2-CMC-Ce beads indicates a positive surface charge of the beads. In conclusion, the electrostatic interaction dominated the sorption, resulting in an increased adsorption capacity.

3.3 Conclusions

A novel adsorbent with high adsorption capacity for fluoride ions was prepared from cerium-carboxymethyl cellulose beads doped with CeO_2 nanoparticles. The optimal adsorption pH was found as pH 6.2. Since the isoelectric point of the CeO_2 nanoparticles used is measured as 8.5, the NPs are positively charged at the optimal adsorption pH. As a result, with the incorporation of CeO_2-NPs into CMC-Ce beads, the adsorbing capacity of the adsorbent increased significantly with the increase of electrostatic attraction towards negatively charged fluoride ions. Both CMC-Ce and CeO_2-CMC-Ce beads followed the Langmuir model, with maximum adsorption capacities of 105 and 312 mg F^-/g, respectively. The CeO_2-CMC-Ce adsorbents have a promising application in the defluoridation of drinking water.

4. SURFACTANT MODIFIED ALGINATE COMPOSITE GELS FOR CONTROLLED RELEASE OF PROTEIN DRUG [3]

In recent years, natural source polymers are of interest due to their, non-toxic, cost-effective, biocompatible, biodegradable, and easily available properties. One of them alginate has been reported as an efficient hydrogel as drug delivery agent [56, 57], adsorbent [7, 8, 10], or wound dressing [12]. Alginate is an anionic polysaccharide mainly produced from marine brown algae and is a copolymer of 1–4 linked-β-d-mannuronate (M) and α-l-guluronate (G) homopolymeric blocks. The main advantage of alginate hydrogel is its easy preparation by ionic cross-linking with multivalent metal ions without the need of toxic chemicals or harsh conditions [58]. The mechanism of gelation has been accepted as an egg-box model for years. The carboxyl groups of two different alginate chains coordinate the metal ions between them, so an egg-box appearance forms.

Protein type drugs degrade in the extreme gastric pH. Such drugs are adsorbed by the intestinal mucosa if they reach the intestine without degradation in the stomach environment [59]. For this reason, researches concentrate on new approaches for colon-targeted delivery systems. A large number of polysaccharide-based delivery systems are becoming a popular option for colon-specific delivery of drugs due to their resistance to gastric and intestinal enzymes, and because anaerobic bacteria metabolize them in the colon [59]. Moreover, the pH-sensitive properties of some polysaccharides make them colon-targeted agents. One of them is alginate. Alginate shrinks in acidic stomach medium and the gel mostly keeps the encapsulated drug [60]. When swelling in the basic intestinal environment, the drug diffuses into the colon. In this respect, it is an ideal polysaccharide for the transport of drugs to the colon. It has been shown that composite materials formed by alginate by the addition of clay, nanoparticles or other polymers [56, 61] reduce the release of protein type drugs in the stomach and provide more controlled release in the intestinal environment. Some researchers have

[3] This chapter was published as “Kahya, N., Erim, F.B. (2019). Surfactant modified alginate composite gels for controlled release of protein drug. Carbohydr. Polym. 225, 115165”.

tried different gel preparation and modification ways to increase the protein retention capacity of alginate. M. Bajpai et al. crosslinked BSA containing alginate gel by diffusion through the dialysis tube technique using calcium or barium ions to increase encapsulation efficiency of alginate for BSA to 90% [62]. A.M. Omer et al. have coated alginate microbeads with aminated chitosan to increase the encapsulation efficiency of BSA to 82% [63].

Interactions of surfactants with synthetic or natural polymers have been explored for decades owing to their widespread applications in the pharmaceutical, food, and cosmetic industries and in biotechnology [64-66]. Recently, it was reported that the incorporation of sodium dodecyl sulfate (SDS) to alginate increases the Young's modulus, i.e. rigidness of alginate gels. The film thickness of alginate-chitosan multilayer films increased with the incorporation of SDS [67]. BSA is widely used as a model protein in many studies. The interaction of SDS with BSA has been reported in different studies [68-71]. With regards to the expected interest of SDS in both alginate and protein, in this present study, calcium alginate beads were modified with the anionic surfactant SDS in order to improve protein entrapment efficiency and controlled release behaviors of calcium alginate hydrogels for the oral delivery of protein. Previously, in two studies, alginate-surfactant composite gels have been tested in the removal of dyes from water [72] and small drug release [73]. To our knowledge, there is no study on the release behaviors of protein-type drugs from SDS-alginate composite hydrogels.

4.1 Experimental

4.1.1 Materials

Alginic acid sodium salt (from brown algae, 4-12 cP, 1% in H_2O) was purchased from Sigma-Aldrich (St. Louis, MO). Sodium dodecyl sulfate (SDS), bovine serum albumin (BSA, fraction V), Coomassie® Brilliant Blue G 250, and ethanol were from Merck (Darmstadt, Germany). Orthophosphoric acid were purchased from Riedel-de Haën (Seelze, Germany). Calcium chloride dihydrate ($CaCl_2.2H_2O$) was obtained from J.T. Baker (Deventer, the Netherlands). All reagents were analytical grade and were used without further purification. All solutions were prepared with deionized water from Elga Purelab Option-Q system (London, UK).

4.1.2 Preparation of Ca-Alg and SDS/Ca-Alg beads

According to the manufacturer's specifications, a 1% w/v solution of alginate used in this study has a viscosity range of 4–12 mPa.s. There is no M/G ratio in the certificate of the product. However, Miller reported that M/G ratio can vary within brown seaweed alginates from 0.33 to 3 [74]. The M/G ratio of alginates varies according to the type of seaweeds, the age, and the season of the collection [75]. Ramos et al. used a 1% solution of alginate with 7 mPa.s viscosity, which is very close to the viscosity of our alginate solution [76]. The M/G ratio of this alginate was reported as 0.42.

Alginate was dissolved in deionized water in order to give a 2% (w/v) polymer solution. The alginate solution was stirred to obtain a homogeneous solution for 2 h at a laboratory room temperature (25 °C). The $CaCl_2$ solution (3% w/v) was prepared by dissolving the necessary amount of calcium chloride dihydrate in deionized water. Alginate beads were formed by dropping 2% alginate solution into 3% $CaCl_2$ solution using a syringe of 0.8 cm inner diameter. The spherical beads waited for 5 min in the crosslinking solution [56]. Then, the beads were collected and taken into deionized water to remove the excess of $CaCl_2$ from the beads. Ca-Alg beads were enrolled in plastic Petri dishes and left to dry at room temperature.

To prepare SDS doped alginate particles, sodium dodecyl sulfate and alginate were dissolved separately in water. Alginate and SDS solutions were combined so that the final solution concentration was 100 mM SDS and 2% (w/v) alginate. SDS/Ca-Alg beads were formed in $CaCl_2$ solution as mentioned above. The washing and drying steps were applied to the beads, respectively.

4.1.3 Preparation of protein loaded beads

In order to prepare bovine serum albumin loaded alginate beads, alginate was dissolved in distilled water until it became a homogeneous solution. BSA was dissolved in distilled water separately. Then, alginate and BSA solutions were combined to give a 2% (w/v) alginate and 1% (w/v) BSA in the final solution. After the mixture became homogeneous, the alginate solution was dropped into a 3% $CaCl_2$ solution and kept for 5 min. The beads were filtered and put into deionized water. After 2 min of waiting in the water, beads were removed. Finally, BSA loaded alginate beads (BSA/Ca-Alg) were dried on Petri dishes at room temperature.

Similar to BSA/Ca-Alg beads, sodium dodecyl sulfate included alginate beads were formed. SDS and BSA were dissolved in deionized water and these were incorporated into the alginate solution to give a final solution of 2% (w/v) alginate, 100 mM SDS, and 1% (w/v) BSA in the mixture. The mixture was dropped into $CaCl_2$ solution. After with 5 min crosslinking time, the beads were filtered, washed, and separated. The BSA/SDS/Ca-Alg beads were dried. BSA containing beads were taken in a laboratory refrigerator at 4 °C before release experiments to prevent the disruption of BSA entrapped in beads.

4.1.4 Characterization of the beads

Fourier transform infrared spectroscopy (FTIR) data were collected using a PerkinElmer Spectrum One FTIR (Shelton, CT, USA). Scanning electron microscopy measurements of alginate beads were conducted by a field-emission scanning electron microscope (FE-SEM, JSM-6335 F, JEOL, Tokyo, Japan). Prior to SEM measurements, the samples were thinly sputtered with gold using an Edwards S150B sputter coater unit (BOC Edwards, UK).

4.1.5 Swelling experiments of the beads

The swelling behaviors of the beads were studied gravimetrically. Simulated gastric fluid, SGF (pH 1.2, 0.2% (w/v) NaCl and 0.7% (v/v) HCl) and simulated intestinal fluid, SIF (pH 7.4, NaH_2PO_4-NaOH buffer) solutions were prepared. Initially, the pre-weighed 0.1 grams of Ca-Alg and SDS/Ca-Alg beads were placed in SGF and SIF solutions and shaken at 250 rpm at 37 ^{o}C temperature water bath (Nüve ST402, Ankara, Turkey). The excess wetness on the bead's surface was eliminated with filter paper, and the mass of the swollen beads was weighed. Swelling experiments were repeated two times. The swelling ratio (SWR%) was calculated using the following expression:

$$SWR\% = \frac{(m_t - m_o)}{m_o}\ x\ 100 \tag{4.1}$$

where m_t is mass of swollen beads determined time intervals and m_o is initial mass of beads in gram.

4.1.6 Protein encapsulation efficiency

The encapsulation efficiency of beads (EE) was calculated according to equation (4.2) by subtracting the total BSA losses (m_l) during the gelation and washing steps from the initial amount of BSA (m_0) added to the alginate solution.

$$Encapsulation\ Efficiency\ (EE)\ \% = \frac{m_0 - m_1}{m_0}\ x\ 100 \qquad (4.2)$$

where m_0 is the initial amount of BSA present in the alginate solutions in milligram and m_1 is the total amount of BSA lost in $CaCl_2$ solution, and in water using to wash the beads and filter paper.

4.1.7 Protein release studies

Alginate beads loaded with BSA were weighed (0.1 g) and put in amber glass bottles containing 30 cm^3 of release media (SGF or SIF). Beads were shaken in a temperature-controlled water bath at 37 ^oC and 250 rpm. At each time interval 0.5 cm^3 of release media was taken into microcentrifuge tubes and fresh release media (SGF or SIF) was added in the same volume to the bottles immediately. BSA content in the samples was determined by Bradford protein assay at 595 nm [77]. Spectrophotometric measurements were performed with a Shimadzu UV spectrophotometer UV-1800 (Kyoto, Japan) using disposable plastic cuvettes. All experiments were performed in triplicate.

4.2 Results and Discussion

4.2.1 Characterization of alginate beads

Scanning electron microscopy analysis of dry calcium alginate and SDS incorporated calcium alginate beads are illustrated in Figure 4.1. Surface morphology of alginate beads were investigated by SEM at different magnifications up to 5000x. Ca-Alg beads have spherical shapes, and compact surface areas. Some squashes on the bead surface are probably due to the contact of the beads on Petri dishes during the air drying process (Figure 4.1 (A-C)). The incorporation of SDS significantly changes the morphology of the beads as seen in Figure 4.1 (D-F). The beads retain their spherical shapes, but their surfaces turn into a leafy structure with many cavities.

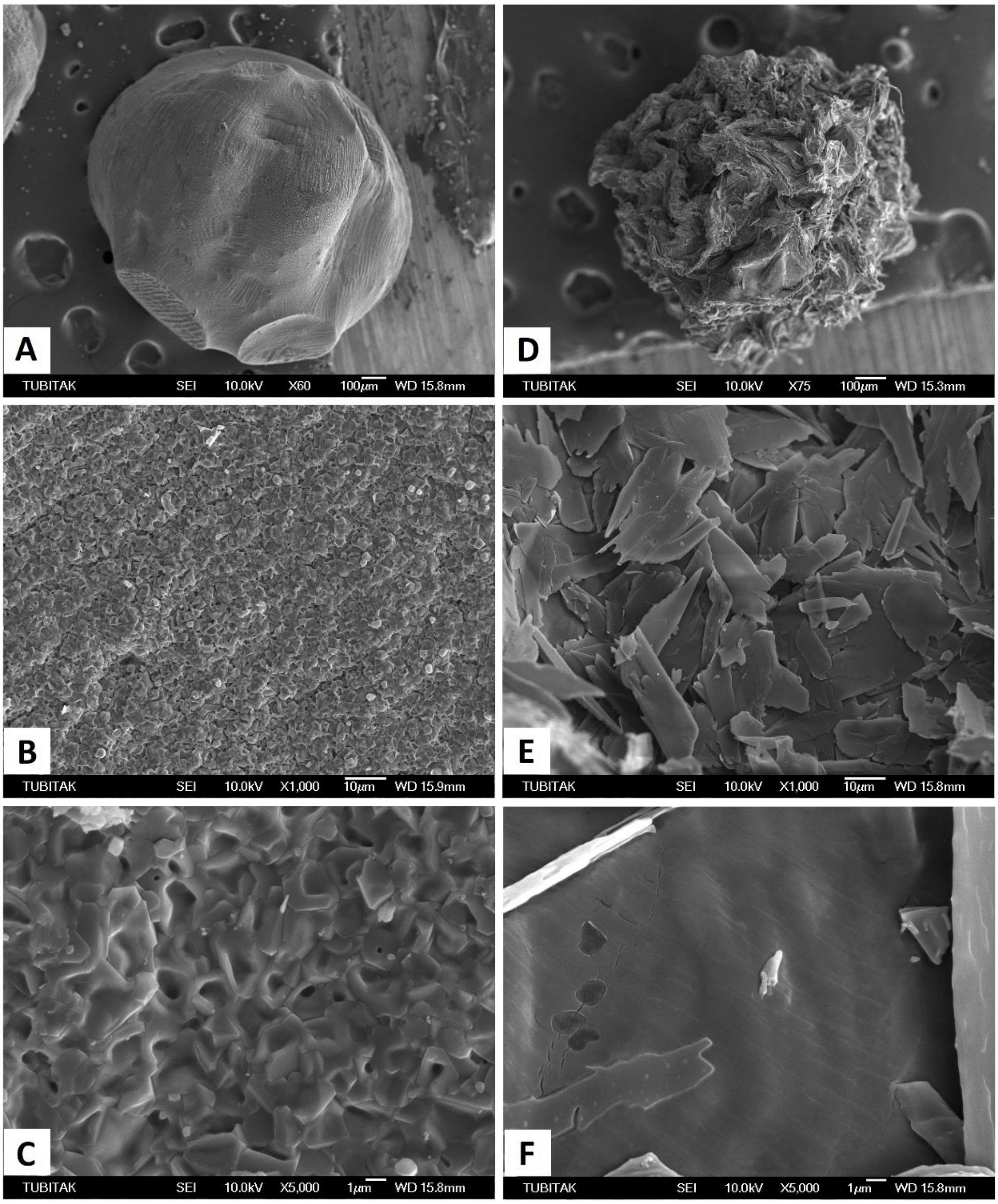

Figure 4.1 : Scanning electron microscope images of the beads: (A), (B) and (C) belongs to calcium alginate, and (D), (E) and (F) belongs to SDS incorporated calcium alginate beads, respectively.

The relationship between water-soluble polymers and surfactants is of particular interest to many researchers, since the importance of these substances in industrial applications. The most accepted model in this regard is the necklace-like model [78]. According to this model, the surfactant is bound to the polymer chains by forming aggregates to form necklace-like complexes. The critical aggregation concentration is 3–4 times below the critical micelle concentration of the surfactant. It has also been shown that the interaction between the surfactant and polymer chains starts even below the critical aggregation concentration [79]. In this study, it can be assumed that similar interactions between SDS and alginate biopolymer create significant changes in morphology. Additionally, Kaygusuz et al. reported that the addition of SDS increases the Young modulus of alginate spheres. Thereby more rigid beads are obtained by the addition of SDS to alginate. It was reported that the incorporation of SDS into alginate-chitosan polyelectrolyte multilayer films affected surface morphologies of films by increasing the film thickness and surface roughness based on AFM results [67].

FTIR spectra of the calcium alginate, SDS incorporated calcium alginate, and BSA loaded version of these alginate beads, are shown in Figure 4.2. Dry state of all the beads was used to obtain FTIR spectra. Stretching vibrations of O–H bonds of alginate, considering appeared in the range of 3347–3370 cm^{-1} [80]. SDS included alginate beads showed two sharp peaks at 2917 and 2850 cm^{-1}, which result from the asymmetric and symmetric stretching vibrations of $-CH_2$ groups of the SDS molecule [81]. SDS/Ca-Alg beads loaded with BSA assigned two characteristic peaks, which indicates the presence of BSA in the beads formulation, at 1641 and 1545 cm^{-1} due to the C=O stretching and the N–H bending mode of amide I, respectively [82]. Three of the spectra showed a distinct peak at 1596 cm^{-1} that belongs to asymmetric stretching of carboxylate group of alginate chains [83]. However, this peak did not appeared sharply in the BSA/SDS/Ca-Alg spectra and it could be overloaded by BSA responsible peaks (1641 and 1545 cm^{-1}) located around it. The peak, which characterizes CH_2 scissoring vibrational mode of SDS, appeared at 1471 cm^{-1} in the SDS containing beads spectra. Besides, asymmetric stretching modes of the sulfate group of the SDS molecule gave two peaks at 1244 and 1214 cm^{-1} with a 30 cm^{-1} frequency difference [84]. The sharp bands at 1105 and 1014 cm^{-1} are assigned to the S-O stretching vibrations of SO_4 from SDS molecule in this study [85]. The peak at 1023 cm^{-1} with a shoulder at 1078 cm^{-1} clearly appeared in Ca-Alg spectra and pointed out the alginate structure of the beads caused due to C-O stretching in C-O-C linkages [60].

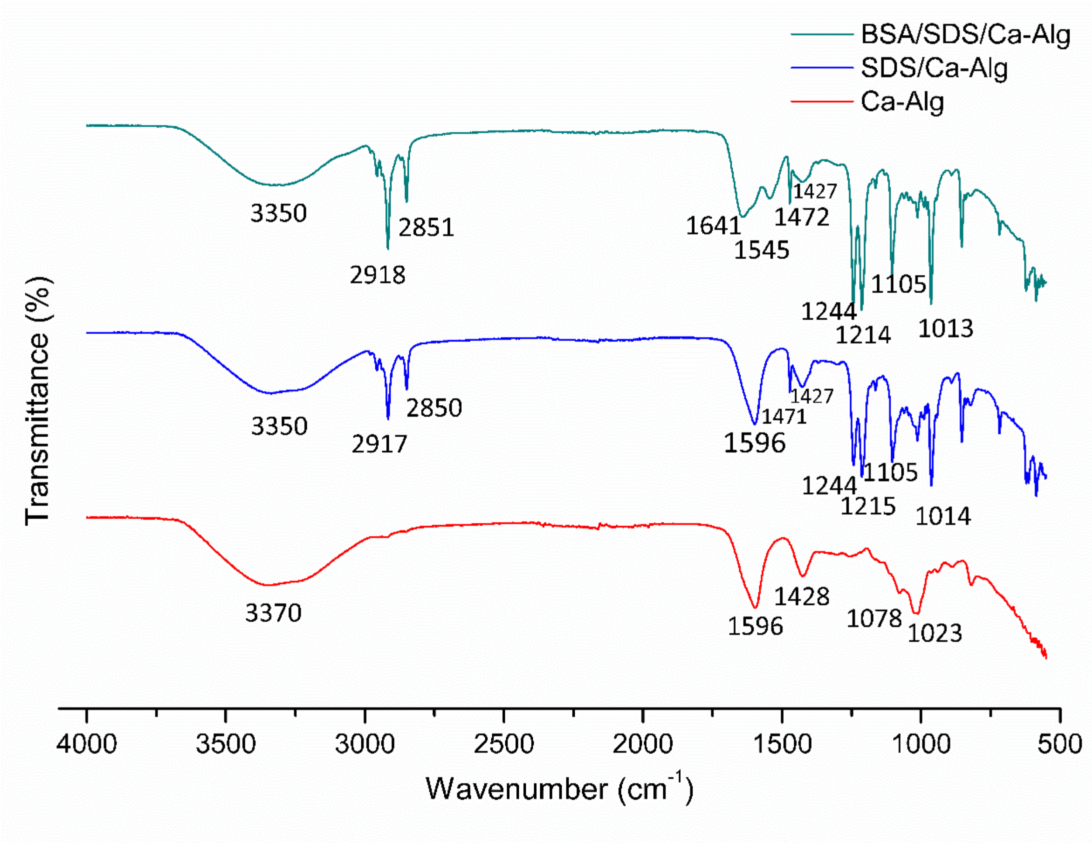

Figure 4.2 : FTIR spectra of the beads.

Figure 4.3 shows swelling ratios of Ca-Alg and SDS/Ca-Alg beads in SGF and SIF solutions, respectively. Alginate is a pH-sensitive copolymer. At the pH values above the pK_a values of the mannuronate (M) and guluronate (G) groups (3.4 and 3.6 for M and G units), alginate has a negative charge due to the dissociation of the carboxylic acid in the structure. Since the carboxylic groups of alginate above pH 5 are completely dissociated, negative charges in the polymer chain repel each other, and the chain expands. Conversely, since the carboxylic groups are fully protonated in the acidic gastric environment, the polymer chain collapses, and the alginate swells very little in the acidic stomach. With the SDS addition, the swelling increases slightly (Figure 4.3 A). It was shown before that with the decrease of pH value from 5 to 3, hydrophobic segments in the alginate chains and consequently hydrophobic interaction between alginate and SDS increase [86]. With the repulsion between SDS groups that bind to the polymer, the alginate chain relaxes and the swelling increase. On the other hand, the presence of SDS in intestinal pH makes the swelling more controlled than naked alginate. The swelling degrees of both Ca-Alg and SDS/Ca-Alg beads increase in the intestinal fluid compared to those in the gastric fluid (Figure 4.3

B). The reason for this is that the dissociation of the alginate in the basic medium increases, consequently negative charge on the polymer and hydrophilic character increase. The lower swelling of the composite material containing SDS is due to the hydrophobic tails of the SDS chain. When the degree of swelling is low, the rate of disintegration of the spheres decreases and they show more stable behavior. The swelling behavior of alginate beads turned to first erosion and finally dissolution after ~150 min. However, the decomposition of SDS containing beads was not observed. Hence, SDS provided robustness to alginate beads to protect their erosion in SIF. This is consistent with the previously published study showing that SDS has improved the stiffness of alginate [67].

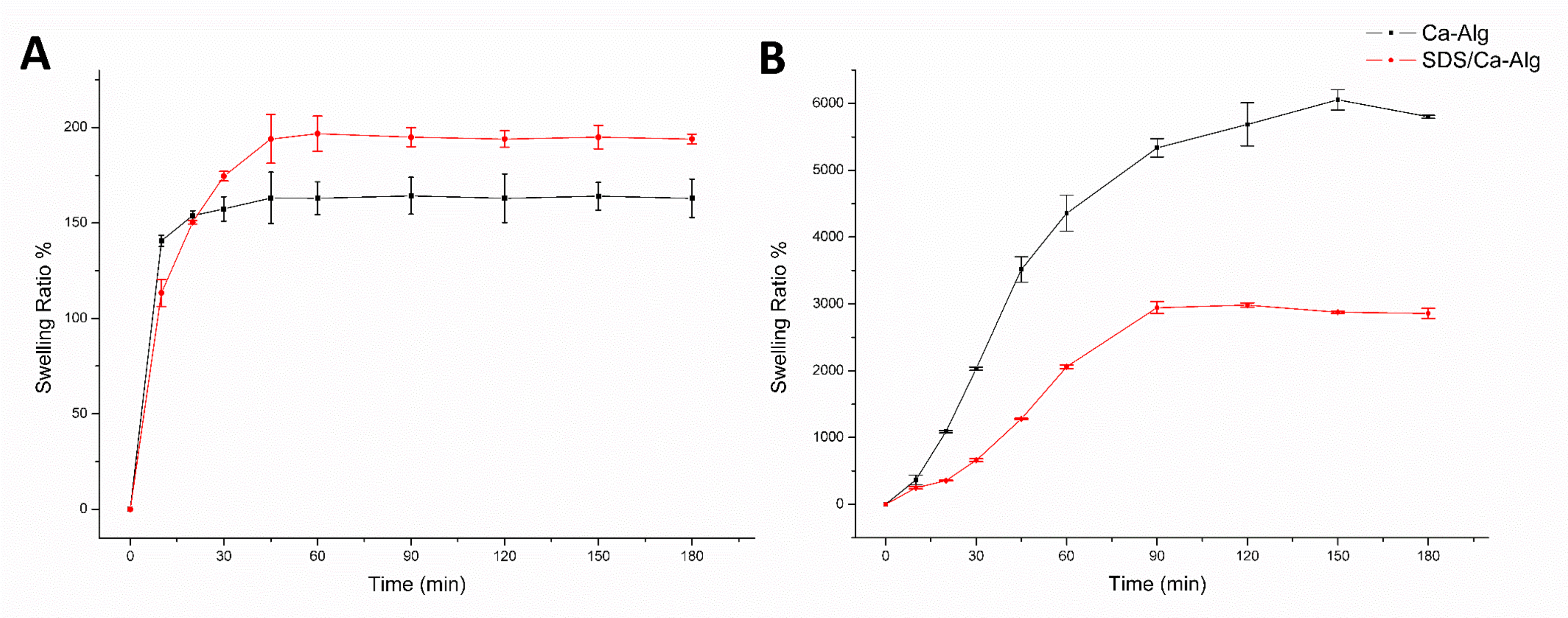

Figure 4.3 : Swelling ratios of the beads in (A) simulated gastric fluid (SGF) and (B) simulated intestinal fluid (SIF).

4.2.2 Encapsulation of BSA by alginate beads

Encapsulation efficiencies of BSA/Ca-Alg beads and BSA/SDS/Ca-Alg beads were calculated by subtracting the lost amounts of BSA during the crosslinking, washing, and filtration steps from the initial amount of BSA. For this, BSA concentration in $CaCl_2$ solution after the gelation process, BSA concentration in washing water used for beads and filter paper were detected spectrophotometrically as explained in the experimental part. Figure 4.4 shows the encapsulated amount of BSA from beads step by step. The last step bars show the final encapsulation efficiency of beads for BSA. As shown in Figure 4.4, Ca-Alg beads performed lower capability to hold the initial amount of BSA in the beads (EE%, 77.1 ± 1.7). However, SDS incorporated alginate beads encapsulated almost all of the loaded BSA (EE%, 96.3 ± 2.1). Thus, the encapsulation efficiency of alginate beads for BSA was significantly enhanced by modification of alginate beads with SDS. Increasing the encapsulation efficiency of BSA in the SDS incorporated beads is mainly due to the interaction of SDS with BSA, and it can be foreseen that the diffusion of the large protein molecule from the depths of the cavities will slow down. The protein and anionic surfactant interaction has been mainly explained with a complexation between protein and SDS and this situation was investigated by different techniques [68-71].

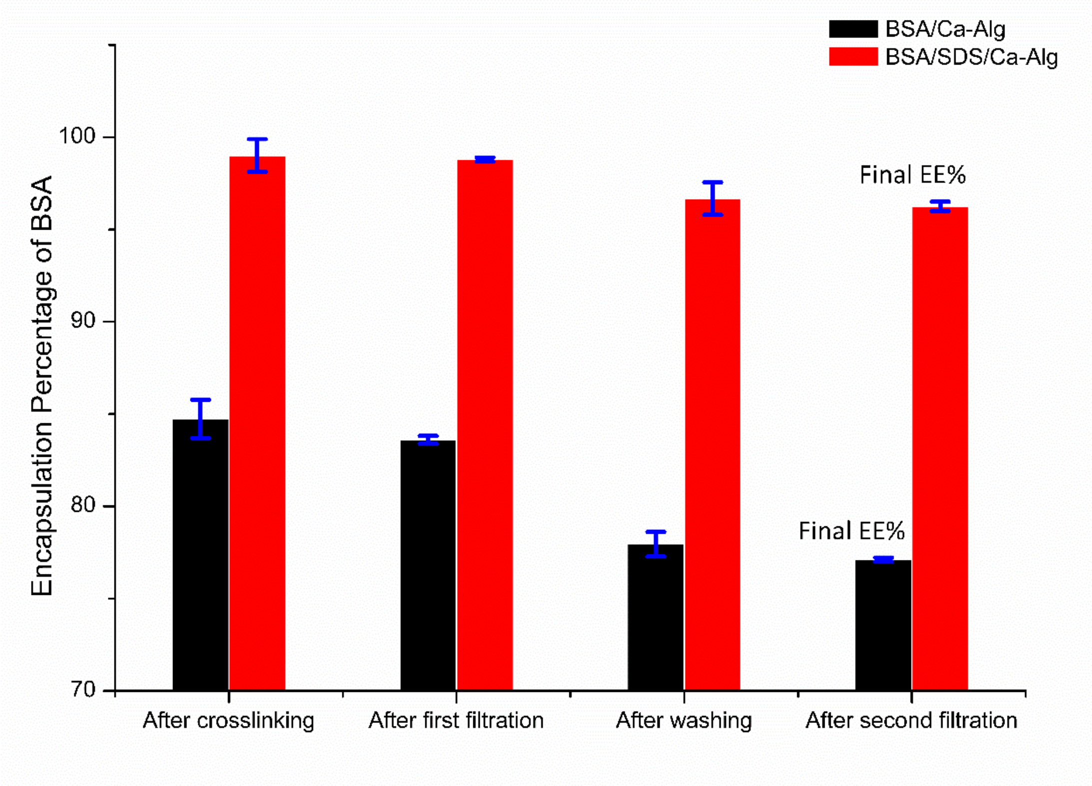

Figure 4.4 : A comparative bar graph of the encapsulated amount of BSA in BSA/SDS/Ca-Alg and BSA/Ca-Alg beads during the beads preparation steps.

4.2.3 Release of BSA from the alginate beads

The protein release experiments were conducted in simulated gastric and intestinal fluids. The transportation of the drug from the stomach to the intestines when it was taken by the oral way was mimicked by holding the beads in acidic SGF media for 120 min. Initially, BSA/Ca-Alg and BSA/SDS/Ca-Alg beads were soaked to acidic SGF media (pH 1.2) for 120 min. In the following process, the beads were taken and immediately put into SIF solutions (pH 7.4) without making an intervention to the beads. Figure 4.5 represents the graphs of the cumulative release percentage of BSA from calcium alginate and SDS included calcium alginate beads by time. It can be seen from Figure 4.5 that compared to 37% of BSA release from BSA/Ca-Alg beads to SGF in two hours, BSA is released in a very low amount (10%) from BSA/SDS/Ca-Alg beads. The release ratio of BSA after 120 min from BSA/SDS/Ca-Alg beads is comparative and significantly very low. As soon as both types of BSA loaded beads with or without SDS were taken into SIF solutions, Ca-Alg beads release the remained BSA together with first erosion and finally dissolution within one hour after they enter the intestine. However, after the rapid release of BSA within the first 10 min, a controlled release profile is observed from the BSA/SDS/Ca-Alg beads in the following period. This behavior is mainly due to the interaction of BSA with SDS. The release continues up to 240 min total time without any degeneration in the shape of the beads. This is mainly due to the increased stiffness of alginate-SDS composite as reported before [67].

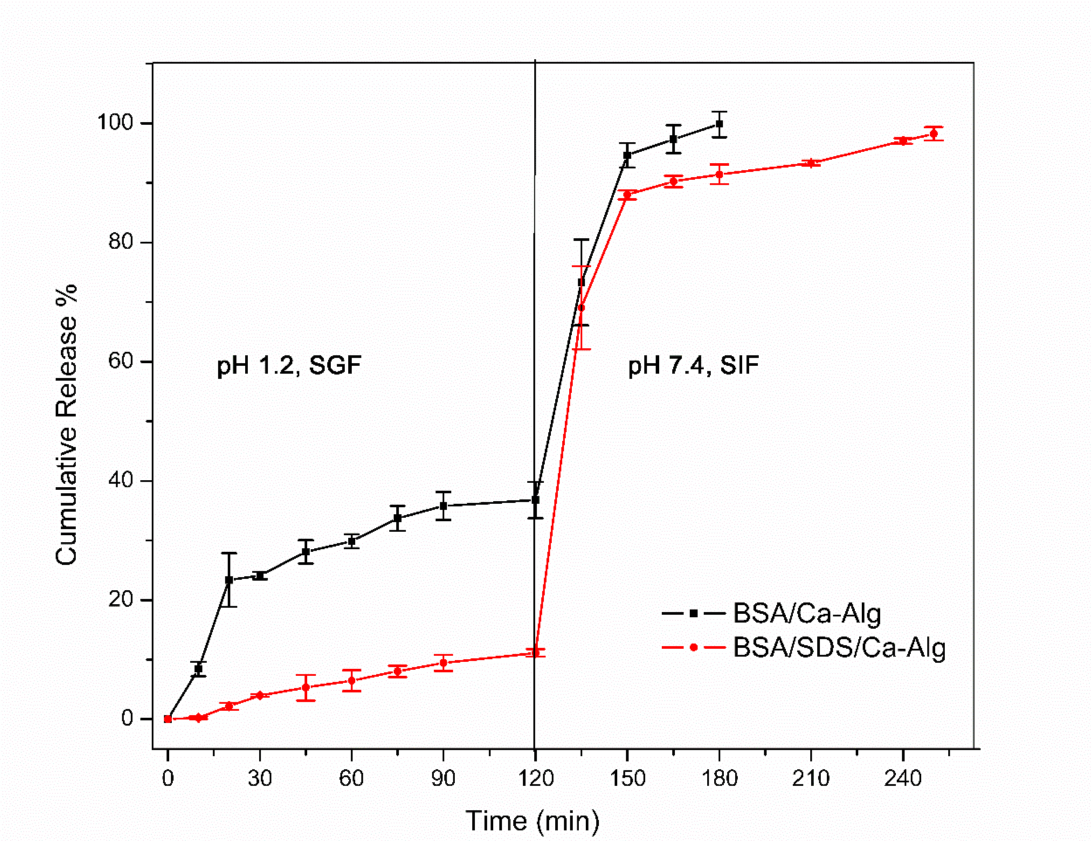

Figure 4.5 : The cumulative release curves of BSA from the alginate beads: Incurring the beads initially in SGF (pH 1.2) during 120 min and then continue to release BSA in SIF (pH 7.4).

In case of reconsideration the swelling profile of SDS/Ca-Alg, it can be seen that the beads have the slightly higher swelling ability in SGF. On the other hand, as it is shown in Figure 4.5, the release behavior of these beads did not show an expected release trend that a higher release profile arises from an excessive swelled polymeric structure as in general. Also from that result, it can be understood that there is a strong interaction between SDS and BSA. In SIF media, Ca-Alg beads have swelled considerably, more than SDS incorporated Ca-Alg beads. In harmony with the swelling of the beads, the burst release of BSA was observed. Modification of beads suppressed swelling and this caused a controlled release in SIF media. On the other hand, the expected increase in the stiffness of the SDS-alginate composition as previously reported [67] may be helpful in the controlled release profile. The most noteworthy result is that protein release from the modified gel in the stomach environment is significantly reduced compared to protein release from the plain alginate gel. Thus, large amounts of BSA can reach the intestine without degradation in the acidic gastric environment. Moreover, in SIF media, a more controlled release occurs than the burst release of alginate.

4.3 Conclusion

Calcium alginate beads were doped with sodium dodecyl sulfate. SDS/Ca-Alg beads were characterized in point of their physical and structural properties. Then, SDS/Ca-Alg beads were used to encapsulate the model protein BSA in order to reveal the drug release capability of the beads. It was observed that SDS incorporated calcium alginate beads performed almost total encapsulation efficiency for BSA before the release experiments. The release ratio of protein from hydrogels was significantly suppressed in the simulated stomach medium with the incorporation of SDS to alginate. This behavior is noteworthy since the major drawback in the oral delivery of protein drugs is the instability and degradation of them in the acidic medium of the stomach. Moreover, the beads showed enough endurance, especially in the basic SIF medium until they reach up to the total protein release. Thereby, we recommend the SDS modified alginate carriers to the pharmaceutical industry as an innovative design for protein-type drugs that are taken orally and are intended to target the colon.

5. BARIUM ION CROSS-LINKED ALGINATE-CARBOXYMETHYL CELLULOSE COMPOSITES FOR CONTROLLED RELEASE OF ANTICANCER DRUG METHOTREXATE[4]

Polysaccharides are natural polymers isolated from plants, microorganisms, and marine sources. They are widely used in food, medicine, and environmental applications in recent years due to their biocompatible, biodegradable and non-toxic properties [87, 90]. Alginate, a natural polysaccharide extracted from brown algae, is one of the more commonly used polysaccharide in food, environment, and pharmaceutical applications [91, 7, 8, 57]. It has a copolymer structure consisting of 1,4-linked β-d-mannuronic acid and α-l-guluronic acid units. Alginate is a pH-sensitive biopolymer due to the carboxylic acid groups in its structure. The great advantage of alginate as a drug carrier in the oral administration is its minimal swelling properties in the acidic gastric environment. Thus, the orally taken drug entrapped into alginate gel is largely transported to the intestinal environment. However, in basic body pH, a burst release of the drug is observed with sudden swelling and decomposition of the alginate gel. The recent innovative studies are on slowing the swelling rate of alginate in a basic environment by some additives such as clay [56] or forming composite materials with alginate and other polysaccharides or polymers [92]. Alginate forms ionically cross-linked hydrogel with multivalent metal ions. The important factor affecting the strength of the alginate gel is the type of metal ion used. Although the most commonly used ion is calcium in the gelation of alginate, barium ion has been used in drug release studies. Ba-alginate gels are shown to be more resistant than calcium alginate and release the drug more controlled [58, 93].

Cellulose based polymeric systems have been used for drug release applications due to eco-friendly and processability properties [94]. Carboxymethyl cellulose is a water-

---

[4] This chapter was published as "Kahya, N., Gölcü, A., Erim, F.B. (2019). Barium ion cross-linked alginate-carboxymethyl cellulose composites for controlled release of anticancer drug methotrexate. J. Drug Deliv. Sci. Technol. 54, 101324".

soluble derivative of cellulose. It has been used in drug release studies to form supplementary composite gels that support other polysaccharides rather than being used alone. Carboxymethyl cellulose also contains carboxylic acid groups similar to alginate and composite gels can ionically cross-link with multivalent metal ions. Seaweed and cellulose-based polysaccharides are biodegradable polymers [95]. Alginate-carboxymethyl cellulose composite gels have been reported as carriers for proteins and small drugs [96-100].

In this study, barium-alginate-carboxymethyl cellulose composite hydrogel beads were prepared as a controlled release agent to slow the sudden release of the cancer drug methotrexate in the PBS with a pH value of 7.4. MTX is an antimetabolite and folic acid antagonist drug that is widely used for the treatment of malignancies and also auto-immune diseases [101, 102]. MTX can be administered clinically via oral, intravenous, subcutaneous and/or intra-muscular administration routes. Since MTX is poorly soluble in water, MTX was dissolved in green solvent DMSO [103, 104] and added to the polymer solution. The effect of DMSO in polymer solution was investigated in terms of morphology and swelling properties of barium-alginate-carboxymethyl cellulose gels. In the literature, release behavior of MTX has been reported from a commercial porous polymeric adsorbent [105], polymeric magnetic nanoparticles [106], bacterial cellulose/carboxymethylcellulose (BC/CMC) biocomposites [107], kappa-carrageenan/chitosan complexes [108], chitosan microparticles [109], thiolated carboxymethyl chitosan [110], folic acid-conjugated chitosan nanoparticles [111], pH-sensitive gelatin microsphere biopolymer [112], mPEG–PCL polymersomes [113], and silica-gelatin aerogel [114]. According to our literature research, this is the first study on MTX release behavior from alginate-carboxymethyl cellulose matrix.

After the tremendous success of cisplatin complexes [115], in recent years, there have been increasing studies on metal-complexes of drugs as new drug candidates [116]. However studies on how to control the drug release rates of metal–drug complexes are still rare [117]. In this study, the release behaviors of Cu(II) and Zn(II) complexes of MTX were examined in comparison with the release behavior of MTX.

5.1 Experimental

5.1.1 Materials

Alginic acid sodium salt (from brown algae, 4–12 cP, 1% in H_2O) and carboxymethyl cellulose (low viscosity) were purchased from Sigma-Aldrich (St. Louis, MO). Barium chloride dihydrate ($BaCl_2.2H_2O$), dimethyl sulfoxide (DMSO), sodium chloride, potassium chloride, sodium dihydrogen phosphate, and sodium hydroxide were obtained from Merck (Darmstadt, Germany). MTX was purchased from a local pharmacy (Kahramanmaraş, Turkey). The Zn and Cu complexes of MTX were prepared in a similar manner to the previous study by our group [118]. All reagents were analytical grade and were used without further purification. All solutions were prepared with deionized water from Elga Purelab Option-Q system (London, UK).

Thermo Orion Dual Star pH Meter (Beverly, MA, USA) was used to adjust pH during PBS solution preparation. The drug release and the swelling experiments were performed in Nüve ST 402 (Ankara, Turkey) model temperature controlled water bath. Fourier transform infrared spectroscopy (FTIR) data were recorded using a PerkinElmer Spectrum One FTIR (Shelton, CT, USA). Morphological analysis of the beads was performed using EVO LS10 model (Carl Zeiss, Oberkochen, Germany) scanning electron microscope (SEM).

The thickness of wet and dry Ba-Alg/CMC beads was measured using a Mitutoyo digital caliper (Tokyo, Japan). All of the measurements were conducted for two sets of beads prepared on different days. Five beads were selected from each set and measured.

5.1.2 Preparation of the Ba-Alg/CMC beads

Alginate and carboxymethyl cellulose polymers were dissolved separately in deionized water by stirring at 40 °C until to obtain complete dissolved polymer solutions. Then, these solutions were combined and stirred 1 h. Methotrexate and its synthesized Cu(II) and Zn(II) metal complexes were weighed and 2 mg from each was dissolved in 1 mL of DMSO. These solutions were separately included in the polymer mixture. The final concentrations of ingredients of polymer solution were: 2% (w/v) Alg, 2% (w/v) CMC, 0.02% (w/v) drug and 10% (v/v) DMSO. The formed solutions which are described above were dropped using a syringe of 0.85 mm inner diameter from a constant height of 15 cm above the gelling solution (i.e. %20 (w/v) $BaCl_2$) under continuous stirring. The dropping step was completed in 5 min. The obtained beads were filtered from a stainless steel filter. The beads were put into a certain amount of deionized water for 1 min to remove excess barium chloride from the surface of the beads and filtered from the washing solution. Finally, the MTX entrapped Ba-Alg/CMC gel beads were placed onto 9 cm diameters of plastic Petri dishes and dried 24 h at room temperature. Control group beads (Ba-Alg/CMC) were prepared in the same steps mentioned above without drug. Moreover, to evaluate if DMSO is vital or not in the control group of bead formulation, alginate and carboxymethyl cellulose solutions were prepared without DMSO just including deionized water instead of DMSO into the polymer mixture.

MTX has given a maximum wavelength at 303 nm in its UV spectra. Amount of copper and zinc complexes of the drug in the solutions were determined also at this wavelength. Calibration curve of the drug was constructed by dissolving about a certain amount of drug in 1:10 solution of DMSO:PBS. The irrepressible lost content of the initial amount of drugs in the gelling $BaCl_2$ solution (12.5 mL) and washing water (10 mL) was determined by measuring of absorbance values of these solutions at 303 nm. By using the calibration curve equations of MTX (y = 0.04807x-0.01126, R^2 = 0.9984), MTX-Cu (y = 0.03911x-0.00752, R^2 = 0.9995), and MTX-Zn (y = 0.04574x+0.02287, R^2 = 0.9996), entrapment efficiency percentage (*EE%*) of drugs was calculated from:

$$(EE\%) \;= \frac{(Amount\ of\ MTX\ remained\ in\ the\ composites\ in\ mg)}{(Initial\ amount\ of\ drug\ in\ the\ polymer\ solution\ in\ mg)} x100 \qquad (5.1)$$

5.1.3 Swelling experiments of the Ba-Alg/CMC beads

In the swelling experiments of Ba-Alg/CMC composites, about 0.1 g of pre-weighed beads in their dry state were immersed in 10 mL PBS containing vessels and shaken at 200 rpm at 37 ± 0.1 °C temperature water bath. The excess wetness on the bead's surface was eliminated gently with filter paper, and the swollen beads mass was weighed. The mass changes of the swelled beads by time was transformed to swelling ratio percentage (*SR%*) using the following empirical equation:

$$Swelling\ Ratio\ Percentage\ (SR\%) = \frac{(M_f - M_i)}{M_i} x100 \qquad (5.2)$$

Here M_f represents the mass of swollen state of the beads by a specific time in gram. M_i is the initial mass of the beads in gram. The measurements were made in dublicate and average data was used for calculations.

5.1.4 MTX release from the Ba-Alg/CMC beads

Drug release experiments from MTX and its metal complexes loaded composites which were named Ba-Alg/CMC/MTX, Ba-Alg/CMC/MTX-Cu, and Ba-Alg/CMC/MTX-Zn were performed. The dry state beads were weighed about 0.1 g and each portion of the beads was put into 10 mL PBS (pH 7.4) containing vessels. The vessels were shaken in a water bath at a constant speed of 200 rpm at 37 ± 0.1 °C. At specific time intervals, 1 mL of aliquots were withdrawn and analyzed spectrophotometrically at 303 nm using a Shimadzu UV-1800 spectrophotometer (Kyoto, Japan). The vessels were not shaken during UV analysis and the measured 1 mL of sample volumes were put into the vessels immediately to keep the release media volume in 10 mL under determined experimental conditions. Two sets of freshly produced drug loaded beads were prepared in different days and the release experiments were done in triplicates per each set.
Cumulative drug release percentages of the drug were calculated using the following equation:

$$Cumulative\ Drug\ Release\ (\%) = \frac{Amount\ of\ MTX\ released\ by\ time}{Total\ amount\ of\ MTX\ encapsulated\ in\ the\ beads}\ x100 \qquad (5.3)$$

Release studies were performed by drug-loaded composites just after their preparation and full drying. To test the shelf life and stability of the drug in Alg/CMC beads, the beads were kept at 23±2 °C and 55±5% humidity conditions during 60 days. After this time, the beads were used again in the release experiment in the same conditions as mentioned above.

5.2 Results and Discussion

5.2.1 Surface properties of the Ba-Alg/CMC beads

Figure 5.1 (A-B) illustrates the appearance of the freshly prepared Ba-Alg/CMC and Ba-Alg/CMC/MTX gel beads. As can be seen from Figure 5.1 A, the freshly prepared composite gel beads were in white color with spherical shapes and thickness of 2.18 ± 0.0602 mm in their wet state. Besides, the average thickness of dry Ba-Alg/CMC beads was measured as 0.896 ± 0.0829 mm. The beads color was changed to pale yellow when they were loaded with MTX (Figure 5.1 B).

Figure 5.1 : A) Ba-Alg/CMC and B) Ba-Alg/CMC/MTX beads.

Drug-free versions of Ba-Alg/CMC beads were prepared as described in Experimental part with the addition of DMSO to polymer mixture. One set of beads were prepared with the same procedure but without DMSO. Figure 5.2 A and Figure 5.2 B show SEM photographs of Ba-Alg/CMC beads prepared without DMSO and with DMSO, respectively. It can be seen from Figure 5.2 A, the dry composite beads without DMSO have a non-spherical shape. With the addition of DMSO, the pellets are transformed into a spherical shape (Figure 5.2 B). Magnified SEM images of beads without DMSO and with DMSO are seen in Figure 5.2 C and Figure 5.2 D, respectively. Beads without DMSO have a flaky surface (Figure 5.2 C), however, beads with DMSO appear as convoluted surface morphology (Figure 5.2 D).

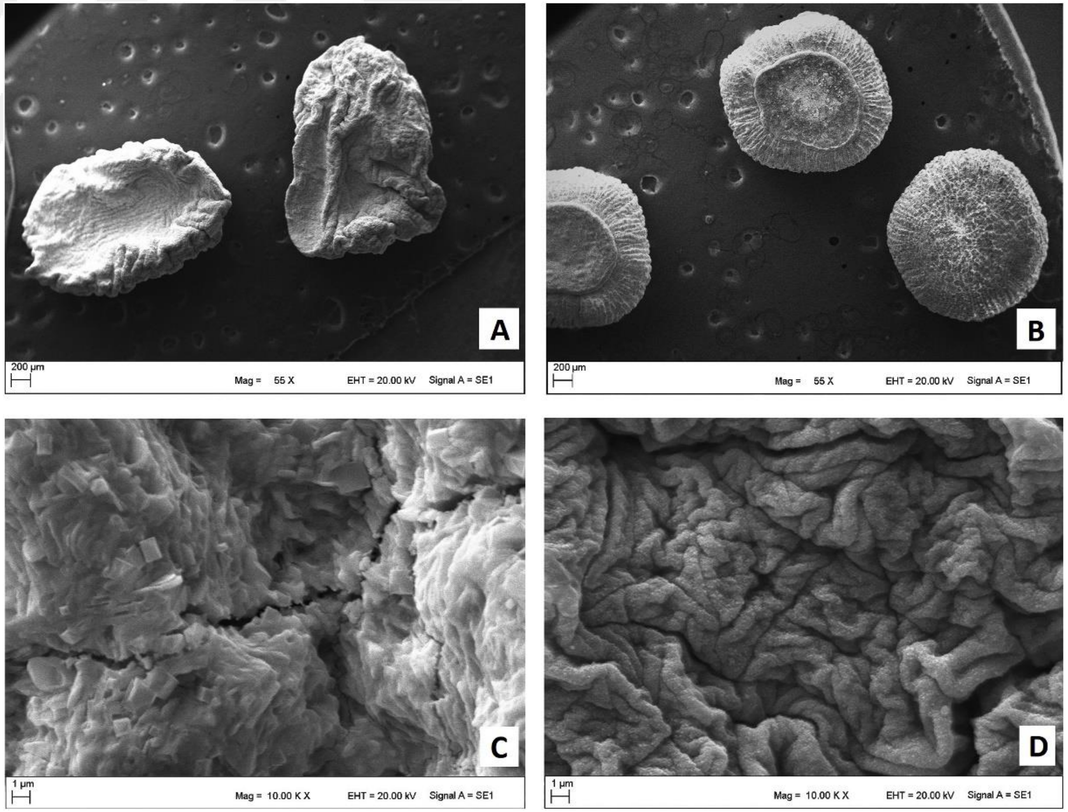

Figure 5.2 : Scanning electron microscope images of Ba-Alg/CMC: DMSO free beads (A, C) and DMSO containing beads (B, D).

5.2.2 Fourier transformed infrared spectroscopy (FTIR)

The FTIR spectra of Ba-Alg/CMC and Ba-Alg/CMC/MTX beads were given in Figure 5.3. In the spectrums, the broad and adjacent two peaks which are at 3331 cm^{-1} and 3233 cm^{-1}, were determined the characteristic peaks illustrated to the stretching vibrations of the -OH groups of the polysaccharides of alginate and carboxymethyl cellulose. An obvious peak for the primary amine stretch at 3455 cm^{-1} was referred to NH_2 group of methotrexate. The peak at 2915 cm^{-1} was identified with the asymmetric -CH stretching in the Ba-Alg/CMC bead spectra. Drug-loaded beads showed two extra peaks in their FTIR spectra which were at 1739 cm^{-1} and 1635 cm^{-1} that could be attributed to C=O stretch and mainly C=O stretch of amide I group of MTX, respectively. Two sequential sharp peaks at 1584 cm^{-1} and 1414 cm^{-1} are attributed to asymmetric and symmetric vibrations for COO^- a group of Alg/CMC composites [98] and these peaks shifted to 1600 and 1417 cm^{-1} after the entrapment of the MTX into the beads. The C–O stretching of methotrexate has appeared at 1217 cm^{-1}. The strong band at 1012 cm^{-1} and sharp band at 952 cm^{-1} could be associated with the stretching of C–O and C–C groups, respectively.

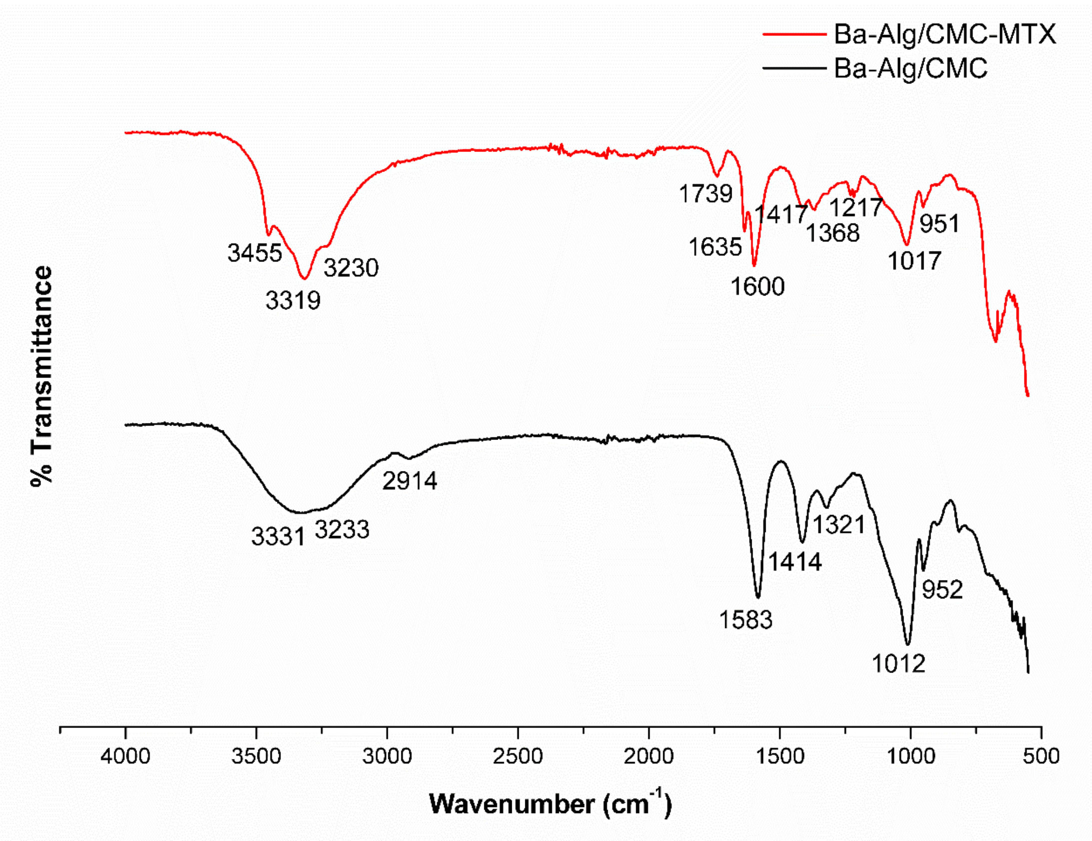

Figure 5.3 : FTIR spectra of Ba-Alg/CMC and Ba-Alg/CMC/MTX beads.

5.2.3 Swelling behaviors of the Ba-Alg/CMC beads

The swelling behaviors of Ba-Alg/CMC beads prepared as described in the experimental section were tested in PBS buffer (pH 7.4) by gravimetric swelling experiments. Additionally, a group of beads was prepared without DMSO to investigate the effect of DMSO in the beads formulation. Figure 5.4 shows swelling ratio percentages of the beads. The swelling equilibrium time of the beads was reached after 2 h treating the beads at drug release conditions. The residence time of the beads in PBS ended in 240 min when SR% of beads remained constant. DMSO, which was added during the preparation of the alginate beads, reduced the swelling ratio of beads by about two times (Figure 5.4). This result showed that DMSO has made a positive effect on the shapes of beads and swellings of alginate-carboxymethyl cellulose composites in PBS.

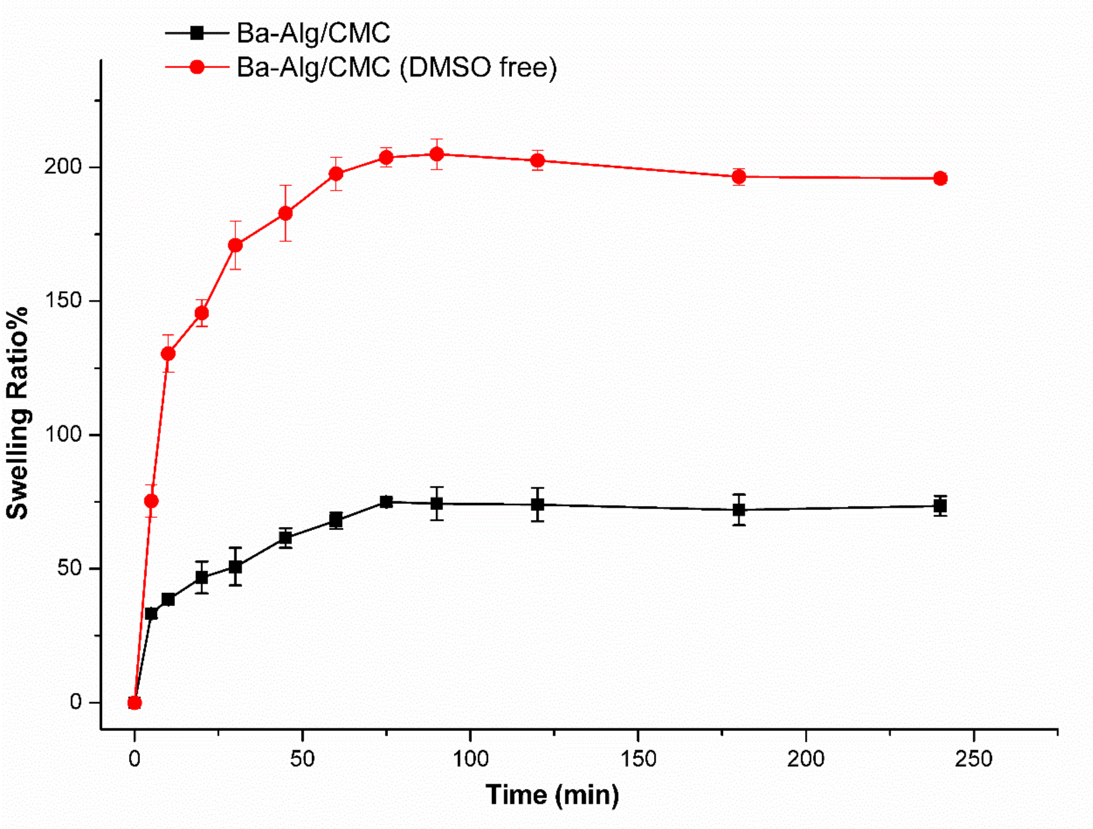

Figure 5.4 : Swelling ratio percentage *vs*. time graphs of DMSO free Ba-Alg/CMC and DMSO containing Ba-Alg/CMC beads. (Mean ± Standard deviation, N = 2).

5.2.4 Entrapment efficiency and drug release kinetics of the Ba-Alg/CMC beads

In order to calculate the final EE% value, the amount of drug remained in the cross-linker solution and the washing water of the beads were taken into account. The entrapment efficiency percentage of Ba-Alg/CMC beads were represented in Table 5.1. As it can be seen from Table 5.1, the EE% of Ba-Alg/CMC for the drugs slightly increases according to MTX-Cu > MTX-Zn > MTX order. This trend shows that MTX-Cu has slightly more interest in alginate-carboxymethyl cellulose composite. There may be a metal-polymer interaction between free metal sides of methotrexate complexes and Ba-Alg/CMC beads.

Table 5.1 : EE% of MTX and its Zn(II) and Cu(II) metal complexes loaded composites. (Mean±Standard deviation, N=2).

Bead Formulation	Entrapment Efficiency%
Ba-Alg/CMC/MTX	58.4±1.22
Ba-Alg/CMC/MTX-Zn	61.8±1.22
Ba-Alg/CMC/MTX-Cu	66.9±1.76

The release studies of the drugs were performed in PBS media at 37 ± 0.1 °C under shaking the vessels at a constant speed in a water bath. Each measurement was repeated three times from separate vessels. Cumulative percentage *vs*. time graphs of three drugs were shown in Figure 5.5. After the first 60 min, the release rate slowed down but continued to 300 min with the final 98% cumulative release. When the swelling behavior Ba-Alg/CMC beads prepared with DMSO is investigated, it is seen that the swelling of beads continues till 60 min and then stabilize. The slowdown of the release profile of MTX after the first 60 min is consistent with the swelling behavior of the beads. To examine the effect of shelf time of 60 days to the release behavior of the MTX loaded beads, the beads were stored after their preparation and drying process under the conditions of 23 ± 2 °C and 55 ± 5% humidity. From Figure 5.5, it cannot be seen a significant change between the release behavior of these beads and that of the immediately tested beads. MTX has been delivered even after two months successively from a biopolymer based Alg/CMC composites to PBS. Thereby, the stability of the drug without losing its effective release actions in PBS was maintained with entrapment.

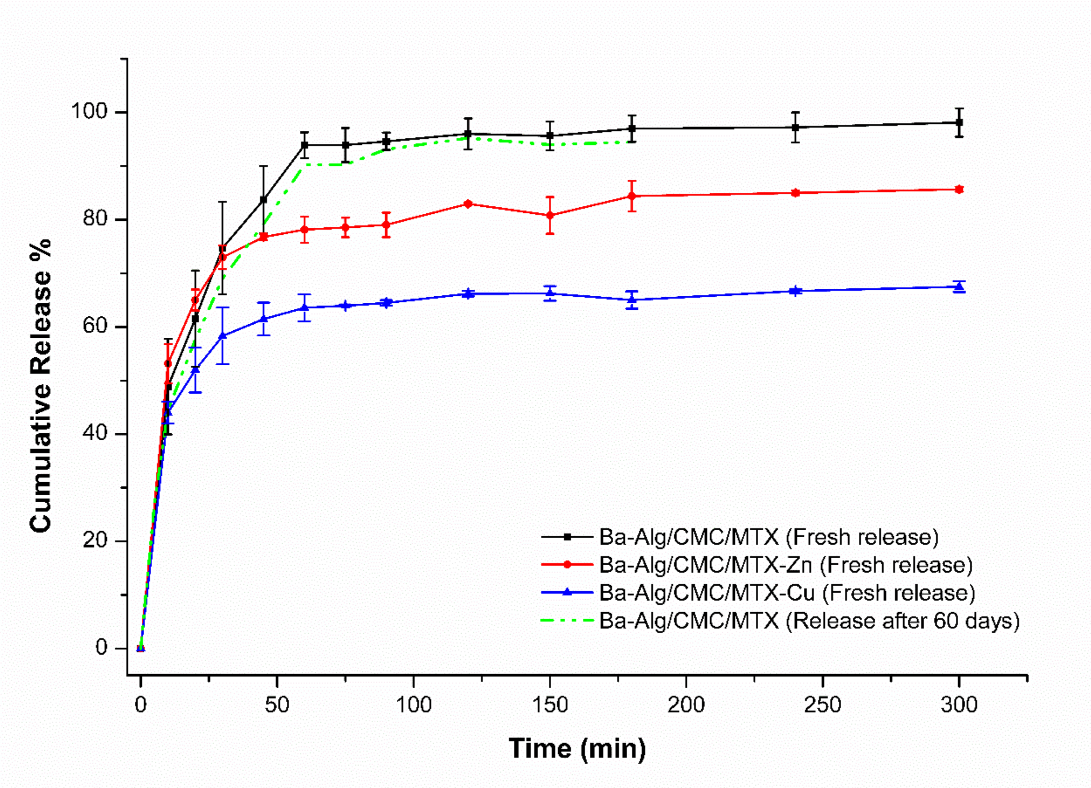

Figure 5.5 : Cumulative drug release profiles of MTX and its metal complexes from the prepared composite gels. MTX release after keeping the beads 60 days at 23 ± 2 °C and 55 ± 5% humidity conditions was shown by dashed line. (Mean ± Standard deviation, N = 2).

The kinetic models were used to describe drug release kinetics of the drugs from Ba-Alg/CMC beads. Cumulative drug release percentages data were used to fit the kinetic models. Table 5.2 shows calculated model parameters for the first-order, Higuchi and Hixson-Crowell kinetic models [119]. The first 120 min release data was fitted to kinetic model equations. From Table 5.2, it can be noticed that the best kinetic model for release of MTX was first-order kinetic model with acceptable R^2 values (>0.94). The other two kinetic models that are Higuchi and Hixson-Crowell models gave R^2 values nearly 0.90. It was not observed significant changes in kinetic modeling between the beads which are studied immediately or after 60 days.

Table 5.2 : MTX release kinetics from Ba-Alg/CMC composites.

Bead Formulation	Cumulative Drug Release % at 6 h	First Order (Fresh release)		Higuchi (Fresh release)		Hixson-Crowell (Fresh release)	
		K_1 (h^{-1}) K_1 (h^{-1})[a]	R^2	K_H ($h^{-1/2}$) K_H ($h^{-1/2}$)[a]	R^2	K_{HC} ($h^{-1/3}$) K_{HC} ($h^{-1/3}$)[a]	R^2
Ba-Alg/CMC/MTX	98.1±2.64	4.13±0.414 5.16±0.513[a]	0.947±0.0403 0.975±0.0146[a]	50.8±11.6 60.9±11.1[a]	0.874±0.0278 0.904±0.0226[a]	1.41±0.222 1.34±0.345[a]	0.900±0.0506 0.902±0.0238[a]

[a]The kinetic models represent the release data obtained from the release after keeping the beads 60 days at 23±2 °C and 55 ± 5% humidity conditions.

5.3 Conclusion

In this present study, Alg/CMC blend beads cross-linked with Ba(II) were prepared by ionic gelation method. Anticancer drug methotrexate was entrapped into Ba-Alg/CMC beads to test the drug release behavior of the beads in phosphate buffer saline (PBS) medium. A small amount of DMSO added in the preparation step of beads to increase the solubility of MTX, gained a significant positive effect on both the morphology and swelling and release behaviors of composite beads. DMSO effected the drug release profile of the beads mainly by decreasing swellings of the beads in PBS. Moreover, Cu(II) and Zn(II) complexes of MTX was loaded to the composites and release behaviors were compared with that of MTX. Cu(II) and Zn(II) complexes of MTX showed lower cumulative drug release percentages than MTX in 5 h of total released time. Ba-Alg/CMC beads being are easy to produce, cheap and biodegradable materials are proposed to subject some other anticancer drug delivery studies similar to MTX structure.

6. CONCLUSIONS

Biopolymers, are naturally derived sources that have been interested for various applications such as adsorption, drug encapsulation, and controlled drug release thanks to their biocompatible, biodegradable, almost non-toxic properties. In recent years, composite materials based on biopolymers have been attracting great attention by allowing the development of novel materials of adsorbents, drug release agents, etc. This thesis focused on biopolymer-based materials and on their composites, for their application as adsorbents in aqueous solutions and drug release agents into mimicked body fluids. Due to the many contaminants, water pollution remains to cause a serious health and environmental threat to the ecosystem. Hereby, the adsorptions of toxicants of SDBS and fluoride using biopolymer based hydrogels have been handled to be an efficient method for the treatment of the pollutants from aqueous solutions as the first two parts of the thesis.

In the first part of the thesis, chitosan biopolymer based adsorbent was prepared and used for the adsorption of an anionic surfactant, which is SDBS, surfactant from aqueous media. To increase the strength of chitosan films in aqueous media, the films were cross-linked ionically in sodium sulfate solutions. The adsorption of SDBS was favorable at pH 2, that is linked by the to the positive charge of chitosan at acidic conditions. Experimental data was best fitted to the pseudo-second order kinetics. From Langmuir isotherm model, maximum adsorption capacity of films for SDBS was calculated as 714 mg/g. Considering very high maximum adsorption capacity value, it is very practical to use easily prepared and environmentally friendly chitosan films for SDBS removal. Prepared adsorbent films are also suggested as potential agents against increasing surfactant pollution in aqueous environments.

In the second part of the thesis, the removal of fluoride ions by the prepared novel cerium-carboxymethyl cellulose composite beads (CMC-Ce) and cerium-carboxymethyl cellulose composite beads incorporated CeO_2 nanoparticles (CeO_2-CMC-Ce) was performed. The fluoride removal efficiency of CMC-Ce and CeO_2-

CMC-Ce adsorbents has shown maximum adsorption capacities of 105 and 312 mg/g, respectively. It was resulted that, the incorporation CeO_2-NPs to biopolymer CMC-Ce adsorbent beads, significantly enhanced the fluoride adsorption ability of the beads. The adsorption data was well fitted to Langmuir isotherm and pseudo-second-order kinetic models. The reusability of the adsorbents up to 9 cycle usage creates opportunity for a sustainable fluoride removal process by the CeO_2-CMC-Ce beads, and this novel adsorbent for the defluoridation of drinking water have been regarded a promising application in the future.

Biopolymers create advantages in drug encapsulation and release methods by yielding efficient drug loading and controlled release profiles. The remaining third and fourth parts of the thesis studied the protein-type drug release to the target colon environment via the biopolymer-based drug encapsulation and the controlled release of an anticancer drug into the body fluid through the biopolymer agent, respectively.

In the third part of the thesis, alginate biopolymer was modified by SDS to increase the entrapment efficiency of alginate for BSA, which is used as a model protein drug, and provide a colon targeted controlled release profile of BSA. SDS modification helped to reduce the release of protein in the acidic stomach environment and transport the drug to the colon medium to reach the total protein release. SDS-modified alginate beads as drug carriers can be proposed for protein-based drugs, that are taken orally and are intended to release to the colon media without any degradation in acidic stomach fluid.

In the fourth part of the thesis, barium alginate-carboxymethyl cellulose composite beads were prepared as a controlled release agent for the cancer drug methotrexate (MTX). MTX is an almost insoluble drug in water. Therefore, the drug was included to the polymer solution following its dissolution in DMSO. The addition of DMSO (10%) to the formulation reduced the swelling of the beads and was also effective in controlling the MTX release. The drug release studies indicated that almost the total amount of MTX release ($98.1 \pm 2.64\%$) was completed during 5 h into PBS at 37 °C. Moreover, release behaviors of the metal complexes of MTX (pre-synthesized Cu(II) and Zn(II) complexes), were compared to MTX and lower cumulative drug releases than MTX were observed. The drug release kinetic models, which are first order, Higuchi and Hixson-Crowell were applied to experimental release data. Consequently, Ba-Alg/CMC beads, with the properties of effortlessly produced, cost efficient, and biodegradable materials are recommended as a drug release agent in monitoring the release of other anticancer drugs in the MTX structure.

As a result of this thesis, the biopolymer-based materials obtained within the scope of the thesis were presented to the literature as a new type of applicable adsorbent in the removal of water pollutants with high removal efficiency. Biopolymeric materials prepared as controlled drug release materials have also been brought to the literature as remarkable materials with their high entrapping efficiencies and controlled release profiles.

REFERENCES

[1] **Ivanković, T., & Hrenović, J.** (2010). Surfactants in the environment, *Archives of Industrial Hygiene and Toxicology*, *61* (1), 95–110.

[2] **Zhang, L., Liu, Y., Wang, S., Liu, B., & Peng, J.** (2015). Selective removal of cationic dyes from aqueous solutions by an activated carbon-based multicarboxyl adsorbent, *RSC Advances, 5*, 99618–99626.

[3] **Zhang, L., Liu, Y., Wang, S., Liu, B., & Peng, J.** (2017). The removal of sodium dodecyl benzene sulfonate by activated carbon modified with quaternary ammonium from aqueous solution, *Journal of Porous Materials*, *24*, 65–73.

[4] **Hozhabr Araghi, S., & Entezari, M.H.** (2015). Amino-functionalized silica magnetite nanoparticles for the simultaneous removal of pollutants from aqueous solution, *Applied Surface Science, 333*, 68–77.

[5] **Özdemir, U., Özbay, B., Veli, S., & Zor, S.** (2011). Modeling adsorption of sodium dodecyl benzene sulfonate (SDBS) onto polyaniline (PANI) by using multi linear regression and artificial neural networks, *Chemical Engineering Journal*, *178*, 183–190.

[6] **Kaygusuz, H., Uzaşçı, S., & Erim, F.B.** (2015). Removal of fluoride from aqueous solution using aluminum alginate beads, *CLEAN: Soil, Air, Water*, *43*, 724–730.

[7] **Kaygusuz, H., Çoşkunirmak, M.H., Kahya, N., & Erim, F.B.** (2015). Aluminum alginate-montmorillonite composite beads for defluoridation of water, *Water, Air, & Soil Pollution*, *226*, 2257.

[8] **Uyar, G., Kaygusuz, H., & Erim, F.B.** (2016). Methylene blue removal by alginate–clay quasi-cryogel beads, *Reactive and Functional Polymers, 106*, 1–7.

[9] **Obeid, L., El Kolli, N., Dali, N., Talbot, D., Abramson, S., Welschbillig, M., Cabuil, V., & Bée, A.** (2014). Adsorption of a cationic surfactant by a magsorbent based on magnetic alginate beads, *Journal of Colloid and Interface Science, 432*, 182–189.

[10] **Uzaşçı, S., Tezcan, F., & Erim, F.B.** (2014). Removal of hexavalent chromium from aqueous solution by barium ion cross-linked alginate beads, *International Journal of Environmental Science and Technology, 11*, 1861–1868.

[11] **Kalaycıoğlu, Z., Torlak, E., Akın-Evingür, G., Özen, İ., & Erim, F.B.** (2017). Antimicrobial and physical properties of chitosan films incorporated with turmeric extract, *International Journal of Biological Macromolecules, 101*, 882–888.

[12] **Kaygusuz, H., Torlak, E., Akın-Evingür, G., Özen, İ., von Klitzing, R., & Erim, F.B.** (2017). Antimicrobial cerium ion-chitosan crosslinked alginate biopolymer films: a novel and potential wound dressing, *International Journal of Biological Macromolecules*, *105*, 1161-1165.

[13] **Berger, J., Reist, M., Mayer, J.M., Felt, O., Peppas, N.A., & Gurny, R.** (2004). Structure and interactions in covalently and ionically crosslinked chitosan hydrogels for biomedical applications, *European Journal of Pharmaceutics and Biopharmaceutics*, *57* (1), 19–34.

[14] **Parhizgar, F., Alishahi, A., Varasteh, H., & Rezaee, H.** (2017). Removing sodium dodecyl benzene sulfonate (SDBS) from aqueous solutions using chitosan, *Journal of Polymers and the Environment, 25*, 836–843.

[15] **Langmuir, I.** (1918). The adsorption of gases on plane surfaces of glass, mica and platinum, *Journal of the American Chemical Society, 40*, 1361–1403.

[16] **Freundlich, H.M.F.** (1906). Über die adsorption in lösungen, *Zeitschrift für Physikalische Chemie, 57*, 385–470.

[17] **Temkin, M.J., & Pyzhev, V.** (1940). Recent modifications to Langmuir isotherms, *Acta Physicochimica USSR*, *12*, 217–222.

[18] **Tseng, R.L., & Wu, F.C.** (2008). Inferring the favorable adsorption level and the concurrent multi-stage process with the Freundlich constant, *Journal of Hazardous Materials, 155*, 277–87.

[19] **Valizadeh, S., Younesi, H., & Bahramifar, N.** (2016). Highly mesoporous K_2CO_3 and KOH/activated carbon for SDBS removal from water samples: batch and fixed-bed column adsorption process, *Environmental Nanotechnology, Monitoring and Management*, *6*, 1–13.

[20] **Mi-Na, Z., Xue-Pin, L., & Bi, S.** (2006). Adsorption of surfactants on chromium leather waste, *Journal of the Society of Leather Technologists and Chemists*, *90* (1), 1–6.

[21] **Öztekin, N.** (2017). Removal of sodium dodecylbenzenesulfonate from aqueous solution using polyethyleneimine-modified bentonite clay, *Desalination and Water Treatment*, *80*, 268–275.

[22] **Tally, M., & Atassi, Y.** (2016). Synthesis and characterization of pH-sensitive superabsorbent hydrogels based on sodium alginate-g-poly(acrylic acid-co-acrylamide) obtained via an anionic surfactant micelle templating under microwave irradiation, *Polymer Bulletin*, *73*, 3183–3208.

[23] **Srivastava, A., Kumari, M., & Prasad., K.S.** (2022). Fluoride occurrence, health issues, and removal using adsorption process, *Proceedings of the Indian National Science Academy, 88*, 129-141.

[24] **Solanki, Y.S., Agarwa, M., Gupta, A.B., Gupta, S., & Shukla, P.** (2022). Fluoride occurrences, health problems, detection, and remediation methods for drinking water: a comprehensive review, *Science of The Total Environment*, *807*, 150601.

[25] **World Health Organization (WHO)** (2011). Guidelines for drinking-water quality, 4th Ed. <https://apps.who.int/iris/handle/10665/44584>, date retrieved 01.02.2023.

[26] **Tolkou, A.K., Manousi, N., Zachariadis, G.A., Katsoyiannis, I.A. & Deliyanni, E.A.** (2021). Recently developed adsorbing materials for fluoride removal from water and fluoride analytical determination techniques: a review, *Sustainability*, *13*, 7061.

[27] **Gai, W.Z., & Deng, Z.Y.** (2021). A comprehensive review of adsorbents for fluoride removal from water: performance, water quality assessment and mechanism, *Environmental Science: Water Research & Technology*, *7*, 1362–1386.

[28] **Wan, K.L., Huang, L., Yan, J., Ma, B.Y., Huang, X.J., Luo, Z.X., Zhang, H.G., & Xiao, T.F.** (2021). Removal of fluoride from industrial wastewater by using different adsorbents: a review, *Science of The Total Environment*, *773*, 145535.

[29] **Ghosh, S., Malloum, A., Igwegbe, C.A., Ighalo, J.O., Ahmadi, S., Dehghani, M.H., Othmani, A., Gokkus, O., & Mubarak, N.M.** (2022). New generation adsorbents for the removal of fluoride from water and wastewater: a review, *Journal of Molecular Liquids*, *346*, 118257.

[30] **Inaniyan, M., & Raychoudhury, T.** (2019). Application of activated carbon–metal composite for fluoride removal from contaminated groundwater in India, *International Journal of Environmental Science and Technology*, *16*, 7545–7554.

[31] **Alhassan, S.I., Huang, L., He, Y.J., Yan, L.J., Wu, B.C., & Wang, H.Y.** (2021). Fluoride removal from water using alumina and aluminum-based composites: a comprehensive review of progress, *Critical Reviews in Environmental Science and Technology*, *51*, 2051–2085.

[32] **Zúñiga-Muro, N.M., Bonilla-Petriciolet, A., Mendoza-Castillo, D.I., Reynel Ávila, H.E., & Tapia-Picazo, J.C.** (2017). Fluoride adsorption properties of cerium-containing bone char, *Journal of Fluorine Chemistry*, *197*, 63–73.

[33] **Kiran, M.S., Bhandari, R., Nehra, A., Manohar, C.S., & Belliraj, S.K.** (2020). Zirconium–cerium and zirconium–lanthanum complexed polyvinyl alcohol films for efficient fluoride removal from aqueous solution, *Journal of Dispersion Science and Technology*, *42* (10), 1550–1565.

[34] **Zhu, T.Y., Zhu, T.H., Gao, J., Zhang, L.F., & Zhang, W.Q.** (2017). Enhanced adsorption of fluoride by cerium immobilized cross-linked chitosan composite, *Journal of Fluorine Chemistry*, *194*, 80–88.

[35] **Liu, H., Deng, S.B., Li, Z.L., Yu, G., & Huang, J.** (2010). Preparation of Al–Ce hybrid adsorbent and its application for defluoridation of drinking water, *Journal of Hazardous Materials*, *179*, 424–430.

[36] **Pansambal, S., Oza, R., Borgave, S., Chauhan, A., Bardapurkar, P., Vyas, S., & Ghotekar, S.** (2022). Bioengineered cerium oxide (CeO_2) nanoparticles and their diverse applications: a review, *Applied Nanoscience*.

[37] **Kargozar, S., Baino, F., Hoseini, S.J., Hamzehlou, S., Darroudi, M., Verdi, J., Hasanzadeh, L., Kim, H.W., & Mozafari, M.** (2018). Biomedical applications of nanoceria: new roles for an old player, *Nanomedicine*, *13* (23), 3051-3069.

[38] **Kalaycioglu, Z., Kahya, N., Adimcilar, V., Kaygusuz, H., Torlak, E., Akin-Evingur, G., & Erim, F.B.** (2020). Antibacterial nano cerium oxide/chitosan/cellulose acetate composite films as potential wound dressing, *European Polymer Journal*, *133*, 109777.

[39] **Kizilkonca, E., Torlak, E., & Erim, F.B.** (2021). Preparation and characterization of antibacterial nano cerium oxide/ chitosan/ hydroxyethylcellulose/ polyethylene glycol composite films, *International Journal of Biological Macromolecules*, *177*, 351-359.

[40] **Lee, J., Jeong, J.S., Kim, S.Y., Lee, S. J., Shin, Y. J., Im, W.J., Kim, S.H., Park, K., Jeong, E.J., Nam, S.Y., & Yu, W.J.** (2020). Safety assessment of cerium oxide nanoparticles: combined repeated-dose toxicity with reproductive/developmental toxicity screening and biodistribution in rats, *Nanotechnology*, *14* (5), 696-710.

[41] **Kalaycioglu, Z., Gecim, B., & Erim, F.B.** (2022). Green synthesis of cerium oxide nanoparticles from turmeric and kinds of honey: characterisations, antioxidant and photocatalytic dye degradation activities, *Advances in Natural Sciences: Nanoscience and Nanotechnology*, *13*, 015016.

[42] **Kaygusuz, H., & Erim, F.B.** (2020). Biopolymer-assisted green synthesis of functional cerium oxide nanoparticles, *Chemical Papers*, *74*, 2357–2363.

[43] **Kang, D.J., Yu, X.L., & Ge, M.F.** (2017). Morphology-dependent properties and adsorption performance of CeO_2 for fluoride removal, *Chemical Engineering Journal*, *330*, 36–43.

[44] **Dong, H., Tang, H., Shi, X.X., Yang, W.L., Chen, W.J., Li, H., Zhao, Y., Zhang, Z.Y., & Hua, M.** (2022). Enhanced fluoride removal from water by nanosized cerium oxides impregnated porous polystyrene anion exchanger, *Chemosphere*, *287*, 131932.

[45] **George, A., Sanjay, M.R., Srisuk, R., Parameswaranpillai, J., & Siengchin, S.** (2020). A comprehensive review on chemical properties and applications of biopolymers and their composites, *International Journal of Biological Macromolecules*, *154*, 329-338.

[46] **Rahman, M.S., Hasan, M.S., Nitai, A.S., Nam, S., Karmakar, A.K., Ahsan, M.S., Shiddiky, M.J.A., & Ahmed, M.B.** (2021). Recent developments of carboxymethyl cellulose, *Polymers*, *13* (8), 1345.

[47] **Gouda, M., Khalaf, M.M., Al-Shuaibi, M.A.A., Mohamed, I.M.A., Shalabi, K., El-Shishtawy, R.M., & El-Lateef, H.M.A.** (2022). Facile synthesis and characterization of CeO_2-nanoparticle-loaded carboxymethyl cellulose as efficient protective films for mild steel: a comparative study of experiential and computational findings, *Polymers*, *14* (15), 3078.

[48] **El Jemli, Y., Mansori, M., Diaz, O.G., Barakat, A., Solhy, A., & Abdelouahdi, K.** (2020). Controlling the growth of nanosized titania via polymer gelation for photocatalytic applications, *RSC Advances*, *10*, 19443-19453.

[49] **Kahya, N., Gölcü, A., & Erim, F.B.** (2019). Barium ion cross-linked alginate-carboxymethyl cellulose composites for controlled release of anticancer drug methotrexate, *Journal of Drug Delivery Science and Technology, 54*, 101324.

[50] **Purohit, S.D., Singh, H., Bhaskar, R., Yadav, I., Chou, C.F., Gupta, M.K., & Mishra, N.C.** (2020). Gelatin-alginate-cerium oxide nanocomposite scaffold for bone regeneration, *Materials Science and Engineering: C, 116*, 111111.

[51] **Gofman, I.V., Nikolaeva, A.L., Khripunov, A.K., Ivan´kova, E.M., Shabunin, A.S., Yakimansky, A.V., Romanov, D.P., Popov, A.L., Ermakov, A.M., Solomevich, S.O., Bychkovsky, P.M., Baranchikov, A.E., & Ivanov, V.K.** (2021). Bacterial cellulose-based nanocomposites containing ceria and their use in the process of stem cell proliferation, *Polymers*, *13* (12), 1999.

[52] **Li, J.F., Liu, Q., Huang, R.H. & Wang, G.D.** (2016). Synthesis of a novel Ce(III)-incorporated cross-linked chitosan and its effective removal of fluoride from aqueous solution, *Journal of Rare Earths*, *34* (10), 1053-1061.

[53] **Nehra, S., Raghav, S., & Kumar, D.** (2020). Biomaterial functionalized cerium nanocomposite for removal of fluoride using central composite design optimization study, *Environmental Pollution*, *258*, 113773.

[54] **Wei, Y.F., Wang, L., & Wang, Y.J.** (2022). Cerium alginate cross-linking with biochar beads for fast fluoride removal over a wide pH range, *Colloids and Surfaces A: Physicochemical and Engineering Aspects*, *636*, 128161.

[55] **Bentouhami, E., Bouet, G.M., Meullemeestre, J., Vierling, F., & Khan, M.A.** (2004). Physicochemical study of the hydrolysis of rare-earth elements (III) and thorium (IV), *Comptes Rendus Chimie*, *7* (5), 537-545.

[56] **Kaygusuz, H., & Erim, F.B.** (2013). Alginate/BSA/montmorillonite composites with enhanced protein entrapment and controlled release efficiency, *Reactive and Functional Polymers*, *73* (11), 1420-1425.

[57] **Kaygusuz, H., Uysal, M., Adimcilar, V., & Erim, F.B.** (2015). Natural alginate biopolymer montmorillonite clay composites for vitamin B2 delivery, *Journal of Bioactive and Compatible Polymers*, *30* (1), 48-56.

[58] **Kaygusuz, H., Erim, F.B., Pekcan, Ö., & Akin Evingür, G.** (2014). Cation effect on slow release from alginate beads: a fluorescence study, *Journal of Fluorescence, 24*, 161-167.

[59] **Amidon, S., Brown, J.E., & Dave, V.S.** (2015). Colon-targeted oral drug delivery systems: design trends and approaches, *AAPS PharmSciTech, 16* (4), 731–741.

[60] **Pasparakis, G., & Bouropoulos, N.** (2006). Swelling studies and in vitro release of verapamil from calcium alginate and calcium alginate-chitosan beads, *International Journal of Pharmaceutics*, *323*, 34-42.

[61] **Reddy, B.H.N., Rauta, P.R., Venkatalakshimi, V., & Sreenivasa, S.** (2018). Synthesis and characterization of cloisite-30B clay dispersed poly (acryl amide/sodium alginate)/AgNp hydrogel composites for the study of BSA protein drug delivery and antibacterial activity, *Materials Research Express, 5*, 025403.

[62] **Bajpai, M., Shukla, P. & Bajpai, S.K.** (2016). Ca (II) + Ba (II) ions crosslinked alginate gels prepared by a novel diffusion through dialysis tube (DTDT) approach and preliminary BSA release study, *Polymer Degradation and Stability*, *134*, 22–29.

[63] **Omer, A.M., Tamer, T.M., Hassan, M.A., Rychter, P., Mohy Eldin, M.S., & Koseva, N.** (2016). Development of amphoteric alginate/aminated chitosan coated microbeads for oral protein delivery, *International Journal of Biological Macromolecules, 92*, 362-370.

[64] **Goldfeld, M., Malec, A., Podella, C. & Rulison, C.** (2015). Proteins as surfactant enhancers for environmental and industrial applications, *Journal of Petroleum & Environmental Biotechnology, 6* (2).

[65] **Li, Y., & Lee, J.** (2019). Staring at protein-surfactant interactions: Fundamental approaches and comparative evaluation of their combinations - a review, *Analytica Chimica Acta*, *1063*, 18-39.

[66] **Mesa, C.L.** (2005). Polymer – surfactant and protein – surfactant interactions, *Journal of Colloid and Interface Science*, *286* (1), 148-157.

[67] **Kaygusuz, H., Akin Evingür, G., Pekcan, Ö., von Klitzing, R. & Erim, F.B.** (2016). Surfactant and metal ion effects on the mechanical properties of alginate hydrogels, *International Journal of Biological Macromolecules*, *92*, 220-224.

[68] **Honda, C., Kamizono, H., Matsumoto, K.I. & Endo, K.** (2004). Studies on bovine serum albumin-sodium dodecyl sulfate complexes using pyrene fluorescence probe and 5-doxylstearic acid spin probe, *Journal of Colloid and Interface Science*, *278* (2), 310-317.

[69] **Matei, I., Ariciu, A.M., Neacsu, M.V., Collauto, A., Salifoglou, A., & Ionita, G.** (2014). Cationic spin probe reporting on thermal denaturation and complexation-decomplexation of BSA with SDS. Potential applications in protein purification processes, *The Journal of Physical Chemistry B, 118* (38), 11238-11252.

[70] **Moriyama, Y., Watanabe, E., Kobayashi, K., Harano, H., Inui, E., & Takeda, K.** (2008). Secondary structural change of bovine serum albumin in thermal denaturation up to 130 ^oC and protective effect of sodium dodecyl sulfate on the change, *The Journal of Physical Chemistry B*, *112* (51), 16585-16589.

[71] **Santos, S.F., Zanette, D., Fischer, H., & Itri, R.** (2003). A systematic study of bovine serum albumin (BSA) and sodium dodecyl sulfate (SDS) interactions by surface tension and small angle X-ray scattering, *Journal of Colloid and Interface Science*, *262* (2), 400-408.

[72] **Parekh, P., Parmar, A., Chavda, S., & Bahadur, P.** (2011). Modified calcium alginate beads with sodium dodecyl sulfate and clay as adsorbent for removal of methylene blue, *Journal of Dispersion Science and Technology*, *32* (10), 1377-1387.

[73] **Taha, M.O., Nasser, W., Ardakani, A., & Alkhatib, H.S.** (2008). Sodium lauryl sulfate impedes drug release from zinc-crosslinked alginate beads: Switching from enteric coating release into biphasic profiles, *International Journal of Pharmaceutics*, *350*, 291-300.

[74] **Miller, I.J.** (1996). Alginate composition of some New Zealand brown seeweeds, *Phytochemistry*, *41* (5), 1315-1317.

[75] **Gómez-Ordóñez, E., &Rupérez, P.** (2011). FTIR-ATR spectroscopy as a tool for polysaccharide identification in edible brown and red seaweeds, *Food Hydrocolloids*, *25* (6), 1514-1520.

[76] **Ramos, P.E., Silva, P., Alario, M.M., Pastrana, L.M., Teixeira, J.A., Cerqueira, M.A., & Vicente, A.** (2018). Effect of alginate molecular weight and M/G ratio in beads properties foreseeing the protection of probiotics, *Food Hydrocolloids*, *77*, 8-16.

[77] **Bradford, M.M.** (1976). A rapid and sensitive method for the quantitation of microgram quantities of protein utilizing the principle of protein-dye binding, *Analytical Biochemistry*, *72*, 248-254.

[78] **Nikas, Y.J., & Blankstein, D.** (1994). Complexation of nonionic polymers and surfactants in dilute aqueous solutions, *Langmuir*, *10*, 3512-3528.

[79] **Öztekin, N., & Erim, F.B.** (2013). Determination of critical aggregation concentration in the poly-(vinylpyrrolidone)–sodium dodecyl sulfate system by capillary electrophoresis, *Journal of Surfactants and Detergents*, *16* (3), 363-367.

[80] **Sartori, C., Finch, D.S., Ralph, B., & Gilding, K.** (1997). Determination of the cation content of alginate thin films by FTi.r. spectroscopy, *Polymer*, *38* (1), 43-51.

[81] **Chatterjee, S., Salaün, F., & Campagne, C.** (2014). The influence of 1-butanol and trisodium citrate ion on morphology and chemical properties of chitosan-based microcapsules during rigidification by alkali treatment, *Marine Drugs*, *12*, 5801-5816.

[82] **Tang, I.M., Krishnamra, N., Charoenphandhu, N., Hoonsawat, R., & Pon-On, W.** (2011). Biomagnetic of apatite-coated cobalt ferrite: A core-shell particle for protein adsorption and pH-controlled release, *Nanoscale Research Letters*, *6* (1), 19.

[83] **Lawrie, G., Keen, I., Drew, B., Chandler-Temple, A., Rintoul, L., Fredericks, P., & Grøndahl, L.** (2007). Interactions between alginate and chitosan biopolymers characterized using FTIR and XPS, *Biomacromolecules*, *8*, 2533-2541.

[84] **Viana, R.B., da Silva, A.B.F., & Pimentel, A.S.** (2012). Infrared spectroscopy of anionic, cationic, and zwitterionic surfactants, *Advances in Physical Chemistry*, *2012*, 903272.

[85] **Leitch, J.J., Collins, J., Friedrich, A.K., Stimming, U., Dutcher, J.R., & Lipkowski, J.** (2012). Infrared studies of the potential controlled adsorption of sodium dodecyl sulfate at the Au(111) electrode surface. *Langmuir*, *28*, 2455-2464.

[86] **Yang, J., Zhao, J., & Fang, Y.** (2008). Calorimetric studies of the interaction between sodium alginate and sodium dodecyl sulfate in dilute solutions at different pH values, *Carbohydrate Research*, *343* (4), 719-725.

[87] **Lovegrove, A., Edwards, C.H., De Noni, I., Patel, H., El, S.N., Grassby, T., Zielke, C., Ulmius, M., Nilsson, L., Butterworth, P.J., Ellis, P.R., & Shewry, P.R.** (2017). Role of polysaccharides in food, digestion, and health, *Critical Reviews in Food Science and Nutrition*, *57* (2), 237-253.

[88] **Laurienzo, P.** (2010). Marine polysaccharides in pharmaceutical applications: an overview, *Marine Drugs*, *8*, 2435-2465.

[89] **Charoenwongpaiboon, T., Wangpaiboon, K., Pichyangkura, R., & Prousoontorn**, **M.H.** (2018). Highly porous core-shell chitosan beads with superb immobilization efficiency for: *Lactobacillus reuteri* 121 inulosucrase and production of inulin-type fructooligosaccharides, *RSC Advances*, *8*, 17008-17016.

[90] **Lisuzzo, L., Cavallaro, G., Parisi, F., Milioto, S., Fakhrullin, R., & Lazzara, G.** (2019). Core/Shell gel beads with embedded halloysite nanotubes for controlled drug release, *Coatings*, *9* (2), 70.

[91] **Ching, S.H., Bansal, N., & Bhandari, B.** (2019). Alginate gel particles–a review of production techniques and physical properties, *Critical Reviews in Food Science and Nutrition*, *57* (6), 1133-1152.

[92] **Poojari, R., & Srivastava, R.** (2013). Composite alginate microspheres as the next-generation egg-box carriers for biomacromolecules delivery, *Expert Opinion on Drug Delivery*, *10* (8), 1061-1076.

[93] **Mørch, Ý.A., Donati, I., Strand, B.L., & Skjåk-Bræk, G.** (2006). Effect of Ca^{2+}, Ba^{2+}, and Sr^{2+} on alginate microbeads, *Biomacromolecules*, *7*, 1471-1480.

[94] **Saber-Samandari, S., Saber-Samandari, S., Gazi, M., Cebeci, F.Ç., & Talasaz, E.** (2013). Synthesis, characterization and application of cellulose based nano-biocomposite hydrogels, *Journal of Macromolecular Science, Part A, 50* (11), 1133-1141.

[95] **Abdul Khalil, H.P.S., Tye, Y.Y., Saurabh, C.K., Leh, C.P., Lai, T.K., Chong, E.W.N., Nurul Fazita, M.R., Hafiidz, J.M., Banerjee, A., & Syakir, M.I.** (2017). Biodegradable polymer films from seaweed polysaccharides: a review on cellulose as a reinforcement material. *Express Polymer Letters*, *11* (4), 244-265.

[96] **Kim, M.S., Park, S.J., Gu, B.K., & Kim, C.H.** (2012). Ionically crosslinked alginate-carboxymethyl cellulose beads for the delivery of protein therapeutics, *Applied Surface Science, 262*, 28-33.

[97] **Agarwal, T., Narayana, S.N.G.H., Pal, K., Pramanik, K., Giri, S., & Banerjee, I.** (2015). Calcium alginate-carboxymethyl cellulose beads for colon-targeted drug delivery, *International Journal of Biological Macromolecules, 75*, 409-417.

[98] **Swamy, B.Y., & Yun, Y.S.** (2015). In vitro release of metformin from iron (III) cross-linked alginate-carboxymethyl cellulose hydrogel beads, *International Journal of Biological Macromolecules*, *77*, 114-119.

[99] **Bulut, E., & Şanli, O.** (2014). Optimization of release conditions of Alzheimer's drug donepezil hydrochloride from sodium alginate/sodium carboxymethyl cellulose blend microspheres, *Journal of Macromolecular Science, Part B*, *53*, 902-917.

[100] **Bannikova, A., Rasumova, L., Evteev, A., Evdokimov, I., & Kasapis, S.** (2017). Protein-loaded sodium alginate and carboxymethyl cellulose beads for controlled release under simulated gastrointestinal conditions, *International Journal of Food Science & Technology, 52* (10), 2171-2179.

[101] **Holmboe, L., Andersen, A.M., Mørkrid, L., Slørdal, L., & Hall, K.S.** (2012). High dose methotrexate chemotherapy: pharmacokinetics, folate and toxicity in osteosarcoma patients, *British Journal of Clinical Pharmacology*, *73* (1), 106-114.

[102] **Cutolo, M., Sulli, A., Pizzorni, C., Seriolo, B., & Straub, R.H.** (2001). Anti-inflammatory mechanisms of methotrexate in rheumatoid arthritis, *Annals of the Rheumatic Diseases, 60* (8), 729-735.

[103] **Alfonsi, K., Colberg, J., Dunn, P.J., Fevig, T., Jennings, S., Johnson, T.A., Kleine, H.P., Knight, C., Nagy, M.A., Perry, D.A., & Stefaniak, M.** (2008). Green chemistry tools to influence a medicinal chemistry and research chemistry based organisation, *Green Chemistry*, *10*, 31-36.

[104] **Henderson, R.K., Jiménez-González, C., Constable, D.J.C., Alston, S.R., Inglis, G.G.A., Fisher, G., Sherwood, J., Binks, S.P., & Curzons, A.D.** (2011). Expanding GSK's solvent selection guide - embedding sustainability into solvent selection starting at medicinal chemistry, *Green Chemistry*, *13*, 854-862.

[105] **Wang, X., & Yan, H.** (2017). Methotrexate-loaded porous polymeric adsorbents as oral sustained release formulations, *Materials Science and Engineering: C, 78*, 598-602.

[106] **Vakilinezhad, M.A., Alipour, S., & Montaseri, H.** (2018). Fabrication and in vitro evaluation of magnetic PLGA nanoparticles as a potential Methotrexate delivery system for breast cancer, *Journal of Drug Delivery Science and Technology*, *44*, 467-474.

[107] **de Lima Fontes, M., Meneguin, A.B., Tercjak, A., Gutierrez, J., Cury, B.S.F., dos Santos, A.M., Ribeiro, S.J.L., & Barud, H.S.** (2018). Effect of in situ modification of bacterial cellulose with carboxymethylcellulose on its nano/microstructure and methotrexate release properties, *Carbohydrate Polymers*, *179*, 126-134.

[108] **Mahdavinia, G.R., Mosallanezhad, A., Soleymani, M., & Sabzi, M.** (2017). Magnetic- and pH-responsive κ-carrageenan/chitosan complexes for controlled release of methotrexate anticancer drug, *International Journal of Biological Macromolecules*, *97*, 209-217.

[109] **Mesquita, P.C., Oliveira, A.R., & Fernandes, M.F.** (2015). Physicochemical aspects involved in methotrexate release kinetics from biodegradable spray-dried chitosan microparticles, *Journal of Physics and Chemistry of Solids*, *81*, 27-33.

[110] **Gao, C., Liu, T., Dang, Y., Yu, Z., Wang, W., Guo, J., Zhang, X., He, G., Zheng, H., Yin, Y., & Kong, X.** (2014). pH/redox responsive core cross-linked nanoparticles from thiolated carboxymethyl chitosan for in vitro release study of methotrexate, *Carbohydrate Polymers*, *111*, 964-970.

[111] **Ji, J., Wu, D., Liu, L., Chen, J., Xu, Y.** (2012). Preparation, characterization, and in vitro release of folic acid-conjugated chitosan nanoparticles loaded with methotrexate for targeted delivery, *Polymer Bulletin*, *68*, 1707-1720.

[112] **Nezhad-Mokhtari, P., Arsalani, N., Javanbakht, S., & Shaabani, A.** (2019). Development of gelatin microsphere encapsulated Cu-based metal-organic framework nanohybrid for the methotrexate delivery, *Journal of Drug Delivery Science and Technology*, *50*, 174-180.

[113] **Nosrati, H., Adinehvand, R., Manjili, H.K., Rostamizadeh, K., & Danafar, H.** (2019). Synthesis, characterization, and kinetic release study of methotrexate loaded mPEG–PCL polymersomes for inhibition of MCF-7 breast cancer cell line, *Pharmaceutical Development and Technology*, *24* (1), 89-98.

[114] **Nagy, G., Király, G., Veres, P., Lázár, I., Fábián, I., Bánfalvi, G., Juhász, I., & Kalmár, J.** (2019). Controlled release of methotrexate from functionalized silica-gelatin aerogel microparticles applied against tumor cell growth, *International Journal of Pharmaceutics*, *558*, 396-403.

[115] **Rosenberg, B.** (1985). Fundamental studies with cisplatin, *Cancer*, *55* (10), 2303-2316.

[116] **Ndagi, U., Mhlongo, N., & Soliman, M.E.** (2017). Metal complexes in cancer therapy – an update from drug design perspective, *Drug Design, Development and Therapy*, *11*, 599-616.

[117] **Wang, H., Hu, T., Wen, R., Wang, Q., & Bu, X.** (2013). In vitro controlled release of theophylline from metal–drug complexes, *Journal of Materials Chemistry B*, *1*, 3879-3882.

[118] **Çeşme, M., & Gölcü, A.** (2019). Metal-based molecular compounds: structure, analytical properties, dsDNA binding studies and in vitro antiproliferative activity on selected cancer cell lines, *Pharmaceutical Chemistry Journal*, *53*, 392-410.

[119] **Dash, S., Murthy, P.N., Nath, L., & Chowdhury, P.** (2010). Kinetic modeling on drug release from controlled drug delivery systems, *Acta Poloniae Pharmaceutica – Drug Research*, *67* (3), 217-223.

CURRICULUM VITAE

Name Surname : Nilay KAHYA

EDUCATION :

- **B.Sc.** : 2014, Istanbul Technical University, Faculty of Science and Letters, Chemistry
- **B.Sc. (Double Major)** : 2020, Istanbul Technical University, Chemical-Metalurgical Engineering, Chemical Engineering
- **M.Sc.** : 2016, Istanbul Technical University, Graduate School of Science, Engineering and Technology, Chemistry

PROFESSIONAL EXPERIENCE AND REWARDS:

- 2015-Present Research Assistant, Chemistry, Istanbul Technical University, Faculty of Science and Letters, Department of Chemistry
- 2017-2020 Researcher, ITU Scientific Research and Development Support Program Projects (40695)
- 2020-2023 Researcher, ITU Scientific Research and Development Support Program Projects (42372)
- 2022-2023 PhD scholarship, TUBITAK 3501 Scientific and Technological Research Projects (221M272)

PUBLICATIONS ON THE THESIS:

- **Kahya, N.,** Kaygusuz, H., Erim, F.B. 2018. Aqueous Removal of Sodium Dodecyl Benzene Sulfonate (SDBS) by Crosslinked Chitosan Films, Journal of Polymers and the Environment, 26, 2166-2172.
- **Kahya, N.,** Erim, F.B. 2019. Surfactant Modified Alginate Gels for Controlled Release of Protein Drug, Carbohydrate Polymers, 224, 115165.

- **Kahya, N.,** Gölcü, A., Erim, F.B. 2019. Barium Ion Cross-linked Alginate-Carboxymethyl Cellulose Composites for Controlled Release of Anticancer Drug Methotrexate, Journal of Drug Delivery Science and Technology, 54, 101324.
- **Kahya, N.,** Erim, F.B. 2023. Removal of Fluoride Ions from Water by Cerium-Carboxymethyl Cellulose Beads Doped with CeO_2 Nanoparticles, International Journal of Biological Macromolecules, 242(1), 124595.

OTHER PUBLICATIONS:

- Balkız, G., Pingo, E., **Kahya, N.,** Kaygusuz, H., Erim, F.B. 2018. Graphene Oxide/Alginate Quasi-Cryogels for Removal of Methylene Blue, Water, Air, & Soil Pollution, 229(131).
- Kalaycıoğlu, Z., **Kahya, N.,** Adımcılar, V., Kaygusuz, H., Torlak, E., Akın-Evingür, G., Erim, F.B. 2020. Antibacterial Nano Cerium Oxide/Chitosan/Cellulose Acetate Composite Films As Potential Wound Dressing, European Polymer Journal, 133, 109777.
- Karadeniz, D., **Kahya, N.,** Erim, F.B. 2022. Effective Photocatalytic Degradation of Malachite Green Dye by Fe (III)-Cross-linked Alginate-Carboxymethyl Cellulose Composites, Journal of Photochemistry and Photobiology A: Chemistry, 428, 113867.
- **Kahya, N.,** Kestir, S.M., Öztürk, S., Yolaç, A., Torlak, E., Kalaycıoğlu, Z., Akın-Evingür, G., Erim, F.B. 2022. Antioxidant and Antimicrobial Chitosan Films Enriched with Aqueous Sage and Rosemary Extracts as Food Coating Materials: Characterization of the Films and Detection of Rosmarinic Acid Release, International Journal of Biological Macromolecules, 217, 470-480.
- **Kahya, N.,** Erim, F.B. 2022. Graphene oxide/Chitosan Based Composite Materials as Adsorbents in Dye Removal, Chemical Engineering Communications, 209(12), 1711-1726.